Biochemical Characterization of Two Aminopeptidases Involved in Hemoglobin Catabolism in the Food Vacuole of *Plasmodium falciparum*

Daniel Raafat Tadros Ragheb

Dissertation submitted to the faculty of
Virginia Polytechnic Institute and State University
in partial fulfillment of the requirement for the degree of

Doctor of Philosophy
In
Biochemistry

Michael W. Klemba, Chair
Dennis R. Dean
James E. Mahaney
Florian D. Schubot

March 31st, 2011

Blacksburg, VA

Keywords: *Plasmodium falciparum*, malaria, PfAPP, PfA-M1, aminopeptidase P, M1 aminopeptidase, food vacuole, hemoglobin degradation

Biochemical Characterization of Two Aminopeptidases Involved in Hemoglobin Catabolism in the Food Vacuole of *Plasmodium falciparum*

Daniel Raafat Tadros Ragheb

ABSTRACT

The parasite *Plasmodium falciparum* is the causative agent of the most severe form of human malaria. During its intraerythocytic life cycle, *P. falciparum* transports red blood cell contents to its acidic organelle, known as the food vacuole, where a series of proteases degrade a majority of the host hemoglobin. Two metalloaminopeptidases, PfAPP and PfA-M1, have been previously localized to the food vacuole (in addition to distinct secondary locations for each), implicating them in the final stages of hemoglobin catabolism. Prior genetic work has determined these enzymes are necessary for efficient parasite proliferation, highlighting them as potential anti-malarial drug targets. This study presents the biochemical basis for the catalytic roles of these two enzymes in the hemoglobin degradation pathway. PfAPP, an aminopeptidase P homolog, is specific for hydrolyzing the N-termini of peptides containing penultimate prolines. PfA-M1 is a member of the expansive M1 family of proteases and exhibits a broad specificity towards substrates. The two enzymes are ubiquitous, found in organisms across all kingdoms of life. Their presence in an acidic environment is unique for aminopeptidase P proteins and rare for M1 homologs. Our immunolocalization results have confirmed the dual distribution of these two enzymes in the parasite. Vacuolar targeting was found to be associated with the *Plasmodium* specific N-terminal extension found in the PfA-M1 sequence by yellow fluorescent protein fusion studies. Kinetic analysis of recombinant forms of PfAPP and PfA-M1 revealed both enzymes are stable and catalytically efficient in the substrate rich, acidic environment of the parasite food vacuole. In addition, mutagenic exploration of the PfA-M1 active site has determined a residue important in dictating substrate specificity among homologs of the same family. These results provide insight into the parasite's functional recruitment of these enzymes to deal with the final stages of hemoglobin catabolism and necessary considerations for inhibitor design.

DEDICATION AND ACKNOWLEDGEMENTS

This dissertation, all my work, and who I am is dedicated to the Person and Glory of Jesus Christ.

I do not think I can accurately convey on this page the sense of gratitude and love I have for the people in my life so I can only hope that I am able to do so better in person.

It is no matter of simple order that I would like to thank Dr. Michael Klemba first for all his years of guiding me through graduate school. You are an amazing scientist and mentor, and a good and humble man whom I am delighted to call a friend. I would not have wanted to be taught by anyone other than you. In the same breath thank you Dr. Seema Dalal for all our wonderful times together, all that I have learned from you, for your friendship, and for the love with which you invited me into your lives with Neal and Kyle. I will miss all four of you dearly.

Thank you Drs. Dennis Dean, James Mahaney, and Florian Schubot for the constant encouragement and advice that marked all my meetings with you. It was a pleasure to have you as my committee these past years.

I appreciate the Biochemistry department and its staff and faculty for all their help. In particular, thank you Dr. Erin Dolan for always having the time to talk and for your dedicated service for the graduate students of this department.

Thank you Titilola Denloye, Priscilla Krai, Alex Kulifay and all the past members of the Klemba lab for being good friends and labmates and for putting up with my singing, whistling, humming, knocking, general abuse and sense of humor. It was always fun to be in lab with you all.

I have had so many treasured friends come and go through Blacksburg that is difficult to mention all of them here, so my apologies to anyone I missed. To my oldest friends from Blacksburg, Shannon and Jarrod Alford, thank you for your continued love and encouragement. To some of the best people I know, Dan Preusser, Robert Howe, Josh Layfield, Mike Wiley and Joe & Krista Allen, thank you for your faithful and true friendships.

To my extended Argentinian family, Pablo, Vanessa, Lucas (Hi Lucccaaaasssss!), and Isabella Tarazaga, the Lord has blessed me with your unwavering love and loyalty for which I can never thank Him enough. You are truly amazing friends whom I love and miss dearly.

I would not have been able to do any of this or matured at all as a person if it were not for my Mom and Dad. I love and miss you both so much, that I think only you two could understand. I don't want to just thank you for your unmatched love and encouragement, but for every step of the way when you were willing to stand firmly for what was right first and teach me accordingly in grace and truth. It is evident in my heart how the Lord has and continues to use you, and you deserve all of the love, honor and respect I can possibly give. Thanks for always being there for me. With this same measure of love do I thank you Ragy for being a wonderful older brother who has never been less than proud of me. Your love and friendship mean the world to me.

And in fitting form, from dedication to the last acknowledgement, my love and gratitude are most for the Lord Jesus Christ. This is no passing word of empty religion but real love for the Divine Man who would take His Cross to bear my and the world's sins upon His very shoulders. As You were raised from the dead, so You called me into the presence of God the Father and blessed me with Your Holy Spirit, and so I walk in the newness of life that You've given me. For this I do not simply thank you Lord, but I live my life eternally for You and Your Glory. And for anyone who has every felt any measure of love from me, please know that it is truly "because He first loved us."

TABLE OF CONTENTS

LIST OF FIGURES

Chapter 2

Chapter 3

Chapter 3 (*continued*)

Chapter 4

LIST OF TABLES

Chapter 2

Chapter 3

Chapter 4

ATTRIBUTION

I performed all the experiments presented in this dissertation except for the following:

Chapter 2 - Preliminary cloning and metal reconstitution assays were performed by K. Bompiani, and cloning of PfAPP and hAPP for recombinant expression as well as immunolocalization studies were done by Dr. S. Dalal.

Chapter 3 - Cloning of PfA-M1 for recombinant expression was done by K. Bompiani, mass spectrometry analysis by Dr. W. K. Ray, and cloning and expression of PfA-M1 N-terminal-YFP fusions for *in vivo* experiments and the associated tissue culture work were all done by Dr. S. Dalal.

Chapter 4 - This project is a collaboration between Dr. S. Dalal and myself. Dr. Dalal performed all the mutagenesis and cloning of the PfA-M1 gene, I determined the metal content associated with the PfA-M1 variants, and the rest of the experiments were done together.

Chapter 1

Introduction

Plasmodium falciparum malaria as a global problem

The disease malaria has devastating effects on the impoverished populations of tropical and subtropical areas worldwide. The treatment and prevention of the disease has in recent years returned to the forefront of political and global health campaigns. Predictions from current statistical models indicate there are just over two billion people at risk of infection by *Plasmodium falciparum*, the most virulent of the five *Plasmodia* species known to cause human malaria. There are approximately 515 million clinical attacks and one to two million deaths attributable to *P. falciparum* malaria every year. Of these cases, 70% are located in sub-Saharan Africa and 25% in South East Asia (1). In highly endemic areas, children under the age of 10 are most at risk of developing malaria, especially where there are low economic resources, poor health infrastructure, inefficient population census measures, and limited access to anti-malarial drugs (2). Fifty years after the Global Malaria Eradication Programme (run by the World Health Organization) populations not treated with chloroquine in areas of uncontrolled mosquito transmission have suffered greatly from the rampant spread of the disease. Even after attention was turned towards malaria-stricken areas, parasite resistance has developed against previously employed first-line anti-malarial drugs (chloroquine, sulfadoxine-pyrimethamine) (3). Concerns of developing resistance against drug treatments, including the current preferred method (artemisinin combination therapy) and their high costs of manufacture and distribution, have prompted research for new, effective and cheap ways to combat the burdensome disease. In addition to current efforts to develop an anti-malarial vaccine and improve mosquito control there is a need for anti-malarial drugs that exploit different pathways in the parasite's biology (4,5). New methods must rapidly kill the blood pathogen, have minimal side effects on the patient, and be manufactured at an inexpensive cost to ensure mass implementation of treatment, even in the most impoverished of areas.

Exploring parasite biology for drug targets

P. falciparum spends its life cycle between its vector, the *Anopheles* mosquito, and human host. As the mosquito takes a blood meal, motile sporozoite-form parasites are transferred to human skin and enter the bloodstream. From there, parasites enter the liver and invade hepatocytes where they remain for six days. At that time, merozoite-stage parasites rupture infected liver cells and proceed to invade erythrocytes. It is during this asexual stage of

the parasite life cycle that the clinical symptoms of malaria present. Over the course of approximately 48 hours, merozoite parasites invade red blood cells (RBC), and mature from young rings through the trophozoite stage to multi-nucleated schizonts. During its stay, the parasite remodels host cell structure, consumes a majority of the cytosolic hemoglobin in the cell, and exports proteins into the cytosol and onto the surface of RBCs. After replication, 8-32 progeny egress from each cell and reinvade uninfected RBCs, completing the erythrocyte life cycle. Various stimuli can induce gametocytogenesis during the RBC life cycle by which the parasite can differentiate into its male and female forms, which are then taken up in the bloodmeal of a mosquito. As the stage of disease in the life of the parasite, the RBC cycle presents a vast array of potential drug targets. (6,7).

The importance of proteases in the P. falciparum life cycle

Enzymes that catalyze the hydrolysis of peptide bonds are involved in a variety of vital biological processes in *P. falciparum*, particularly in the erythrocyte cycle. Some of these pathways are typical of eukaryotic cells such as the proteasome complex, responsible for protein turnover. Others are more unique to the needs of the obligate parasite and have been presented as attractive drug targets. These enzymes vary in mechanistic classification, including aspartic, cysteine, serine, and metalloproteases and substrate preference including both endo- and exopeptidases. In recent years, proteolytic enzymes have been identified in multiple events required for parasite proliferation including RBC invasion, the export of proteins into the host cell, parasite egress, and hemoglobin degradation (8-11). The focus of my research is two aminopeptidases, PfAPP and PfA-M1, implicated in hemoglobin catabolism in the food vacuole, an acidic organelle in the parasite.

The requirement of hemoglobin degradation for parasite proliferation

Hemoglobin, the protein responsible for oxygen binding and delivery in the human body, comprises approximately 95% of soluble protein in the red blood cell. Over the course of its life cycle within the cell, *P. falciparum* will consume close to three fourths of RBC hemoglobin, mainly during the trophozoite stage (12). Hemoglobin degradation provides the parasite with amino acids (of which only 16% are used for protein synthesis), space within the RBC, and a potential mechanism of osmotic regulation to preserve host cell integrity (12-14). It has been

shown that blocking hemoglobin catabolism causes enlarged food vacuole phenotypes and prevents parasite maturation and replication (15). Proteases essential to the pathway have consequently been identified as potential drug targets.

RBC cytosol is ingested through the cytostome of the parasite and transported to the acidic food vacuole where resident aspartic (plasmepsins I, II, and IV), histo-aspartic, and cysteine proteases (falcipain-2, 2', 3') begin to degrade native hemoglobin (16). Polypeptide fragments generated from these proteases are further hydrolyzed by a metallo-enzyme, falcilysin (17). Dipeptidyl-aminopeptidase 1 can generate dipeptides from the subsequent oligopeptides produced (18).

Previous work on hemoglobin degradation in *P. falciparum* led to the hypothesis that dipeptides were exported from the food vacuole into the cytosol in order to be hydrolyzed by aminopeptidases. This model was based primarily on a study that found aminopeptidase activity in whole parasite lysate, but not in food vacuole extracts (19). Due to the lack of carboxypeptidases in the *P. falciparum* genome, researchers have assumed the final step of hemoglobin degradation to be the result of cytosolic aminopeptidases (20).

However, work in recent years has localized two metalloaminopeptidases, PfAPP and PfA-M1, to the food vacuole. These enzymes are able to generate amino acids that are then transported out of the food vacuole. Gene disruption studies revealed that PfAPP and PfA-M1 are required for efficient parasite proliferation, highlighting both enzymes as important drug targets (21). PfAPP is an aminopeptidase P homolog from the M24 family that hydrolyzes N-terminal amino acids from peptides containing a penultimate proline. PfA-M1 is a much less discriminatory enzyme from the M1 family, termed an aminopeptidase N homolog, that catalyzes the hydrolysis of amino acids from substrates with a wide variety of permitted residues in the P1 and P1' position (Schechter and Berger nomenclature).

An introduction to metalloaminopeptidases

Two particular aspects of function typically define proteases: the catalytic reaction mechanism employed for hydrolysis and general substrate specificity. Enzymes within a particular family may share the same reaction mechanism, but due to arrangement of active site architecture have a preference for cleaving within a peptide sequence as opposed to cleaving a single amino acid from either the N or C-terminus. PfAPP and PfA-M1 are both described as

metalloaminopeptidases; the two enzymes require the presence of a metal ion in the active site for efficient catalysis and act exclusively as exopeptidases upon the N-termini of substrates. Conserved active site scaffolds in these enzymes bind one or two metal ions (either in PfAPP but more commonly only one in PfA-M1) that are necessary for efficient catalysis. These metal ions can serve to activate the nucleophile of the reaction, coordinate substrates, or stabilize transition states. The dependence of activity on the metal ion varies between enzymes (even between individual homologs of the same protein) but requires at least the presence of one ion for full activity (22). The presence of these proteins in the acidic organelle of *P. falciparum* highlights a new location for the aminopeptidase P homolog and an uncommon environment for the M1 aminopeptidase.

The study of PfAPP and PfA-M1

In the chapters to follow, we will discuss the role of these two enzymes in hemoglobin catabolism in the malaria parasite. Chapters 2 and 3 detail the localization and biochemical characterization of aminopeptidase P and M1 aminopeptidase homologs, respectively. The preliminary results of a mutagenic study exploring a structurally important factor relating to substrate specificity in M1 aminopeptidases are presented in Chapter 4. This work as a whole offers insight into the characteristics of the two enzymes and necessary considerations for effective inhibitor and anti-malarial design.

REFERENCES

1. Snow, R. W., Guerra, C. A., Noor, A. M., Myint, H. Y., and Hay, S. I. (2005) *Nature* **434**, 214-217
2. Smith, D. L., McKenzie, F. E., Snow, R. W., and Hay, S. I. (2007) *PLoS Biol* **5**, e42
3. Greenwood, B. M., Fidock, D. A., Kyle, D. E., Kappe, S. H. I., Alonso, P. L., Collins, F. H., and Duffy, P. E. (2008) *The Journal of Clinical Investigation* **118**, 1266-1276
4. Vaughan, A. M., Wang, R., and Kappe, S. H. (2010) *Hum Vaccin* **6**
5. Takken, W., and Knols, B. G. J. (2009) *Trends in Parasitology* **25**, 101-104
6. Sherman, I. W. (2005) The Life of *Plasmodium*: an Overview. in *Molecular Approaches to Malaria* (Sherman, I. W. ed.), American Society for Microbiology, Washington, D.C. pp 3-11
7. Bannister, L. H., Margos, G. M., and Hopkins, J. M. (2005) Making a Home for *Plasmodium* Post-Genomics: Ultrastructural Organization of the Blood Stages. in *Molecular Approaches to Malaria* (Sherman, I. W. ed.), American Society for Microbiology, Washington, D.C. pp 24-49
8. Yeoh, S., O'Donnell, R. A., Koussis, K., Dluzewski, A. R., Ansell, K. H., Osborne, S. A., Hackett, F., Withers-Martinez, C., Mitchell, G. H., Bannister, L. H., Bryans, J. S., Kettleborough, C. A., and Blackman, M. J. (2007) **131**, 1072-1083
9. Koussis, K., Withers-Martinez, C., Yeoh, S., Child, M., Hackett, F., Knuepfer, E., Juliano, L., Woehlbier, U., Bujard, H., and Blackman, M. J. (2009) *EMBO J* **28**, 725-735
10. Boddey, J. A., Moritz, R. L., Simpson, R. J., and Cowman, A. F. (2009) *Traffic* **10**, 285-299
11. Klemba, M., and Goldberg, D. E. (2002) *Annual Review of Biochemistry* **71**, 275-305
12. Krugliak, M., Zhang, J., and Ginsburg, H. (2002) *Molecular and Biochemical Parasitology* **119**, 249-256
13. Allen, R. J. W., and Kirk, K. (2004) *Trends in Parasitology* **20**, 7-10
14. Lew, V. L., Tiffert, T., and Ginsburg, H. (2003) *Blood* **101**, 4189-4194
15. Rosenthal, P. J., and Meshnick, S. R. (1996) *Molecular and Biochemical Parasitology* **83**, 131-139

16. Rosenthal, P. J. (2005) Proteases and Hemoglobin Degradation. in *Molecular Approaches to Malaria* (Sherman, I. W. ed.), American Society for Microbiology, Washington, D.C. pp 311-326
17. Murata, C. E., and Goldberg, D. E. (2003) *Journal of Biological Chemistry* **278**, 38022-38028
18. Klemba, M., Gluzman, I., and Goldberg, D. E. (2004) *J. Biol. Chem.* **279**, 43000-43007
19. Kolakovich, K. A., Gluzman, I. Y., Duffin, K. L., and Goldberg, D. E. (1997) *Molecular and Biochemical Parasitology* **87**, 123-135
20. Gardner, M. J., Hall, N., Fung, E., White, O., Berriman, M., Hyman, R. W., Carlton, J. M., Pain, A., Nelson, K. E., Bowman, S., Paulsen, I. T., James, K., Eisen, J. A., Rutherford, K., Salzberg, S. L., Craig, A., Kyes, S., Chan, M.-S., Nene, V., Shallom, S. J., Suh, B., Peterson, J., Angiuoli, S., Pertea, M., Allen, J., Selengut, J., Haft, D., Mather, M. W., Vaidya, A. B., Martin, D. M. A., Fairlamb, A. H., Fraunholz, M. J., Roos, D. S., Ralph, S. A., McFadden, G. I., Cummings, L. M., Subramanian, G. M., Mungall, C., Venter, J. C., Carucci, D. J., Hoffman, S. L., Newbold, C., Davis, R. W., Fraser, C. M., and Barrell, B. (2002) *Nature* **419**, 498-511
21. Dalal, S., and Klemba, M. (2007) *Journal of Biological Chemistry* **282**, 35978-35987
22. Lowther, W. T., and Matthews, B. W. (2002) *Chem. Rev.* **102**, 4581-4608

Chapter 2

Evidence for catalytic roles for *Plasmodium falciparum* aminopeptidase P in the food vacuole and cytosol

Daniel Ragheb, Kristin Bompiani, Seema Dalal and Michael Klemba

Published in: *Journal of Biological Chemistry* 284: 24806-24815 (2009)

ABSTRACT

The metalloenzyme aminopeptidase P catalyzes the hydrolysis of amino acids from the N-termini of peptides with a prolyl residue in the second position. The human malaria parasite *Plasmodium falciparum* expresses a homolog of aminopeptidase P during its asexual intraerythrocytic cycle. *P. falciparum* aminopeptidase P (PfAPP) shares with mammalian cytosolic aminopeptidase P a three-domain, homodimeric organization and is most active with Mn(II) as the cofactor. A distinguishing feature of PfAPP is a 120-amino acid N-terminal extension that appears to be removed from the mature protein. PfAPP is present in the parasite's food vacuole and cytosol, a distribution that suggests roles in vacuolar hemoglobin catabolism and cytosolic peptide turnover. To evaluate the plausibility of these putative functions, the stability and kinetic properties of recombinant PfAPP were evaluated at the acidic pH of the food vacuole and at the near-neutral pH of the cytosol. PfAPP exhibited high stability at 37 °C in the pH range 5.0 to 7.5. In contrast, recombinant human cytosolic APP1 was unstable and formed a high molecular weight aggregate at acidic pH. At both acidic and slightly basic pH values, PfAPP efficiently hydrolyzed the amino terminal X-Pro bond of the nonapeptide bradykinin and of two globin pentapeptides that are potential *in vivo* substrates. These results provide support for roles for PfAPP in peptide catabolism in both the food vacuole and the cytosol and suggest that PfAPP has evolved a dual distribution in response to the metabolic needs of the intraerythrocytic parasite.

INTRODUCTION

Malaria remains one of the most deadly global infectious diseases with an estimated 500 million clinical cases and 2 million deaths annually (1,2). Clinical manifestations of the disease arise as the protozoan malaria parasite replicates asexually within human erythrocytes. Five species of the genus *Plasmodium* infect humans. The cytoadherent properties of red blood cells infected with *Plasmodium falciparum*, coupled with the parasite's ability to reach high parasitemia, make it the most virulent species. The emergence of strains of *P. falciparum* that are resistant to affordable anti-malarial drugs such as chloroquine has complicated efforts to manage malaria and new drugs are urgently needed.

Aminopeptidases catalyze the hydrolysis of amino acids from the N-termini of proteins and peptides. They participate in a wide range of biological processes including peptide catabolism, protein maturation, antigen presentation on immune cells, and regulation of hormone activity. During the malaria parasite's asexual erythrocytic replication cycle, aminopeptidases contribute to the catabolism of peptides generated by two major proteolytic pathways. One of these is initiated at the proteasome, a multi-functional protease that plays an important role in the turnover of ubiquitinated cellular proteins in the cytosol (3-5). In addition, the parasite transports host red blood cell cytosol (consisting primarily of hemoglobin) to an acidic degradative organelle, the food vacuole, where it is degraded in a proteasome-independent pathway (6,7). As up to 75% of the host cell hemoglobin is catabolized during the parasite's intraerythrocytic cycle (8,9), flux through the vacuolar pathway is substantial. Three aminopeptidases have been identified as key players in recycling amino acids from peptides generated by the proteasomal and vacuolar catabolic pathways: leucine aminopeptidase (PfLAP), aminopeptidase N (PfA-M1) and aminopeptidase P (10-14). The latter two enzymes have been found in the parasite's food vacuole and therefore may play a direct role in hemoglobin catabolism (11). An aspartyl aminopeptidase is also expressed in asexual stage parasites and hydrolyzes N-terminal aspartyl and glutamyl substrates (15); however, disruption of its gene does not prevent efficient intraerythrocytic replication (11).

Aminopeptidase P (APP) homologs exhibit high specificity for proline in the second position of the substrate (the P1' position in the nomenclature of Schechter and Berger (16)) and catalyze the hydrolysis of the X-Pro amide bond, where X is any aminoacyl residue (17). Because of the cyclic nature of the proline sidechain, X-Pro-containing peptides are not easily

accommodated in the active sites of broad-specificity aminopeptidases (17). In mammals, three APP isozymes have been identified. APP1 is found in the cytosolic fraction of cell lysates and has been characterized from a variety of tissues (18-20). Although this enzyme has not, to our knowledge, been localized in intact cells, the apparent lack of specific targeting information is consistent with a role in cytosolic peptide turnover. Active cytosolic forms of APP have been reported in plants (21), fruit flies (22), the microsporidian parasite *Encephalitozoon cuniculi* (23) and in intestinal cells in *Ceanorhabditis elegans* (24), where is it believed to play a role in the catabolism of peptides produced from ingested bacteria. Mammalian APP2 is a glycosylated ectoenzyme anchored into the membrane of endothelial and epithelial cells with a glycosylphosphotidylinositol attachment (25). The best characterized role of APP2 is the inactivation of the plasma hormone bradykinin, a nonapeptide, through cleavage of the Arg-Pro amino terminal peptide bond (26,27). Inhibition of APP2 potentiates the vasodilatory and cardioprotective properties of bradykinin and APP2 has been considered a target for the development of cardiovascular drugs (28-30). A third isoform, APP3, has been identified in the human genome and may be a mitochondrial enzyme but has not yet been characterized (31). Prokaryotic APP homologs contribute to intracellular peptide turnover (32).

P. falciparum aminopeptidase P (PfAPP) appears to be important for intraerythrocytic growth, as parasites with a disrupted PfAPP gene could not be isolated (11). We have previously localized a PfAPP-yellow fluorescent protein fusion to the food vacuole and the cytosol of the parasite (11). The cytosolic pool of PfAPP probably fulfills a role in peptide turnover and amino acid recycling that is orthologous to those of the cytosolic enzymes described above. In contrast, there is no report to our knowledge of an aminopeptidase P homolog functioning in an acidic environment akin to the malarial food vacuole. Moreover, characterization of mammalian aminopeptidase P homologs typically reveals a pH optimum of 7 to 8 with relatively little, if any, activity in the pH range 5.0 to 5.5 (18-20). Although we have previously detected PfAPP activity at acidic pH (11), the catalytic efficiency of the enzyme has not been characterized. Thus, at the outset of this study it was not clear whether PfAPP has a significant catalytic role in the food vacuole.

Here, we have localized untagged, native PfAPP in the parasite and have confirmed the dual cytosolic/vacuolar distribution of the enzyme. The domain organization, quaternary structure and metal requirement of PfAPP were characterized. To evaluate the plausibility of a

catalytic role for PfAPP at acidic and near-neutral pH, its stability in the pH range 5.0 to 7.5 was assessed and compared to that of human cytosolic APP1, an enzyme that does not, to our knowledge, have a physiological role in an acidic environment. The catalytic efficiency of PfAPP at a range of pH values was characterized with three X-Pro-containing peptides, two of which are found in the sequences of human a- and b-globin and therefore represent potentially physiological substrates.

EXPERIMENTAL PROCEDURES

Parasite culture and isolation

P. falciparum clone 3D7 parasites were cultured in human O^+ erythrocytes (Interstate Blood Bank) in RPMI 1640 medium supplemented with 27 mM sodium bicarbonate, 11 mM glucose, 0.37 mM hypoxanthine, 10 mg/mL gentamicin and 5 g/L Albumax I (Invitrogen). Cultures were synchronized by sorbitol treatment (33). Parasites used for immunoblotting and gel filtration chromatography were isolated from intact red blood cells by treatment with 1 mg/mL saponin (34).

Recombinant protein expression and purification

DNA coding for residues 129-777 of *P. falciparum* aminopeptidase P (gene ID PF14_0517) was amplified by PCR from clone 3D7 genomic DNA using the forward primer 5'-GCACGGGATCC*CGAAAACCTGTATTTTCAGAGC*GATAATAATCCTGCTGCTAGATTAG and the reverse primer 5'-GCACGAAGCTTTTAATTGTTATGAATCGCAATTGGTTC. PCR products were digested with BamH1 and HindIII (underlined) and ligated into the same sites in the T7 expression vector pET45b (Novagen). The sequence encoding full-length human cytosolic aminopeptidase P1 (XPNPEP1) was amplified from a plasmid containing a cDNA from an ovarian adenocarcinoma cell line (Mammalian Gene Collection-10592, American Type Tissue Collection) with primers 5'-GCACGGGTACC*GAAAACCTGTATTTTCAGAGC*ATGCCTCCAAAGGTGACTTCAGAG and 3'- GCACGAAGCTTTTAATGCTGTTTGGAGATGGGTTGC and was cloned into the KpnI and HindIII sites of pET45b. Both aminopeptidase sequences were in frame with a vector-encoded N-terminal hexahistidine tag and a primer-encoded tobacco etch virus (TEV) protease

cleavage site ENLYFQS ((35); italicized sequence in the 5'-primers). Coding sequences were verified by DNA sequencing.

E. coli BL21(DE3) Rosetta 2 cells (Novagen) containing the PfAPP or hAPP1 expression plasmid were grown to an optical density at 600 nm of 0.8 and protein expression was induced by adding 1 mM isopropyl b-D-thiogalactopyranoside for 3 h at 37 °C (PfAPP) or 25 °C (hAPP1). Cell pellets were resuspended in immobilized metal affinity chromatography (IMAC) buffer (20 mM NaH_2PO_4 pH 7.4, 500 mM NaCl, 30 mM imidazole) supplemented with 1 mM 4-(2-aminoethyl)benzenesulfonyl fluoride and 1 mg/mL hen egg white lysozyme and were incubated on ice for 30 minutes. After sonication, the lysate was clarified by centrifugation at 20,000 g for 15 minutes at 4 °C. Protamine sulfate was added to the supernatant at 16 mg per gram of cell pellet wet weight. The mixture was stirred on ice for 15 minutes and the precipitated material was removed by centrifugation as above. The clarified lysate was loaded onto a Ni^{2+}-charged HisTrap column (GE Biosciences) equilibrated in IMAC buffer and the column was washed thoroughly. Bound protein was eluted with a linear gradient from 30 – 500 mM imidazole in IMAC buffer. Active fractions were dialyzed into 50 mM Tris-HCl pH 7.5, 200 mM NaCl at 4 °C. To remove the hexahistidine tag, protein was incubated with His-tagged TEV protease (expressed and purified as described (36)) at an aminopeptidase:TEV protease molar ratio of 10:1 (PfAPP) or 30:1 (hAPP1) in 50 mM Tris-HCl pH 8.0 overnight at 4 °C. The cleavage mixture was passed over a Ni^{2+}-charged HisTrap column and the TEV protease-cleaved protein eluting in the flow-through was dialyzed into 50 mM Tris-HCl pH 7.5, 200 mM NaCl at 4 °C and then concentrated in an Ultra-4 centrifugal device (Amicon). The protein was injected onto a Superdex 200 10/30 gel filtration column (GE Healthcare) equilibrated in 50 mM Tris-HCl pH 7.5, 200 mM NaCl. For PfAPP, the major (dimer) peak was collected, concentrated and repurified on the Superdex column. Purified protein was supplemented with 1 mM $MnCl_2$, snap frozen in liquid nitrogen and stored at -80 °C. Protein concentrations were determined by absorbance at 280 nm using extinction coefficients of 62,370 $M^{-1}cm^{-1}$ (PfAPP) and 104,280 $M^{-1}cm^{-1}$ (hAPP1), which were calculated from the amino acid sequences using the ProtParam tool on the Expasy website (ca.expasy.org).

Native and recombinant PfAPP quaternary structure

Approximately 10^9 trophozoite-stage, saponin-treated parasites were suspended in 50 mM Tris-HCl pH 7.5, 200 mM NaCl containing 1 μM *N-(trans*-epoxysuccinyl)-L-leucine 4-guanidinobutylamide, 1 μM pepstatin, and 0.5 mM 4-(2-aminoethyl)benzenesulfonyl fluoride. After sonication, the lysate was clarified by centrifugation at 100,000 *g* for 60 minutes at 4°C. The supernatant was injected onto a Superdex 200 10/300 column equilibrated in 50 mM Tris-HCl pH 7.5, 200 mM NaCl. PfAPP activity in eluted fractions was determined using the fluorogenic substrate (*N*-2-aminobenzoyl)-lysyl-prolyl-proline-4-nitroanilide (Lys(Abz)-Pro-Pro-NA; see "Enzyme assays and kinetic analysis"). 90 μg of purified recombinant PfAPP was injected onto the gel filtration column and assayed in the same fashion. The molecular mass of PfAPP was estimated from a calibration curve generated with ferretin (440 kDa), catalase (232 kDa), aldolase (158 kDa), albumin (67 kDa), ovalbumin (43 kDa), chymotrypsinogen A (25 kDa) and ribonuclease A (14 kDa). The void volume was estimated with blue dextran 2000.

Antibodies and immunoblotting

Anti-PfAPP sera were produced in rabbits using IMAC-purified recombinant PfAPP as the immunogen (Cocalico Biologicals). Serum VP167 was used in all experiments presented here. This serum was diluted 1:10,000 in immunoblotting experiments. Signal was detected by chemiluminescence using a horse radish peroxidase-conjugated anti-rabbit secondary antibody and the ECL kit (GE Biosciences) and was detected on film.

Immunofluorescence and cryo-immunoelectron microscopy

For immunofluorescence assays, clone 3D7 parasites were fixed in suspension with 4% paraformaldehyde and 0.0075% glutaraldehyde, permeabilized and blocked as previously described (37). Fixed parasitized erythrocytes were incubated with anti-PfAPP serum or pre-immune serum (1:2,700 dilution) for 1 hour at room temperature, washed, and incubated with an Alexa 594-conjugated anti-rabbit secondary antibody (Invitrogen). Cells were allowed to settle onto polyethylenimine-coated cover slips and were mounted with ProLong Gold (Invitrogen). Images were collected on a Zeiss AxioImager M1 equipped with an MRm Axiocam digital camera using a 100x/1.4NA objective lens. Images were converted to TIF files and contrast was adjusted using Adobe Photoshop CS2. Pixel intensity profiles were generated with AxioVision

software (release 4.5; Zeiss). Immunoelectron microscopy was carried out at the Molecular Microbiology Imaging Facility, Washington University, St. Louis, MO. Parasitized erythrocytes were fixed with 4% paraformaldehyde and 0.1% glutaraldehyde and were labeled with anti-PfAPP serum (1:2,500 dilution) as previously described (38).

Generation of apoenzyme and metal reconstitution

PfAPP was dialyzed against 50 mM Tris-HCl pH 7.5, 200 mM NaCl, 1 mM ethylenediaminetetraacetic acid (EDTA) for 2 hours at 4 °C to chelate metal ions and then against two changes of 50 mM Tris-HCl pH 7.5, 200 mM NaCl overnight at 4 °C to remove EDTA. Dialyzed PfAPP was incubated for 30 minutes at 37 °C without metal or in the presence of 1 mM $MnCl_2$, $MgCl_2$, $ZnCl_2$, $CoCl_2$, $NiCl_2$ or $CuCl_2$. Activity was measured at 37 °C against the fluorogenic substrate Lys(Abz)-Pro-Pro-NA (see "Enzyme assays and kinetic analysis"). The effect of manganese concentration on PfAPP activity was determined with 1 mM bradykinin in 50 mM Tris-HCl pH 7.5, 200 mM NaCl and 0 – 4 mM $MnCl_2$. Rates of cleavage were determined as described in "Enzyme assays and kinetic analysis". Less than 10% of substrate was converted to product in these assays.

Assay of enzyme stability

PfAPP (730 ng) or hAPP1 (7.5 mg) was diluted from a concentrated stock solution into 100 mM buffer (Tris-HCl pH 7.5, Bis-Tris-HCl pH 6.5, sodium succinate pH 5.5 or sodium succinate pH 5.0), 1 mM $MnCl_2$ and 100 mg/mL bovine serum albumin (BSA) to a final volume of 100 mL. Immediately after mixing and at 10-minute intervals thereafter, a 2 mL aliquot was transferred to 98 mL of 100 mM Tris-HCl pH 7.5, 1 mM $MnCl_2$ and 100 mg/mL BSA on ice. Residual activity was assayed by warming to 37 °C and adding 300 mM Lys(Abz)-Pro-Pro-NA. Human APP1 activity data were fit to the exponential decay equation $y = a + be^{-cx}$ in Kaleidagraph 4.0. To assess oligomerization state as a function of pH, hAPP (50 μg) or PfAPP (15 μg) were diluted into 50 mM sodium succinate pH 5.5 or 50 mM Tris-HCl pH 7.5 supplemented with 200 mM NaCl and 1 mM $MnCl_2$ and then dialyzed against the same buffer for 3 hours at 8 °C. Dialyzed samples were incubated at 37°C for 30 minutes and transferred to ice. Quaternary structure was analyzed on a Superdex 200 column equilibrated in the same buffer as was used for dialysis.

Enzyme assays and kinetic analysis

Routine PfAPP or hAPP1 assays were carried out using the quenched fluorogenic substrate Lys(Abz)-Pro-Pro-NA ((39); Bachem) at 100 mM (unless otherwise stated) in 50 mM Tris-HCl pH 7.5, 1 mM $MnCl_2$. Assays were read in microplates at 37 °C using a Victor^3 fluorometer (PerkinElmer) with excitation and emission wavelengths of 340 and 430 nm, respectively.

PfAPP-catalyzed hydrolysis of the peptide substrates bradykinin (Bachem) and HbPep1 and HbPep2 (custom synthesized at >95% purity by EZBiolab) was monitored using a high-pressure liquid chromatography (HPLC)-based assay (40). PfAPP (4 to 73 ng) was incubated in 100 mM buffer (Tris-HCl pH 7.5, Bis-Tris-HCl pH 6.5, sodium succinate pH 5.5, or MES pH 5.5), 1 mM $MnCl_2$, and a range of substrate concentrations at 37°C for 30 minutes. Reactions were stopped by adding 10 mL glacial acetic acid and were injected onto a Prevail C18 column (5 mm particle size, 250 x 4.6 mm; Alltech) equilibrated in 4% acetonitrile/0.08% phosphoric acid. Substrate and product were resolved with a linear gradient from 20 to 45% acetonitrile in 0.08% phosphoric acid and were detected by absorbance at 214 nm. Product concentrations were calculated by relating peak area to that of a known quantity of bradykinin$_{2\text{-}9}$ (Bachem) or of HbPep1 or HbPep2 that had been quantitatively converted to product by incubation with PfAPP. The amount of enzyme used depended on the substrate and pH and was adjusted so that less than 10% of substrate was converted to product. Kinetic parameters were obtained by non-linear regression fit to the Michaelis-Menten equation

$$v = \frac{[E]_o[S]k_{cat}}{K_m + [S]}$$

where v is the initial rate, $[E]_o$ is the enzyme concentration, and [S] is the substrate concentration, using Kaleidagraph 4.0. Where substrate inhibition was observed, the data were fit by non-linear regression to an equation for uncompetitive substrate inhibition

$$v = \frac{[E]_o[S]k_{cat}}{K_m + [S] + [S]^2/K_{si}},$$

where K_{si} is the inhibition constant (41).

Mass spectrometry

PfAPP-catalyzed hydrolysis products were purified by HPLC using the conditions described in "Enzyme assays and kinetic analysis" but with phosphoric acid in the mobile phase replaced with 0.1% formic acid. Samples were dried under vacuum and resuspended in 10 mL of 50% acetonitrile, 0.1% trifluoroacetic acid, 0.2% formic acid in a sonicating water bath for 5 minutes. Samples were mixed 1:1 with matrix solution (20 mg/ml 2,5-dihydroxybenzoic acid in 50% acetonitrile, 0.1% trifluoroacetic acid, 1% phosphoric acid) and one microliter of the mix was spotted onto a MALDI target plate and allowed to air dry. Data were collected in positive reflectron mode using an Applied Biosystems 4800 MALDI TOF/TOF.

RESULTS

Distribution of aminopeptidase P in protozoa

A single-exon gene (PF14_0517) on chromosome 14 of *P. falciparum* encodes a 777-amino acid homolog of aminopeptidase P (termed PfAPP). Single putative orthologs of PfAPP were found in the genome sequences of mammalian and avian *Plasmodium* species (*P. vivax*, *P. knowlesi*, *P. berghei* and *P. gallinaceum* [incomplete fragment]) as well as in other apicomplexans for which high-quality genome sequence was available (*Toxoplasma gondii*, *Neospora caninum*, *Cryptosporidium hominis* and *Theileria parva*; Supplemental Table 2-S1). A BLAST search of protozoan genomes using the catalytic domain of PfAPP as a query sequence revealed the presence of putative APP homologs in the genomes of the trypanosomatids *Trypanosoma cruzi*, *T. brucei* and *Leishmania major* as well as in *Dictyostelium discoidin* and *Tetrahymena thermophila*. APP homologs were not found in the genome sequences of *Giardia lamblia* and *Trichomonas vaginalis*; however, our search turned up multiple putative prolidase homologs (X-Pro dipeptidase; Supplemental Table 2-S1). Prolidase is related to APP and hydrolyzes an amino terminal X-Pro amide bond; however, unlike APP, prolidase only accepts dipeptide substrates. These results indicate that APP is present in all apicomplexan species examined and is widely, but perhaps not universally, distributed among protozoa. It does appear, however, that the ability to catalyze the hydrolysis of an amino-terminal X-Pro bond is encoded in all protozoan genomes examined (either as APP or prolidase or both) and may therefore be an essential metabolic activity.

Localization of native PfAPP

We have previously shown that endogenous PfAPP tagged with yellow fluorescent protein (YFP) exhibits a bipartite distribution in the parasite's food vacuole and cytosol (11). To confirm that this unusual distribution occurs in the absence of the YFP tag, native PfAPP was localized in aldehyde-fixed parasites using antibodies raised against recombinant PfAPP. In indirect immunofluorescence experiments, an anti-PfAPP serum strongly labeled the parasite's food vacuole with somewhat weaker labeling of the cytosol (Fig. 2-1A). A similar vacuolar/cytosolic pattern of anti-PfAPP/immunogold labeling was observed by cryo-electron microscopy (Fig. 2-1B). The distribution of gold particles in the food vacuole (70, 79% of total) and outside of the food vacuole but within the parasite (19, 21% of total) in Fig. 2-1B agrees well in a qualitative sense with the relative vacuolar and cytosolic fluorescence intensities in Fig. 2-1A. In both experiments, no labeling was observed with pre-immune serum. These results are in accord with the previously reported distribution of PfAPP-YFP (11) and confirm the presence of vacuolar and cytosolic pools of PfAPP in the parasite.

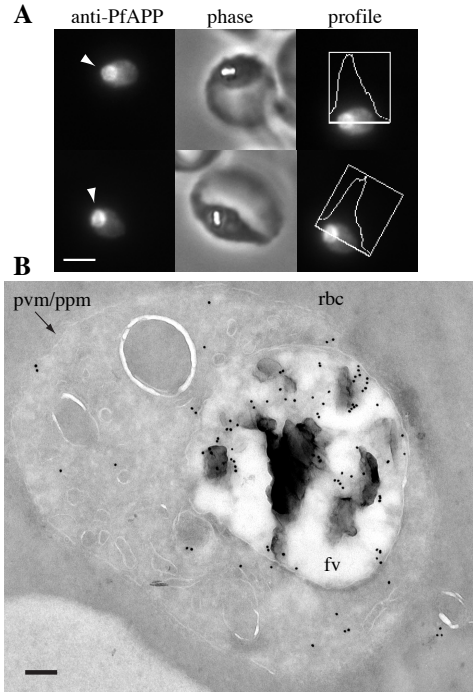

Figure 2-1: Localization of native PfAPP. (A) Indirect immunofluorescence localization of PfAPP in aldehyde-fixed trophozoite-stage parasites. Left column: anti-PfAPP associated fluorescence; middle column, phase contrast image; right column, relative fluorescence intensity along a line bisecting the parasite. The food vacuole is indicated by an arrowhead. Bar, 2 mm. (B) Localization of PfAPP by cryo-immunoelectron microscopy. rbc, red blood cell; fv, food vacuole; pvm/ppm, parasitophorous vacuole membrane/parasite plasma membrane. Bar, 200 nm.

Characterization of native PfAPP

Although mammalian APP1 and *E. coli* APP catalyze the same reaction, they differ in the number of domains and in quaternary structure. *E. coli* APP possesses two domains: a C-terminal catalytic domain and smaller N-terminal domain that contributes to the formation of the tetrameric quaternary structure (42). In human APP1 (hAPP1), which forms a dimer, two domains (I and II) precede the C-terminal catalytic domain (III). Domains I and II share sequence similarity and both are structurally similar to the N-terminal domain of *E. coli* APP (43). Alignment of PfAPP with hAPP1 and with predicted sequences from other apicomplexan genomes reveals that the apicomplexan enzymes contain the three-domain organization of hAPP1 rather than the two-domain structure of prokaryotic APP (Supplemental Figure 2-S1). The alignment also reveals in PfAPP an N-terminal extension of 120 amino acids relative to the start of hAPP1 that is not present in the other apicomplexan homologs (Supplemental Figure 2-S1). Analysis of the first 70 residues of this N-terminal extension with the signal peptide prediction algorithm SignalP 3.0 (44) reveals a putative signal peptide from residues 5 to 16 (Supplemental Table 2-S1 and Figure 2-S1). No signal peptide was detected in any of the apicomplexan homologs (Supplemental Table 2-S1). Possible roles for the PfAPP N-terminal extension are discussed in the "Discussion".

To characterize native PfAPP, polyclonal antibodies against recombinant enzyme (see "Expression of recombinant proteins") were raised in two rabbits. Both anti-PfAPP sera (but not the pre-immune sera) recognized a single major band with a molecular mass of approximately 73 kDa in an extract of trophozoite- and schizont-stage parasites (Fig. 2-2A and data not shown). Minor species at around 90 and 55 kDa were also apparent. To determine which of these bands corresponds to active PfAPP, an extract of soluble trophozoite-stage proteins was fractionated on a gel filtration column and PfAPP activity was quantified (Fig. 2-2B). PfAPP eluted in a single peak with an apparent molecular weight of 157 kDa. Anti-PfAPP immunoblotting of active fractions revealed that both the major 73 kDa and the minor 55 kDa species co-migrated with activity (Fig. 2-2C). Native PfAPP is therefore a homodimer if a monomer molecular mass of 73 kDa is assumed. It appears from these data that full length PfAPP, with a predicted molecular mass of 90 kDa, is processed into a 73 kDa mature form, likely through removal of the N-terminal extension. The 55 kDa species, which migrates with active, dimeric PfAPP, probably represents a minor fraction of mature PfAPP that has been proteolytically clipped at an internal

site. Consistent with this idea, we observe a 20 kDa band on overexposed immunoblots that likely represents the second proteolytic fragment.

The dimer interface of hAPP1 is dominated by hydrophobic interactions between the catalytic domains (domain III) of the monomers (43). Of the 11 residues identified in the hydrophobic interface, seven are conserved in hydrophobic character in PfAPP (Supplemental Table 2-S2). The four that are not conserved in PfAPP lie at the edge of the interface and are likely able to reposition their polar sidechains to interact with bulk solvent. We propose that PfAPP, like hAPP1, forms a homodimer through interaction of two catalytic domains.

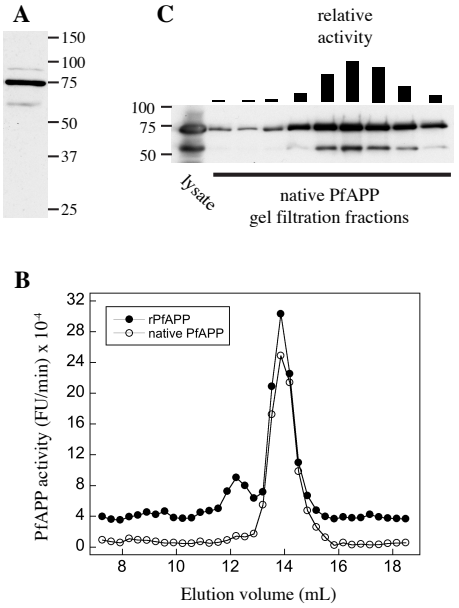

Figure 2-2: Polypeptide size and quaternary structure of PfAPP. (A) Anti-PfAPP immunoblot of an SDS extract of trophozoite- and schizont-stage parasites. A single major 73 kDa species and minor species of 90 and 55 kDa are observed. The sizes of markers are indicated at right. (B) Gel filtration elution profiles of native (open circles) and recombinant (filled circles) PfAPP. The profiles have been offset slightly for clarity. (C) Anti-PfAPP immunoblot of selected gel filtration fractions from the native PfAPP profile in (B). The relative activity of each fraction is indicated with a bar at the top. In the far left lane is the clarified parasite lysate that was injected onto the column. Sizes of markers are indicated at left.

Expression of recombinant proteins

To characterize in detail the enzymatic properties of PfAPP, we expressed it in *Escherichia coli*. As the major form of the enzyme in parasites appears to lack the N-terminal extension, we expressed an N-terminally truncated form of PfAPP (residues 129-777). The

recombinant protein, termed rPfAPP, carried an amino-terminal hexahistidine tag with a tobacco etch virus (TEV) protease recognition sequence between the tag and rPfAPP. After purification and cleavage of the His_6 tag with TEV protease (Fig. 2-3A), rPfAPP had a nearly identical mobility on a sodium dodecyl sulfate (SDS)-polyacrylamide gel to that of native PfAPP (Fig.2-3B). When analyzed by gel filtration chromatography, the major peak of rPfAPP activity co-eluted with that of dimeric native PfAPP (Fig. 2-2B). An active, minor peak (estimated ~20% of total activity) that might represent a dimer of dimers (4.9 polypeptides based on a monomer mass of 73 kDa) was observed. This species appeared to be in equilibrium with the dimeric species, as it could not be depleted by purifying the major (dimer) peak. Human APP1 (residues 1-623) was purified in a similar fashion (Fig. 2-3C) and migrated on a gel filtration column as expected for a dimeric species (data not shown).

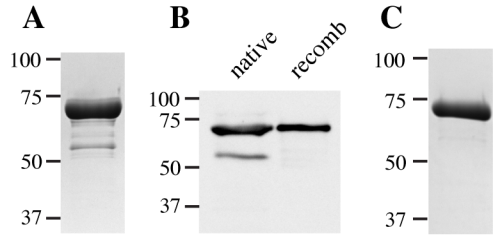

Figure 2-3: **Recombinant PfAPP and hAPP1.** (A) Coomassie-stained polyacrylamide gel of purified recombinant PfAPP (6 μg). Several minor species reproducibly co-migrate with purified rPfAPP, the identities of which are not known. (B) Anti-PfAPP immunoblot comparing the polyacrylamide gel mobilities of SDS-denatured native and recombinant PfAPP ("recomb"). (C) Coomassie-stained polyacrylamide gel of purified recombinant hAPP1 (5 μg). In all panels, the sizes of markers are indicated at the left.

Effect of metal ions on rPfAPP activity

Metal ions in the active site of aminopeptidase P play a key role in catalysis by polarizing a bound water molecule and facilitating deprotonation to the nucleophilic hydroxide species (42). In the x-ray crystal structures of *E. coli* APP and hAPP1, two Mn^{2+} ions are bound in the active site by one histidine, two glutamate and two aspartate ligands (43,45). In contrast, pig kidney APP2 has been reported to contain one molar equivalent of Zn^{2+} (46). To assess the metal requirement of PfAPP, the enzyme was dialyzed against 1 mM EDTA. After this treatment, activity decreased over 80% (Fig. 2-4A); residual activity was probably due to incomplete removal of active site metal ions. Following removal of EDTA, re-activation of the enzyme was attempted by addition of various bivalent cations. Addition of 1 mM Mn^{2+} resulted in a return to

the control (undialyzed) level of activity (Fig. 2-4A). Co^{2+} partially activated the enzyme whereas Mg^{2+} had no effect and Zn^{2+}, Ni^{2+} and Cu^{2+} were inhibitory at 1 mM. These data are consistent with a role for Mn^{2+} rather than Zn^{2+} in the active site of PfAPP.

To examine the relationship between Mn^{2+} concentration and activity against a peptide substrate, rates of PfAPP catalysis of bradykinin hydrolysis were determined at exogenous Mn^{2+} concentrations ranging from 0 – 4 mM (Fig. 2-4B). Low millimolar levels of Mn^{2+} resulted in a three- to four-fold increase in PfAPP activity. Similar levels of activation in the presence of millimolar concentrations of Mn^{2+} have been observed with mammalian cytosolic APP1 (18-20,47,48). Exogenous Mn^{2+} may stimulate activity by promoting occupation of the low-affinity Mn^{2+} site in the enzyme's active site (see "Discussion"). For this reason, we routinely added 1 mM $MnCl_2$ to PfAPP assays.

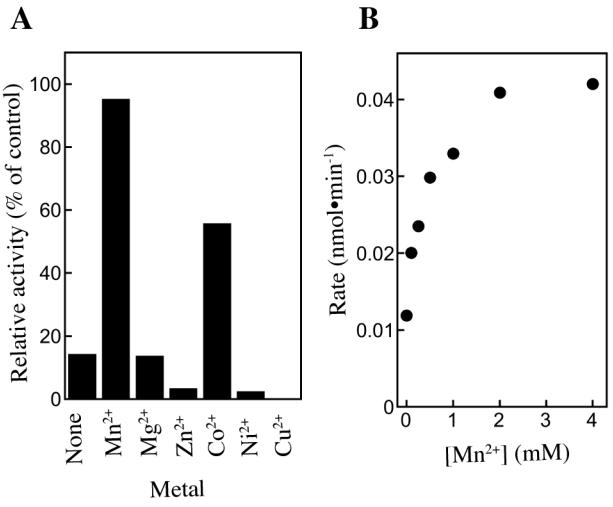

Figure 2-4: Recombinant PfAPP is maximally active in the presence of manganese(II) ions. (A) Re-activation of apo-rPfAPP by various metal ions. Apo-rPfAPP was generated by dialysis against EDTA. After removal of excess EDTA, rPfAPP activity against Lys(Abz)-Pro-Pro-NA was determined in the absence of exogenous metal (None) or in the presence of 1 mM concentrations of various metal ions (indicated below the bars). Data are expressed as the percentage activity compared to an undialyzed sample of rPfAPP (in the presence of 1 mM $MnCl_2$) and are the average of triplicate assays. (B) Effect of exogenous $MnCl_2$ concentration on rates of bradykinin cleavage by rPfAPP. Data points are from duplicate assays.

Stability of rPfAPP and hAPP1

pH can be an important factor in the stability of an enzyme's activity over time. A pH of 7.2 has been reported for the *P. falciparum* cytosol (49) and published values for the food vacuole have ranged from 4.5 to 5.8 with most determinations falling within the range 5.0 to 5.5

(49-53). To assess the functional potential of PfAPP in both cellular compartments, we measured the stability of PfAPP activity at 37 °C over 1 hour at pH values ranging from 5.0 to 7.5. As metalloenzymes are often stabilized in the presence of metal ligand, we included 1 mM $MnCl_2$ in the assay. In addition, bovine serum albumin was added at 100 mg/mL to prevent non-specific adsorption of the enzyme to surfaces following dilution into the activity assay. At pH 7.5 and 6.5, no loss of activity was observed over the course of the 60 minute incubation (Fig. 2-5A). At pH 5.5 and 5.0, PfAPP activity was only slightly less stable, with about 80% retention of activity after 60 minutes.

To determine whether stability in the pH range of 5.0 – 7.5 is a property intrinsic to aminopeptidase P enzymes, we evaluated the stability of recombinant hAPP1. Human APP1 was chosen for this comparison because it shares with PfAPP a three-domain organization, a dimeric quaternary structure, and high activity with Mn(II) in the active site; however, unlike PfAPP, hAPP1 is not known to function in an acidic environment. In marked contrast with PfAPP, hAPP1 rapidly lost activity at pH 5.5 with only 30% of initial activity present after a 10 minute incubation (Fig. 2-5B). At all pH values examined, loss of activity appeared to be a biphasic process having an initial exponential phase (Fig. 2-5B). At pH 5.5, over 90% of initial activity was lost in the exponential phase, during which enzyme activity decayed with a half-time of 6 minutes. Stability of activity at pH 5.5 was not affected by the buffer in the assay: succinate, citrate and MES yielded similar results. Likewise, addition of 10% glycerol to the assay or substitution of BSA with 0.1% Triton X-100 did not enhance hAPP1 stability at pH 5.5. It has been reported that hAPP1 purified from *E. coli* cells grown in standard Luria-Bertini broth has sub-stoichiometric levels of Mn^{2+} and, in addition, contains substantial amounts of the presumed non-physiological metals Mg^{2+} and Fe^{2+} (43). To assess whether inappropriate or incomplete occupancy of the metal-binding sites of hAPP1 could explain its low stability at acidic pH, we i) dialyzed hAPP1 against 1 mM $MnCl_2$ overnight and ii) purified hAPP1 from cells grown in medium containing 1 mM $MnCl_2$, a condition which was shown to yield nearly full Mn^{2+} occupancy of the divalent metal active site (43). In neither case was enzyme stability enhanced at pH 5.5.

Li *et al* have shown that mutation of a tryptophan residue in the hAPP1 dimer interface to glutamate (W477E) results in a monomeric protein (43). The W477E mutant exhibited less than 10% of wild-type activity, which suggests that monomeric hAPP1 has weak, if any, activity. We

speculated that dimer instability of hAPP1 at acidic pH might be the reason for the inactivation observed in Fig. 2-5B. To test this idea, we dialyzed hAPP1 into pH 5.5 or pH 7.5 buffer (including in both cases 1 mM $MnCl_2$ and 200 mM NaCl), incubated the dialyzed enzyme at 37 °C for 30 minutes, and assessed the oligomerization state at each pH by gel filtration (Fig. 2-5C). At pH 7.5, hAPP1 had the expected dimeric quaternary structure (43). At pH 5.5, a dramatic alteration of hAPP1 structure occurred such that the protein eluted as a high molecular weight aggregate in the column void volume, with no apparent dimeric or monomeric protein. It appears that the aggregate consisted mainly of inactive enzyme, as the activity of hAPP1 following dialysis and incubation at pH 5.5 was only 8% of that in the pH 7.5 control .

When the same experiment was conducted with rPfAPP, the results were very different (Fig. 2-5C). At both pH 7.5 and 5.5, the dimeric species was the major form of the enzyme. At pH 5.5, a minor, broad peak appeared at lower elution volume (centered at 10 mL in the right panel of Fig. 2-5C), which suggested the formation of a small amount of aggregate at acidic pH. At both pH 7.5 and 5.5, a small fraction of rPfAPP eluted in the void volume; however, the size of this peak did not vary with pH. Together, our data point to a substantial difference in the stabilities of PfAPP and hAPP1 at acidic pH.

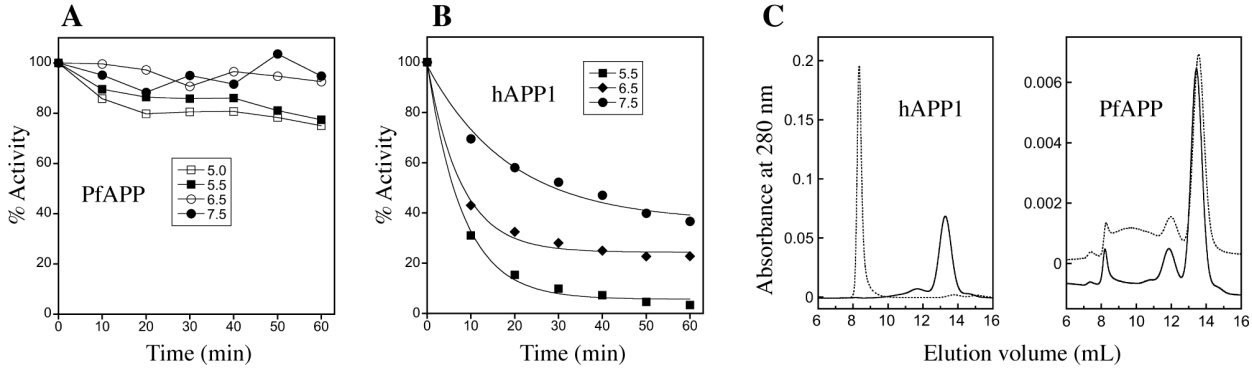

Figure 2-5: Effect of pH on the stability of PfAPP and hAPP1. rPfAPP (A) or hAPP1 (B) were incubated at pH values ranging from 5.0 to 7.5 (rPfAPP) or 5.5 to 7.5 (hAPP1). Immediately after addition of enzyme (time= 0) and at 10 minute intervals thereafter, aliquots were removed to ice with simultaneous adjustment of the pH to 7.5. Percent activity is reported relative to the activity at the initial time point. Each data point is the average of two independent experiments. In (B), the first phase of the biphasic loss of activity was fit to an exponential decay curve. (C) Gel filtration profiles of hAPP1 (left panel) and rPfAPP (right panel) after dialysis for 3 hours and then incubation at 37 °C for 30 minutes at pH 5.5 (dashed line) or pH 7.5 (solid line). The void volume of the column is 8.2 mL. Based on the elution volumes of a set of reference proteins, the predicted elution volumes for dimeric and monomeric rPfAPP are 13.5 and 14.8 mL, respectively, and for dimeric and monomeric hAPP1 are 13.7 and 14.9 mL, respectively.

pH dependence of rPfAPP catalysis

If the notion of catalytic roles for PfAPP in the food vacuole and cytosol is to be plausible, the enzyme must not only be stable but must also function as an efficient catalyst at acidic and near-neutral pH. We determined the pH dependence of the kinetic parameters for the PfAPP-catalyzed hydrolysis of three peptide substrates having an X-Pro amino-terminal sequence. The first peptide we analyzed was the nonapeptide hormone bradykinin (RPPGFSPFR), a physiological substrate of mammalian APP2. Although this peptide is almost certainly not a physiological substrate of PfAPP, it has been used to characterize the properties of both eukaryotic and prokaryotic APP homologs and therefore serves as a point of comparison between homologs. Plots of initial rate against substrate concentration for rPfAPP-catalyzed hydrolysis of bradykinin at pH 7.5, 6.5 and 5.5 fit well to the Michaelis-Menten equation (Supplemental Figure 2-S2). Kinetic constants for hydrolysis of bradykinin by rPfAPP and by mammalian APP1 and APP2 and *E. coli* APP are compiled in Table 2-1. At pH 7.5 and 6.5, the catalytic constants (K_m, k_{cat} and k_{cat}/K_m) of rPfAPP are similar to those of eukaryotic and prokaryotic homologs. One difference that stands out is the substantially lower K_m for hydrolysis of bradykinin by rat APP2; this difference is probably attributable to the fact that bradykinin is a physiological substrate of APP2 but not of PfAPP. As the pH of the reaction is lowered to 5.5 both K_m and the k_{cat} for rPfAPP hydrolysis increase significantly (48-fold and 10-fold increases from pH 7.5 to 5.5, respectively). The net result is that the catalytic efficiency (k_{cat}/K_m) at pH 5.5 is 5-fold lower than at pH 7.5.

Table 2-1: Kinetic parameters for the hydrolysis of X-Pro peptides by PfAPP and selected homologs. The sequence of each substrate is given in single-letter amino acid code. All values were determined at 37 °C except for those for E. coli APP, which were determined at 40 °C. A dash in the Ksi (uncompetitive substrate inhibition constant) column indicates that substrate inhibition was not observed (PfAPP) or reported previously (human APP1, rat APP2, and E. coli APP).

Enzyme	pH	K_m	k_{cat}	k_{cat}/K_m	K_{si}	Ref.
		mM	s^{-1}	$M^{-1}\ s^{-1}$		
Substrate, bradykinin (RPPGFSPFR)						
PfAPP	7.5	0.14	16	1.1×10^5	-	This study
PfAPP	6.5	0.97	88	9.1×10^4	-	This study
PfAPP	5.5	6.7	1.6×10^2	2.3×10^4	-	This study
hAPP1	8.0	0.078	3.8	4.9×10^4	-	43
APP2	6.8	0.021	12	5.7×10^5	-	67
E. coli APP	8.0	0.36	69	1.9×10^5	-	66
Substrate, HbPep1 (FPHFD)						
PfAPP	7.5	0.51	8.6	1.7×10^4	-	This study
PfAPP	5.5	0.86	5.4	6.3×10^3	-	This study
Substrate, HbPep2 (YPWTQ)						
PfAPP	7.5	1.4	1.5×10^2	1.1×10^5	4.4	This study
PfAPP	5.5	1.8	12	6.5×10^3	-	This study

We next evaluated the ability of rPfAPP to catalyze the hydrolysis of the X-Pro bond in two potentially physiological pentapeptide substrates found in the sequences of human a- and b-globin. Both globin chains contain seven proline residues and catabolism of these polypeptides in the food vacuole is likely to give rise to peptides with a proline in the second position. We selected the sequences FPHFD (from a-globin; termed HbPep1) and YPWTQ (from b-globin; termed HbPep2). These sequences were chosen as they contain bulky residues preceding and following the prolyl residue and were thus considered to be stringent test cases for the ability of PfAPP to act on globin-derived peptides. HbPep1 was cleaved around 5-fold less efficiently than bradykinin at pH 7.5 (Table 2-1 and Supplemental Figure 2-S3). The K_m and k_{cat} values for hydrolysis of HbPep1 at pH 5.5 differed by less than a factor of two from those at pH 7.5; the resulting catalytic efficiency was reduced by a factor of 2.7. With HbPep2, a decrease in the rate of product formation at pH 7.5 was observed as the substrate concentration exceeded 1 mM (Fig. 2-6). The rate data were fit to an equation for an uncompetitive substrate inhibition mechanism in which a second molecule of substrate binds the enzyme-substrate complex and prevents conversion of substrate to product (41). A close fit of the line to the data in Fig. 2-6 is consistent

with (but does not prove) an uncompetitive inhibition mechanism and yields an uncompetitive substrate inhibition constant (K_{si}) of 4.4 mM. The catalytic efficiency of PfAPP at pH 7.5 with HbPep2 was similar to that with bradykinin. At pH 5.5, the k_{cat} dropped around 10-fold whereas the K_m increased slightly, leading to a 17-fold decrease in catalytic efficiency when compared to that at pH 7.5.

Peptide products generated by the rPfAPP-catalyzed hydrolysis of bradykinin, HbPep1 and HbPep2 were analyzed by MALDI-TOF mass spectrometry. For hydrolysis of bradykinin at pH 7.5 and 5.5, the dominant product was bradykinin$_{2\text{-}9}$ (i.e. bradykinin lacking the N-terminal Arg residue; Supplemental Table S3). We estimate that less than 10% of the product consisted of bradykinin$_{3\text{-}9}$,which co-migrated with bradykinin$_{2\text{-}9}$ in the HPLC assay. Bradykinin$_{3\text{-}9}$ was presumably generated through two consecutive hydrolysis reactions, as the octapeptide product of the first reaction, PPGFSPFR, also conforms to the X-Pro specificity of the enzyme. Products of HbPep1 and HbPep2 hydrolysis were the expected tetrapeptides (Supplemental Table 2-S3).

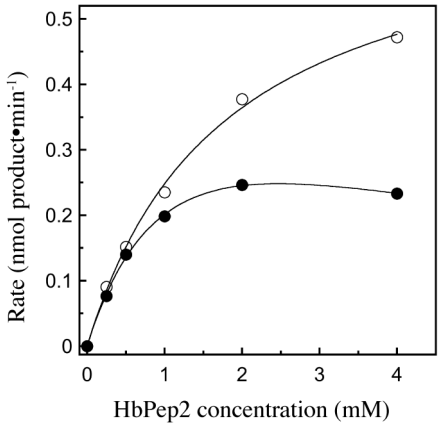

Figure 2-6: Substrate inhibition of rPfAPP by HbPep2. Rates of product formation at pH 7.5 (filled circles) and pH 5.5 (open circles) are plotted against substrate concentration. Data were fit by non-linear regression to equations for uninhibited Michaelis-Menten kinetics (pH 5.5) or for an uncompetitive substrate inhibition mechanism (pH 7.5).

DISCUSSION

The only enzymes known to efficiently catalyze the hydrolysis of an N-terminal X-Pro amide bond are the related metallopeptidases aminopeptidase P (APP) and prolidase (54). An APP homolog is encoded in the genomes of human, rodent and avian malaria parasites, as well as in genomes of several other apicomplexan organisms. No prolidase homologs were found in the genomes of *Plasmodium* spp; thus, in this genus APP appears to be the only enzyme capable of catalyzing the hydrolysis of an amino-terminal X-Pro bond. All protozoan genomes examined here possess at least one (putative) enzyme that can catalyze the hydrolysis of the X-Pro bond. These observations point to a critical role for this activity in protozoan metabolism. The idea that APP/prolidase provide an essential metabolic activity is reinforced by a previous study of 34 genomes across the three domains of life that identified APP/prolidase as one of 80 universally conserved orthologous groups (55). It was also suggested that X-Pro hydrolytic activity was present in the last common ancestor of life (55).

In *P. falciparum*, aminopeptidase P (PfAPP) has an intriguing bipartite distribution in the acidic food vacuole, the site of hemoglobin catabolism, and in the cytosol. While a cytosolic role for APP in peptide turnover in eukaryotes as diverse as mammals, plants, fruit flies and nematodes is well established (18-22,24), this is the first example, to our knowledge, of an APP homolog residing in an acidic intracellular compartment.

PfAPP has the three-domain, dimeric structure of human cytosolic APP1 (hAPP1). Conservation of the hydrophobic dimer interface of hAPP1 (43) in PfAPP suggests that the quaternary structures are very similar in both enzymes. Unlike hAPP1 and the other apicomplexan sequences, PfAPP possesses an N-terminal extension of 120 amino acids that precedes the first conserved domain. Near the beginning of this extension lies a putative signal peptide for import into the endoplasmic reticulum. We speculate that full-length PfAPP traffics to the food vacuole *via* the endoplasmic reticulum as has been observed for several other vacuolar peptidases (56-58). The apparent lack of a signal peptide from the other apicomplexan APP sequences accords with the absence of a food vacuole in these organisms; these APP homologs likely reside in the cytosol. Based on the size of the major PfAPP species in parasite extracts and the co-elution on a gel filtration column of the native enzyme with recombinant PfAPP lacking the N-terminal extension, it appears likely that the N-terminal extension is absent from the mature protein. We attempted to confirm the absence of the N-terminal extension by N-

terminal sequencing of immunopurified native PfAPP but were unable to obtain a sequence for unknown reasons.

Recombinant PfAPP (rPfAPP) activity was greatly reduced following dialysis against EDTA-containing buffer and was nearly fully restored in the presence of 1 mM Mn^{2+}. Similar observations have been made with mammalian cytosolic and *E. coli* APP homologs, which have lead to the conclusion that APP is an Mn(II)-dependent enzyme (18,19,45). Structural studies of hAPP1 and *E. coli* APP have revealed a di-Mn^{2+} cluster, with a water/hydroxide molecule bridging the two metal ions in a position to undertake nucleophilic attack of the X-Pro bond (42,43). However, uncertainty regarding the architecture of the APP active site *in vivo* persists. Metal-enzyme stoichiometries of 1:1, rather than 2:1, have been reported for recombinant human APP1 and pig kidney APP2 (46,47). Moreover, the metal found in APP2 was Zn(II) rather than Mn(II) (46). While atomic structures of the homologous enzyme methionine aminopeptidase at first revealed a di-Co(II) active site very similar in structure to that of APP, more recent evidence suggests that the enzyme is active with a single metal ion in the active site (59). In our opinion, three lines of evidence favor the di-Mn(II) configuration as the best current model for the APP active site. First, recombinant human APP1 that was extensively dialyzed against metal-free buffer retained two Mn(II) ions in the active site (43). Second, a mutant (D260A) of *E. coli* APP that contains only the putative essential Mn(II) ion is inactive (60). Third, an inactive mutant (H243A) of *E. coli* APP that contains an intact di-Mn(II) active site complexed with a tripeptide substrate reveals an interaction between the substrate amino terminus and the putative non-essential Mn(II) ion, which suggests a role for this metal in substrate binding (61). We found that low millimolar levels of Mn(II) stimulated rPfAPP activity several-fold, as has been previously observed with mammalian APP1 (18-20,47,48). There is evidence that one of the two metal sites in the active site of methionine aminopeptidase, and possibly also in *E. coli* APP, has a low affinity for metal (45,59). The stimulation of APP activity observed in the presence of millimolar levels of Mn(II) may result from occupancy of this low-affinity metal binding site. Whether the putative low-affinity site of PfAPP is occupied *in vivo*, and if so by which metal ion, is an interesting question for further study. The inhibition of PfAPP by Zn^{2+} (and possibly also Ni^{2+} and Cu^{2+}) is likely due to stabilization of the enzyme-product complex as observed for *E. coli* APP (45).

Recombinant PfAPP activity was highly stable at 37 °C over one hour in the pH range 5.0 to 7.5, which suggests that this enzyme is sufficiently robust to function in the food vacuole lumen. Contrasting with the high stability of rPfAPP, hAPP1 activity was lost rapidly at pH 5.5. Our observations are consistent with a literature report of low stability of native hAPP1 purified from human platelets (20); therefore, it seems unlikely that hAPP1 is post-translationally modified in a way that would enhance its stability at acidic pH. Loss of activity of hAPP1 appeared to be associated with the formation of a high-molecular weight aggregate. These data suggest that the stability at acid pH found with PfAPP is not an universal feature of three-domain, dimeric aminopeptidase P.

Using three peptide substrates, we found that PfAPP has catalytic efficiencies at pH 7.5 of 10^4 - 10^5 $M^{-1}s^{-1}$, which are similar to those of prokaryotic and eukaryotic APP homologs. At pH 5.5, catalytic efficiencies for each substrate were somewhat lower than the respective values at pH 7. 5 but still ranged around 10^4 $M^{-1}s^{-1}$. We conclude from these data that PfAPP is an efficient catalyst at pH values expected for both the food vacuole and the parasite cytosol. There was no consistent trend in the pH-dependence of K_m or k_{cat} for the three PfAPP substrates examined, which suggests that the effect of pH on these parameters is complex and may be strongly affected by the particular sequence of the substrate. We attempted to determine the kinetic constants for hAPP1-catalyzed hydrolysis of bradykinin at pH 5.5 using a one-minute assay to minimize loss of activity. While we were able to detect activity in this assay, the experiments were not sufficiently reproducible to allow confident determination of kinetic constants. Mass spectrometric identification of the products of PfAPP-mediated hydrolysis are consistent with strict X-Pro aminopeptidase activity. We found that PfAPP can slowly hydrolyze the Pro-Pro bond in bradykinin$_{2-9}$. This finding is significant as the sequence Pro-Pro is found in b-globin.

Together, the data presented here support our model for intracellular peptide catabolism in the malaria parasite (11) in which PfAPP has catalytic roles in both the cytosol and the food vacuole. By analogy with other organisms, the cytosolic pool of PfAPP likely has a housekeeping role in the turnover of peptides generated by the proteasome. We suggest that *Plasmodium* spp. have recruited PfAPP to the food vacuole to facilitate hemoglobin catabolism. Human a- and b-globin each contain seven proline residues. Food vacuole endopeptidases such as plasmepsins and falcipains could directly generate peptides with an X-Pro amino terminus as

they are able to cleave substrates with a P2' proline residue (62-64). Peptide trimming by broad-specificity aminopeptidases has been shown to generate aminopeptidase P substrates in the bacterial cytosol (32). We have localized *P. falciparum* aminopeptidase N to the food vacuole (11), where it could perform an analogous role. Finally, we note that the millimolar K_m values observed at pH 5.5 do not rule out a catalytic role for PfAPP in the vacuole. Hemoglobin is the predominant soluble protein of the red blood cell cytosol at a concentration of 20 mM protomer (65). Even taking into account a dilution of 10-fold in the lumen of the food vacuole, oligopeptide concentrations could still reasonably be expected to exist at low millimolar concentrations, which would be sufficiently high for PfAPP to be a significant factor in peptide catabolism.

The available phylogenetic, biochemical and genetic evidence suggests that PfAPP may present an interesting new target for the development of peptidase-directed anti-malarial drugs. Given the apparent universal conservation of X-Pro hydrolytic activity (55) and its catalytic roles in the intraerythrocytic parasite, we predict that inhibition of PfAPP activity would be detrimental to parasite growth and replication. Our inability to obtain parasites with a disrupted PfAPP coding sequence (11) is consistent with this idea. While inhibition of host APP homologs would be a concern in a strategy targeting PfAPP, we note that PfAPP, unlike its mammalian APP2 homolog (66), can act on substrates with a bulky P2' residue (HbPep2). Thus, specificity for PfAPP over APP2 could potentially be achieved by taking advantage of differences in the S2' subsites.

ACKNOWLEDGEMENTS

We are grateful to W. Beatty for carrying out the immunoelectron microscopy experiments, R. Helm and W.K. Ray for mass spectrometric analysis, D. Jacobus for WR99210 and S. Geherin for technical assistance. This work was supported by a grant from the Thomas F. and Kate Miller Jeffress Memorial Trust, National Institutes of Health grant AI077638 and by the Institute for Biomedical and Public Health Studies at Virginia Tech.

LIST OF ABBREVIATIONS

APP, aminopeptidase P; BSA, bovine serum albumin; EDTA, ethylenediaminetetraacetic acid; hAPP1, human aminopeptidase P1; IMAC, immobilized metal affinity chromatography; Lys(Abz)-Pro-Pro-NA, lysine(N^{ϵ}-2-aminobenzoyl)-Pro-Pro-4-nitroanilide; PfAPP, *Plasmodium falciparum* aminopeptidase P; SDS, sodium dodecyl sulfate; TEV, tobacco etch virus; YFP, yellow fluorescent protein.

SUPPLEMENTARY INFORMATION

Supplemental Table 2-S1: Putative aminopeptidase P and prolidase homologs in selected protozoan organisms.

Organism	Gene ID	BLAST E-value (exponent)[1]	SignalP 3.0 score[2]	
			D-score[3]	Probability[4]
Aminopeptidase P homologs				
P. falciparum[5]	PF14_0517	-	**0.619**	0.45, 0.41
P. vivax	PVX117760	-137	**0.443**	0.11, 0.03
P. knowlesi	PKH_125210	-134	**0.495**	0.18, 0.32
P. berghei	PB000628.00.0	-126	**0.602**	0.84, 0
P. gallinaceum[6]	Pgal0883f06.q1k	-118		
Toxoplasma gondii	TGGT1_008630	-87	0.027	0, 0
Neospora caninum	NC_LIV_091620	-83	0.037	0, 0
Cryptosporidium hominis	Chro.40331	-57	0.051	0, 0.01
Theileria parva	529.m03931	-75	0.068	0, 0
Trypanosoma cruzi	7200.m00011	-59		
	4854.m00002	-59		
Trypanosoma brucei	Tb927.3.2090	-60		
Leishmania major	LmjF02.0040	-54		
	LmjF25.2430	-53		
Dictyostelium discoidin	DDB0304433	-61		
Tetrahymena thermophila	TTHERM_00624780	-52		
Prolidase homologs				
Toxoplasma gondii	TGGT1_114170	-3		
Neospora caninum	NC_LIV_102300	-5		
Dictyostelium discoidin	DDB0266378	-3		
Tetrahymena thermophila	TTHERM_00281000	-2		
Trypanosoma cruzi	8455.m00012	-3		
Trypanosoma brucei	Tb09.211.4330	-5		
Leishmania major	LmjF35.2350	-5		
Giardia lamblia	GL50803_16722	-2		
	GL50803_17327	-2		
Trichomonas vaginalis	TVAG_386080	-6		
	TVAG_321430	-4		
	TVAG_255940	-4		
	TVAG_227590	-4		
	TVAG_437930	-4		

[1] BLAST query sequence was the PfAPP catalytic domain (residues 476-777).
[2] Calculated from the first 70 residues of the predicted sequence.
[3] D-score from the SignalP 3.0 neural network. Values above the cutoff (0.43) are bold.
[4] Probabilities of signal peptides and signal anchors predicted by the Hidden Markov Model algorithm in SignalP 3.0. Values are expressed as: probability of a signal peptide, probability of a signal anchor.
[5] The sequence of PfAPP reported under PF14_0517 in the *Plasmodium* genome database (PlasmoDB; www.plasmodb.org) is annotated to begin at an internal methionine and is missing the first 13 amino acids.
[6] Partial sequence.

Supplemental Table 2-S2: Identities of residues in PfAPP that are homologous to residues in the dimer interface of hAPP1. Charged/polar residues are in bold.

hAPP1 residue[1]	Homologous PfAPP residue	Comments
Y439	**E594**	At edge of interface
F459	F614	
P460	A615	
L468	L623	
F471	I626	
W477	F632	Mutation to Glu causes hAPP1 dimer dissociation
L481	M636	
L484	**N639**	At edge of interface
Y526	Y679	
Y549	**D702**	At edge of interface

[1] As reported in Fig. 1 in Li *et al* (2008) J. Biol. Chem. **283**, 22858-22866.

Supplemental Table 2-S3: Predicted and MALDI-TOF experimental masses for products of recombinant PfAPP-catalyzed peptide hydrolysis.

Substrate	Product	Predicted mass (Da)	Observed mass (Da)
Bradykinin	PPGFSPFR ($Bradykinin_{2-9}$)	904.0	903.5
	PGFSPFR[1] ($Bradykinin_{3-9}$)	806.9	806.4
HbPep1	PHFD	514.5	514.2
HbPep2	PWTQ	530.6	530.2

[1] Minor quantity (estimated less than 10% of total reaction product)

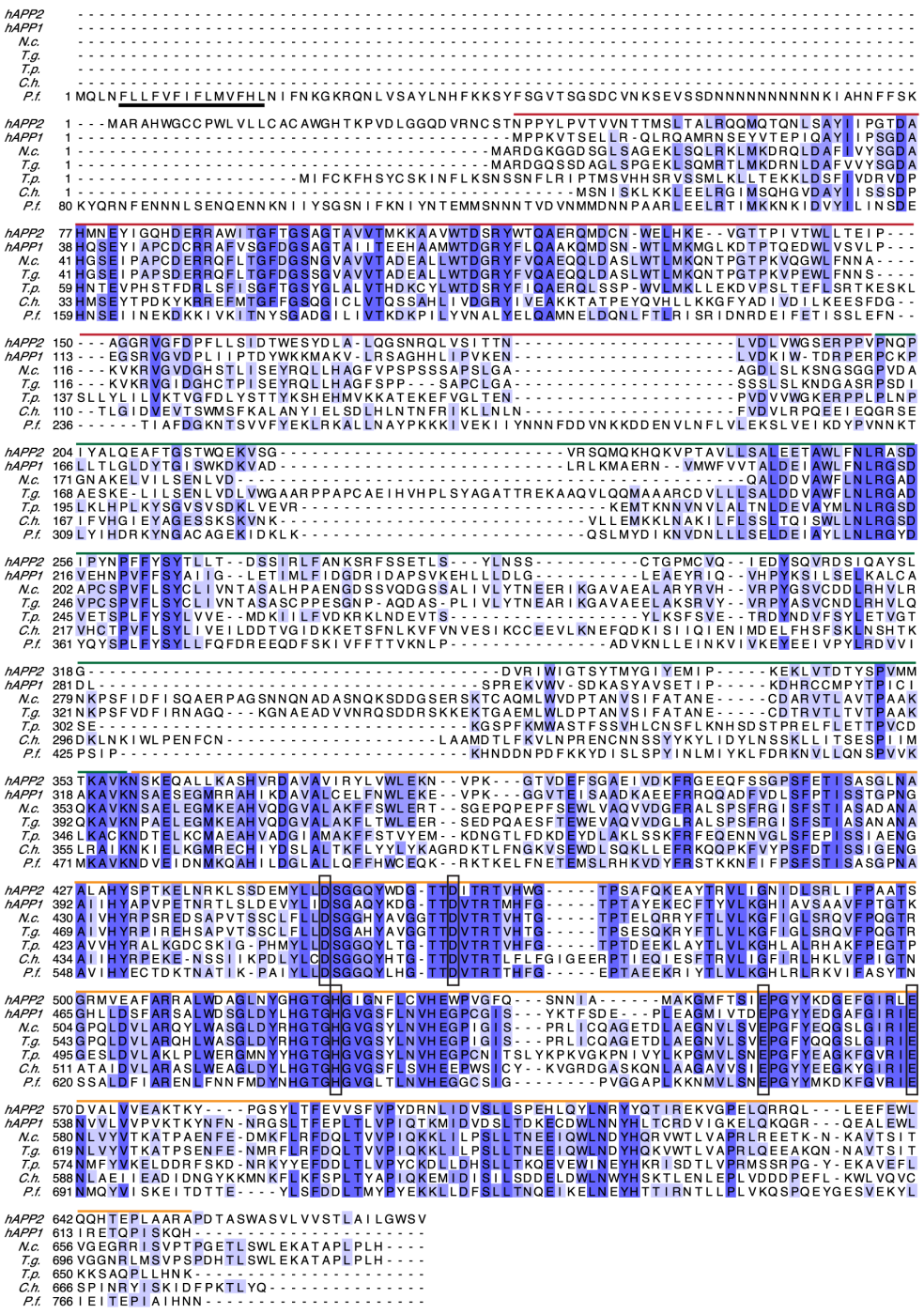

Supplemental Figure 2-S1: Alignment of apicomplexan and human aminopeptidase P sequences. Conserved residues are shaded blue (darker shades indicate higher levels of conservation). The putative signal peptide in the P. falciparum sequence is indicated with a black bar. Regions corresponding to Domain I (red line), Domain II (green line) and Domain III (orange line) of hAPP1 (Li et al (2008) J. Biol. Chem. 283, 22858-22866) are shown above the alignment. Residues forming the di-Mn2+ cluster are boxed. Sequence IDs are in Supplemental Table 2-S1. The alignment was generated with ClustalW and colored using Jalview 2.4 (Waterhouse et al (2009) Bioinformatics 25, 1189-1191). hAPP1, human cytosolic aminopeptidase P1; hAPP2, human membrane aminopeptidase P2. Apicomplexan APP homologs: N.c., Neospora caninum; T.g., Toxoplasma gondii; T.p., Theileria parva; C.h., Cryptosporidium hominis; P.f., Plasmodium falciparum.

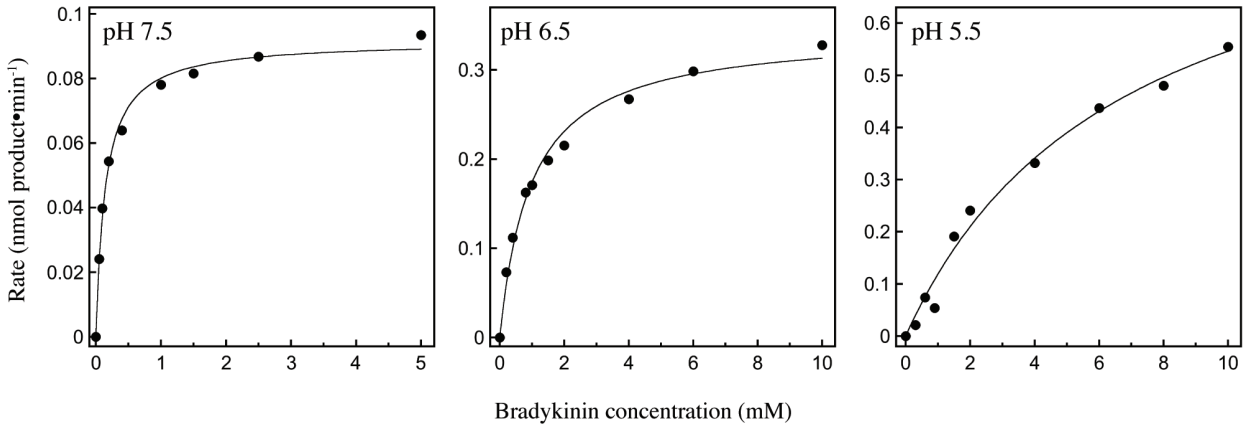

Supplemental Figure 2-S2: Rates of PfAPP-catalyzed bradykinin hydrolysis vs. substrate concentration at pH 7.5, 6.5 and 5.5. Data points are the average of two independent experiments. Lines are non-linear regression fits of the data to the Michaelis-Menten equation.

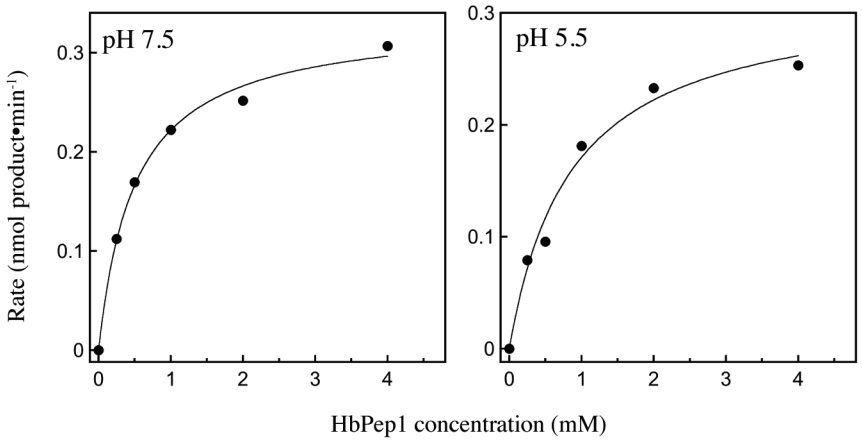

Supplemental Figure 2-S3: Rates of PfAPP-catalyzed HbPep1 hydrolysis vs. substrate concentration at pH 7.5 and 5.5. Data points are the average of two independent experiments. Lines are non-linear regression fits of the data to the Michaelis-Menten equation.

REFERENCES

1. Greenwood, B., and Mutabingwa, T. (2002) *Nature* **415**, 670-672
2. Snow, R. W., Guerra, C. A., Noor, A. M., Myint, H. Y., and Hay, S. I. (2005) *Nature* **434**, 214-217
3. Gantt, S. M., Myung, J. M., Briones, M. R., Li, W. D., Corey, E. J., Omura, S., Nussenzweig, V., and Sinnis, P. (1998) *Antimicrob. Agents Chemother.* **42**, 2731-2738
4. Hatabu, T., Hagiwara, M., Taguchi, N., Kiyozawa, M., Suzuki, M., Kano, S., and Sato, K. (2006) *Exp. Parasitol.* **112**, 179-183
5. Lindenthal, C., Weich, N., Chia, Y. S., Heussler, V., and Klinkert, M. Q. (2005) *Parasitology* **131**, 37-44
6. Goldberg, D. E. (2005) *Curr. Top. Microbiol. Immunol.* **295**, 275-291
7. Rosenthal, P. J. (2004) *Int. J. Parasitol.* **34**, 1489-1499
8. Krugliak, M., Zhang, J., and Ginsburg, H. (2002) *Mol. Biochem. Parasitol.* **119**, 249-256
9. Loria, P., Miller, S., Foley, M., and Tilley, L. (1999) *Biochem. J.* **339**, 363-370
10. Allary, M., Schrevel, J., and Florent, I. (2002) *Parasitology* **125**, 1-10
11. Dalal, S., and Klemba, M. (2007) *J. Biol. Chem.* **282**, 35978-35987
12. Gardiner, D. L., Trenholme, K. R., Skinner-Adams, T. S., Stack, C. M., and Dalton, J. P. (2006) *J. Biol. Chem.* **281**, 1741-1745
13. McGowan, S., Porter, C. J., Lowther, J., Stack, C. M., Golding, S. J., Skinner-Adams, T. S., Trenholme, K. R., Teuscher, F., Donnelly, S. M., Grembecka, J., Mucha, A., Kafarski, P., Degori, R., Buckle, A. M., Gardiner, D. L., Whisstock, J. C., and Dalton, J. P. (2009) *Proc. Natl. Acad. Sci. USA* **106**, 2537-2542
14. Stack, C. M., Lowther, J., Cunningham, E., Donnelly, S., Gardiner, D. L., Trenholme, K. R., Skinner-Adams, T. S., Teuscher, F., Grembecka, J., Mucha, A., Kafarski, P., Lua, L., Bell, A., and Dalton, J. P. (2007) *J. Biol. Chem.* **282**, 2069-2080
15. Teuscher, F., Lowther, J., Skinner-Adams, T. S., Spielmann, T., Dixon, M. W., Stack, C. M., Donnelly, S., Mucha, A., Kafarski, P., Vassiliou, S., Gardiner, D. L., Dalton, J. P., and Trenholme, K. R. (2007) *J. Biol. Chem.* **282**, 30817-30826
16. Schechter, I., and Berger, A. (1967) *Biochem. Biophys. Res. Commun.* **27**, 157-162
17. Cunningham, D. F., and O'Connor, B. (1997) *Biochim. Biophys. Acta* **1343**, 160-186
18. Harbeck, H. T., and Mentlein, R. (1991) *Eur. J. Biochem.* **198**, 451-458

19. Rusu, I., and Yaron, A. (1992) *Eur. J. Biochem.* **210**, 93-100
20. Vanhoof, G., De Meester, I., Goossens, F., Hendriks, D., Scharpe, S., and Yaron, A. (1992) *Biochem. Pharmacol.* **44**, 479-487
21. Hauser, F., Strassner, J., and Schaller, A. (2001) *J. Biol. Chem.* **276**, 31732-31737
22. Kulkarni, G. V., and Deobagkar, D. D. (2002) *J. Biochem.* **131**, 445-452
23. Chavant, P., Taupin, V., El Alaoui, H., Wawrzyniak, I., Chambon, C., Prensier, G., Metenier, G., and Vivares, C. P. (2005) *Int. J. Parasitol.* **35**, 1425-1433
24. Laurent, V., Brooks, D. R., Coates, D., and Isaac, R. E. (2001) *Eur. J. Biochem.* **268**, 5430-5438
25. Hooper, N. M., and Turner, A. J. (1988) *FEBS Lett.* **229**, 340-344
26. Orawski, A. T., Susz, J. P., and Simmons, W. H. (1987) *Mol. Cell Biochem.* **75**, 123-132
27. Prechel, M. M., Orawski, A. T., Maggiora, L. L., and Simmons, W. H. (1995) *J. Pharmacol. Exp. Ther.* **275**, 1136-1142
28. Ersahin, C., Euler, D. E., and Simmons, W. H. (1999) *J. Cardiovasc. Pharmacol.* **34**, 604-611
29. Kitamura, S., Carbini, L. A., Carretero, O. A., Simmons, W. H., and Scicli, A. G. (1995) *Br. J. Pharmacol.* **114**, 6-7
30. Wolfrum, S., Richardt, G., Dominiak, P., Katus, H. A., and Dendorfer, A. (2001) *Br. J. Pharmacol.* **134**, 370-374
31. Ersahin, C., Szpaderska, A. M., Orawski, A. T., and Simmons, W. H. (2005) *Arch. Biochem. Biophys.* **435**, 303-310
32. Miller, C. G., and Green, L. (1983) *J. Bacteriol.* **153**, 350-356
33. Lambros, C., and Vanderberg, J. P. (1979) *J. Parasitol.* **65**, 418-420
34. Benting, J., Mattei, D., and Lingelbach, K. (1994) *Biochem. J.* **300**, 821-826
35. Kapust, R. B., Tozser, J., Copeland, T. D., and Waugh, D. S. (2002) *Biochem. Biophys. Res. Commun.* **294**, 949-955
36. Kapust, R. B., Tozser, J., Fox, J. D., Anderson, D. E., Cherry, S., Copeland, T. D., and Waugh, D. S. (2001) *Protein Eng.* **14**, 993-1000
37. Tonkin, C. J., van Dooren, G. G., Spurck, T. P., Struck, N. S., Good, R. T., Handman, E., Cowman, A. F., and McFadden, G. I. (2004) *Mol. Biochem. Parasitol.* **137**, 13-21
38. Klemba, M., Gluzman, I., and Goldberg, D. E. (2004) *J. Biol. Chem.* **279**, 43000-43007

39. Stockel-Maschek, A., Stiebitz, B., Koelsch, R., and Neubert, K. (2003) *Anal. Biochem.* **322**, 60-67
40. Lloyd, G. S., Hryszko, J., Hooper, N. M., and Turner, A. J. (1996) *Biochem. Pharmacol.* **52**, 229-236
41. Cornish-Bowden, A. (2004) *Fundamentals of enzyme kinetics*, Portland Press, London
42. Wilce, M. C., Bond, C. S., Dixon, N. E., Freeman, H. C., Guss, J. M., Lilley, P. E., and Wilce, J. A. (1998) *Proc. Natl. Acad. Sci. USA* **95**, 3472-3477
43. Li, X., Lou, Z., Zhou, W., Ma, M., Cao, Y., Geng, Y., Bartlam, M., Zhang, X. C., and Rao, Z. (2008) *J. Biol. Chem.* **283**, 22858-22866
44. Bendtsen, J. D., Nielsen, H., von Heijne, G., and Brunak, S. (2004) *J. Mol. Biol.* **340**, 783-795
45. Graham, S. C., Bond, C. S., Freeman, H. C., and Guss, J. M. (2005) *Biochemistry* **44**, 13820-13836
46. Hooper, N. M., Hryszko, J., Oppong, S. Y., and Turner, A. J. (1992) *Hypertension* **19**, 281-285
47. Cottrell, G. S., Hooper, N. M., and Turner, A. J. (2000) *Biochemistry* **39**, 15121-15128
48. Maruyama, S., Kobayashi, T., Ohmori, T., Tanaka, H., and Maeda, H. (1994) *Biosci. Biotechnol. Biochem.* **58**, 2107-2108
49. Kuhn, Y., Rohrbach, P., and Lanzer, M. (2007) *Cell. Microbiol.* **9**, 1004-1013
50. Bennett, T. N., Kosar, A. D., Ursos, L. M., Dzekunov, S., Singh Sidhu, A. B., Fidock, D. A., and Roepe, P. D. (2004) *Mol. Biochem. Parasitol.* **133**, 99-114
51. Hayward, R., Saliba, K. J., and Kirk, K. (2006) *J. Cell Sci.* **119**, 1016-1025
52. Klonis, N., Tan, O., Jackson, K., Goldberg, D., Klemba, M., and Tilley, L. (2007) *Biochem. J.* **407**, 343-354
53. Krogstad, D. J., Schlesinger, P. H., and Gluzman, I. Y. (1985) *J. Cell Biol.* **101**, 2302-2309
54. Vanhoof, G., Goossens, F., De Meester, I., Hendriks, D., and Scharpe, S. (1995) *FASEB J.* **9**, 736-744
55. Harris, J. K., Kelley, S. T., Spiegelman, G. B., and Pace, N. R. (2003) *Genome Res.* **13**, 407-412
56. Francis, S. E., Banerjee, R., and Goldberg, D. E. (1997) *J. Biol. Chem.* **272**, 14961-14968

57. Klemba, M., Beatty, W., Gluzman, I., and Goldberg, D. E. (2004) *J. Cell Biol.* **164**, 47-56
58. Subramanian, S., Sijwali, P. S., and Rosenthal, P. J. (2007) *J. Biol. Chem.* **282**, 24961-24969
59. D'Souza V, M., Bennett, B., Copik, A. J., and Holz, R. C. (2000) *Biochemistry* **39**, 3817-3826
60. Graham, S. C., Lilley, P. E., Lee, M., Schaeffer, P. M., Kralicek, A. V., Dixon, N. E., and Guss, J. M. (2006) *Biochemistry* **45**, 964-975
61. Graham, S. C., and Guss, J. M. (2008) *Arch. Biochem. Biophys.* **469**, 200-208
62. Beyer, B. B., Johnson, J. V., Chung, A. Y., Li, T., Madabushi, A., Agbandje-McKenna, M., McKenna, R., Dame, J. B., and Dunn, B. M. (2005) *Biochemistry* **44**, 1768-1779
63. Siripurkpong, P., Yuvaniyama, J., Wilairat, P., and Goldberg, D. E. (2002) *J. Biol. Chem.* **277**, 41009-41013
64. Subramanian, S., Hardt, M., Choe, Y., Niles, R. K., Johansen, E. B., Legac, J., Gut, J., Kerr, I. D., Craik, C. S., and Rosenthal, P. J. (2009) *PLoS ONE* **4**, e5156
65. Hellerstein, S., Spees, W., and Surapathana, L. O. (1970) *J. Lab. Clin. Med.* **76**, 10-24
66. Yoshimoto, T., Orawski, A. T., and Simmons, W. H. (1994) *Arch. Biochem. Biophys.* **311**, 28-34
67. Orawski, A. T., and Simmons, W. H. (1995) *Biochemistry* **34**, 11227-11236

Chapter 3

Insights into the functional specialization of an M1-family aminopeptidase in the human malaria parasite *Plasmodium falciparum*

Daniel Ragheb, Seema Dalal, Kristin M. Bompiani, W. Keith Ray and Michael Klemba

Manuscript under revision for the *Journal of Biological Chemistry*

ABSTRACT

Aminopeptidases catalyze amino-terminal peptide bond hydrolysis and occupy multitudinous, highly diversified roles across all domains of life. Here, we present evidence that an M1-family aminopeptidase, PfA-M1, has been recruited to specialized roles in the malaria parasite *Plasmodium falciparum*. PfA-M1 is abundant in two subcellular compartments in asexual intraerythrocytic parasites: the food vacuole, where the catabolism of host hemoglobin takes place, and the nucleus. A unique N-terminal extension that precedes the catalytic domains of PfA-M1 contributes to the observed dual targeting. PfA-M1 exists as two major isoforms, a nuclear 120 kDa species and a processed vacuolar species consisting of a complex of 68 and 35 kDa fragments. PfA-M1 is both stable and active at the acidic pH of the food vacuole lumen. Determination of steady-state kinetic parameters over the pH range 5.5 – 8.5 revealed that k_{cat} is relatively insensitive to pH whereas K_m increases at pH values below 6.5. These changes cause a ~10-fold decrease in catalytic efficiency at pH 5.5 compared with pH 7.5; however, the magnitude of the catalytic efficiency at pH 5.5 remains high at ~10^4 $M^{-1} \bullet s^{-1}$. pH is also an important factor governing the potency of the PfA-M1 inhibitors bestatin and bestatin methyl ester. Together, these results support a catalytic role for PfA-M1 in the production of amino acids from short, hemoglobin-derived peptides in the food vacuole lumen. They also suggest a second, distinct function for this enzyme in the parasite nucleus.

INTRODUCTION

Human malaria is responsible for around one million deaths annually (1). Five species of the genus *Plasmodium* cause malaria in humans as they replicate within host erythrocytes. The cytoadherent properties of intraerythrocytic *Plasmodium falciparum,* coupled with its ability to invade mature erythrocytes, makes it the most virulent of the species that infect humans. During its erythrocytic replication cycle, *P. falciparum* endocytoses and catabolizes over two-thirds of soluble erythrocyte proteins (2,3), the majority of which is hemoglobin. Hemoglobin catabolism provides amino acids for protein synthesis, general metabolism, and isoleucine import (4,5) and may also prevent premature hemolysis by reducing the colloid osmolarity of the erythrocyte (6). Blocking hemoglobin catabolism with protease inhibitors prevents parasite replication; therefore, enzymes that catalyze this process are attractive targets for the development of novel anti-malarial drugs (7).

Hemoglobin is extensively catabolized by the parasite within an acidic organelle called the food vacuole or digestive vacuole. In the vacuole, numerous types of endo- and exopeptidases act in a complementary and concerted manner to catalyze the hydrolysis of the a- and b-globin chains of hemoglobin. Aspartic proteases (plasmepsin I, II, IV and histo-aspartic protease) and cysteine endoproteases (falcipain-2, -2' and -3) initiate cleavage of the globin chains and generate polypeptide fragments (8,9). The metallopeptidase falcilysin produces oligopeptides from these fragments (10), which are further reduced to dipeptides by the exopeptidase dipeptidyl aminopeptidase 1 (11,12). Peptides with a proline residue in the second position are trimmed by the aminopeptidase P homolog PfAPP (13).

What happens next is less clearly understood. The liberation of amino acids from globin peptides requires the action of broad-specificity aminopeptidases or carboxypeptidases. As of yet, no carboxypeptidases have been found to participate in globin peptide catabolism (14). Rather, two aminopeptidases have been implicated in this process: the M1-family aminopeptidase N homolog PfA-M1 (15-19) and the M17-family leucine aminopeptidase homolog PfLAP (19-21).

One model for the generation of amino acids from globin di- and oligopeptides that gained early traction is the "peptide export" model (for a recent elaboration of this model, see (18)). According to this view, short peptides are transported out of the vacuole to the cytosol, where the final hydrolytic steps are catalyzed by aminopeptidases (14). Early support for this

model included the apparent absence of aminopeptidase activity from enriched food vacuoles (14) and the neutral-to-basic pH optima of parasite aminopeptidase activities (22,23). The apparent localization of PfA-M1 and PfLAP to the cytosol appeared to provide further evidence for this model (15,18,21). More recently, a study in which these aminopeptidases were tagged with yellow fluorescent protein by allelic modification confirmed a cytosolic distribution for PfLAP but found that PfA-M1 exhibited a dual distribution in the food vacuole and the nucleus (24). This observation provided the first evidence that extensive amino acid production could occur in the acidic lumen of the food vacuole and was bolstered by the enrichment of PfA-M1 activity in food vacuole preparations (24). Recently, however, two alternate interpretations of the food vacuole localization of Dalal and Klemba (24) have been advanced that do not invoke a role for PfA-M1 in the vacuole lumen. Whisstock *et al* (25) have proposed that PfA-M1 is an integral membrane protein anchored in the food vacuole membrane with the catalytic domains in the cytosol, and Azimzadeh *et al* (16) have suggested that PfA-M1 accumulates in cytosolic vesicles that reside proximal to the food vacuole. The idea that PfA-M1 plays a catalytic role in the vacuole has also been questioned on the basis of an apparent pH optimum for PfA-M1 catalysis that precludes significant activity at pH values below 6 (18), such as that found in the *P. falciparum* food vacuole (26-29). However, a rigorous evaluation of the stability and kinetic properties of PfA-M1 at acidic pH has not yet been reported and its catalytic potential under these conditions remains unclear.

PfA-M1 is a member of the expansive M1 family of metallo-aminopeptidases. Twelve members of this family have been identified in humans (30); however, PfA-M1 appears to be more closely related to prokaryotic M1-family enzymes such as *Escherichia coli* PepN (18). PfA-M1 possesses a ~190-amino acid sequence preceding the catalytic domains that is not found in PepN (18). Crystal structures of PfA-M1 and PepN reveal that these aminopeptidases consist of four conserved domains, with a buried active site in the thermolysin-like domain II (18,31,32). A single metal ion, presumed to be zinc(II), is observed in the active site and is thought to activate a water molecule and co-ordinate the tetrahedral intermediate (32). The dipeptide mimetic bestatin exploits this active site configuration. A potent inhibitor of PfA-M1 (18), bestatin resembles a Phe-Leu dipeptide but contains a modified amino-terminal residue with a b-hydroxy group (33). In the bestatin-PfA-M1 co-crystal structure, bestatin occupies the active site with the b-hydroxy group displacing the catalytic water molecule (18).

In this study, we tested the hypothesis that PfA-M1 has a catalytic role in globin degradation inside the food vacuole lumen. First, we localized untagged, native PfA-M1 to determine whether it could contribute to peptide catabolism within the vacuole. Next, we analyzed the stability and steady-state kinetic parameters of PfA-M1 over the pH range 5.0 to 8.5. To further examine the role of pH in substrate binding, we determined its effect on inhibition of PfA-M1 by the substrate analogs bestatin and bestatin methyl ester.

EXPERIMENTAL PROCEDURES

Parasite culture and isolation

P. falciparum 3D7 parasites were cultured in human O^+ erythrocytes (Interstate Blood Bank) in RPMI 1640 medium supplemented with 27 mM sodium bicarbonate, 11 mM glucose, 0.37 mM hypoxanthine, 10 mg/mL gentamicin and 5 g/L Albumax I (Invitrogen). Cultures were synchronized by sorbitol treatment (34). In certain experiments, variants of 3D7 were employed in which the genomic PfA-M1 or PfLAP coding sequence had been modified to encode a C-terminal hemagglutinin (HA) tag (24).

Purification of native PfA-M1

PfA-M1 was purified from a modified 3D7 parasite line that expressed PfLAP with a C-terminal HA tag (24). Trophozoite stage parasites were isolated from infected red blood cells with 0.15% (w/v) saponin in Dulbecco's phosphate-buffered saline (PBS). To remove any remaining hemoglobin, which co-purified with PfA-M1, parasite pellets were frozen at -80 °C, thawed and washed three times in PBS supplemented with 10 μM N-(trans-epoxysuccinyl)-L-leucine 4-guanidinobutylamide, 10 μM pepstatin, and 1 mM 4-(2-aminoethyl)-benzenesulfonyl fluoride. The pellet was then resuspended in 20 mM bis-tris•HCl pH 6.0 with the same inhibitor concentrations and cells were disrupted by sonication. Parasite lysate was centrifuged at 100,000 *x* g for 1 hour and the supernatant was loaded onto a Mono Q 5/50 GL (GE Healthcare) column equilibrated with 20 mM bis-tris•HCl pH 6.0. The flow-through, which contained PfA-M1 activity, was adjusted to pH 7.5 by adding Tris base to 15 mM and was injected onto a Mono Q 5/50 GL column equilibrated with 20 mM Tris-HCl pH 7.5. Bound protein was eluted with a linear gradient from 0 to 1 M NaCl in 20 mM Tris-HCl pH 7.5. PfA-M1 eluted at around 330 mM NaCl. Fractions with PfA-M1 activity were concentrated in an Ultra-4 centrifugal device

(Amicon) and were injected onto a Superdex 200 10/30 gel filtration column (GE Healthcare) equilibrated in 50 mM Tris-HCl pH 7.5, 200 mM NaCl. Fractions were subjected to immunoblotting with anti-PfA-M1 serum to assess the distributions of the PfA-M1 species. Fractions enriched in p120 over p68/p35 and those enriched in p68/p35 over p120 were combined separately. Purity of the pools was assessed on a silver stained polyacrylamide gel. For long-term protein storage, Triton-X-100 was added to 0.1% (v/v) and aliquots were snap-frozen in liquid nitrogen and stored at -80 °C. Protein concentrations were calculated by quantitative immunoblotting as described in "Immunoblotting and immunolocalization" using a standard curve generated with recombinant PfA-M1. Because the p68 fragment is two-thirds of the size of the recombinant PfA-M1 standard used to generate the polyclonal antibodies, it was assumed that the antibody signal per molecule of p68 was two-thirds that of the standard (i.e., antibodies binding to p35 were lost from the quantitation). To adjust for this, the amounts of p68 calculated from the standard curve were multiplied by a factor of 1.5.

Expression and purification of recombinant PfA-M1

DNA coding for residues 192-1085 of *P. falciparum* PfA-M1 (gene ID MAL13P1.56) was amplified by PCR from clone 3D7 genomic DNA using the forward primer 5'-GCACGGGATCC*CGAAAACCTGTATTTTCAGAGC*AAAAAGAACGAACCAAAAATACATTATAGG and the reverse primer 5'-GCACGGCGGCCGCTTATAATTTATTTGTTAATCTTAATAAATA. The PCR product was digested with BamH1 and NotI (underlined) and ligated into the same sites in the T7 expression vector pET45b (Novagen), which appended an N-terminal hexahistidine tag. The PfA-M1 coding sequence was immediately preceded by the primer-encoded tobacco etch virus (TEV) protease cleavage site ENLYFQS ((35); italicized sequence in the forward primer). The sequence was confirmed by DNA sequencing.

The expression plasmid was transformed into *Escherichia coli* BL21(DE3) Rosetta 2 (Novagen). Bacterial cultures were grown to an optical density of 0.8 at 600 nm and protein expression was induced by the addition of 1 mM isopropyl-D-thiogalactopyranoside for 12 hours at 25 °C. Recombinant PfA-M1 was purified by immobilized metal affinity chromatography (IMAC) as described previously for *P. falciparum* aminopeptidase P (13). Fractions containing PfA-M1 were pooled and dialyzed at 4 °C into 50 mM Tris-HCl pH 7.5, 200 mM NaCl. To

remove the N-terminal histidine tag, PfA-M1 was incubated with hexahistidine-tagged tobacco etch virus (TEV) protease (purified as described in (36)) at a molar PfA-M1:TEV protease ratio of 10:1 in 50 mM Tris-HCl pH 8.0 at 4 °C overnight. Cleaved PfA-M1 was purified and concentrated as previously described (13) and dialyzed into 50 mM Tris-HCl pH 7.5, 200 mM NaCl overnight at 4 °C. The dialysate was injected onto a Superdex 200 10/30 gel filtration column (GE healthcare) equilibrated in 50 mM Tris-HCl pH 7.5, 200 mM NaCl. Fractions containing active PfA-M1 were pooled, dialyzed overnight at 4 °C into 50 mM Tris-HCl pH 7.5 containing 10 μM $ZnCl_2$, snap frozen in liquid nitrogen and stored at -80 °C. Protein concentration was determined from absorbance at 280 nm using a calculated extinction coefficient of 1.150 x 10^5 M^{-1}•cm^{-1}.

Immunoblotting and immunolocalization

Rabbit anti-PfA-M1 serum was produced using recombinant PfA-M1 as the immunogen (Cocalico Biologicals). An affinity column was generated by covalently coupling rPfA-M1 to AminoLink Coupling Resin (Pierce) according to the manufacturer's instructions. Anti-PfA-M1 antibodies were bound, eluted at acidic pH and rapidly neutralized according to an established procedure (37). The affinity purified antibodies were dialyzed overnight at 4 °C against PBS pH 7.4, flash frozen in liquid nitrogen and stored at -80 °C.

In immunoblotting experiments, anti-PfA-M1 serum was used at a 1:10,000 dilution or affinity-purified anti-PfA-M1 antibodies were used at a concentration of 0.13 mg/mL. Other antibodies employed were rabbit anti-HA antibody (Invitrogen; 0.25 mg/mL), rabbit anti-plasmepsin II serum 737 (1:5,000; (38)) and mouse anti-plasmepsin V monoclonal antibody 23.1.2 (1:400; (39)). These were followed by a horse radish peroxidase-conjugated anti-rabbit or anti-mouse secondary antibody. Chemiluminescent signal was developed with ECL Plus (GE Healthcare) and recorded on a Storm 840 imager. Band quantitation was performed with ImageQuant TL 7.0 software (GE Healthcare) using Rolling Ball background subtraction set to a radius of 100.

For localization of PfA-M1 by immunofluorescence, parasitized erythrocytes were fixed in 4% paraformaldehyde/0.0075% glutaraldehyde in PBS, permeabilized with 0.1% Triton X-100 in PBS and blocked as previously described (40). Fixed cells were labeled with affinity-purified anti-PfA-M1 antibodies (0.5 mg/mL) followed by an Alexa 594-conjugated anti-rabbit

IgG secondary antibody (2 mg/mL; Invitrogen). Alternately, dried thin smears of parasitized erythrocytes were fixed with 1:1 methanol/ethanol at -20 °C for two minutes, washed with PBS, blocked with 3% bovine serum albumin in PBS and labeled as described for aldehyde-fixed parasites. In both cases, samples were mounted in Prolong Gold (Invitrogen) containing 4',6-diamidino-2-phenylindole (DAPI). Images were collected on a Zeiss Axioimager M1 fluorescence microscope equipped with an Axiocam MRm digital camera and a 100x/1.4NA objective lens. Contrast was adjusted using Adobe Photoshop.

Cryo-immunoelectron microscopy was carried out at the Molecular Microbiology Imaging Facility, Washington University, St. Louis, MO. Parasite-infected erythrocytes were enriched on a MACS magnetic LD column (41), fixed with 4% paraformaldehyde and 0.1% glutaraldehyde and labeled with affinity-purified anti-PfA-M1 polyclonal antibody (0.4 mg/mL) as previously described (11). Image contrast was adjusted with Adobe Photoshop.

Expression of a PfA-M1 N-terminal extension-YFP fusion in parasites

The PfA-M1 N-terminal extension (NTE)-YFP fusion was introduced into the genome of *P. falciparum* in a single copy using the mycobacterium Bxb1 integrase system (42). The plasmid pLN-ENR-GFP (42) was modified to contain the NTE-YFP fusion with expression driven by the PfA-M1 promoter as follows. The green fluorescent protein sequence in pLN-ENR-GFP was replaced with the citrine allele of yellow fluorescent protein (24,43) by PCR amplification of citrine from plasmid pPM2CIT2 (24) with forward primer 5'-GTACGACTAGTCTCGAGATCGCCTAGGGAAAATTTATATTTTCAA (SpeI, XhoI and AvrII sites underlined) and reverse primer 5'-GTACGCTTAAGGCGGCCGCTTAACTTCCTCCTAATCCTGCAT (AflII and NotI sites underlined). The PCR product was digested with SpeI and AflII and ligated into the AvrII and AflII sites of pLN-ENR-GFP to generate pLN-YFP. DNA coding for residues 1 to 200 of PfA-M1 as well as the preceding 25 bases of the 5' untranslated region was then amplified from genomic DNA by PCR with forward primer 5'-GTACGCTCGAGTATATATTTGTATATATATTACAAAATGAA and reverse primer 5'-GTACGCCTAGGATAATGTATTTTTGGTTCGTTCTTTTTAAC, digested with XhoI and AvrII (sites underlined), and cloned into the same sites in pLN-YFP to generate pLN-NTE-YFP. The calmodulin promoter was replaced with the 5'-untranslated region of PfA-M1 (bases -868 to

-22), which was PCR amplified from genomic DNA with forward primer 5'-GTACGGGGCCCAATAAATTATTTCTATTGATATAACAATAC and reverse primer 5'-GTACGCTCGAGTATATAAAAAAAAAAAAATTAAATAAAAATTA, digested with ApaI and XhoI (sites underlined), and cloned into the same sites in pLN-NTE-YFP to generate pAPNp-NTE-YFP.

The expression plasmid was co-transfected with pINT into the parasite line $3D7^{attB}$, which has an attB site integrated into the cg6 locus, as previously described (42). Parasites were selected with 2.5 mg/mL blasticidin and resistant parasites were cloned by limiting dilution; clone D3 was used for this study. Integration of pAPNp-NTE-YFP at the genomic attB locus was confirmed by Southern blotting (Supplemental Fig. 3-S1). Confocal microscopy was performed on a Zeiss LSM 510 META laser scanning microscope using a Zeiss 63x/1.4 NA Plan-Apochromat objective on an Axio Observer Z1 base. YFP was visualized using a 488-nm argon laser and a 505-550 nm band pass filter.

Parasite fractionation

Parasite food vacuoles were enriched from trophozoite-stage parasites as previously described (24,44). Food vacuoles and matching trophozoites were suspended in 50 mM Tris•HCl pH 6.8, 10% glycerol, 0.7 M b-mercaptoethanol, 2% (w/v) sodium dodecyl sulfate and 1.4 mM bromophenol blue supplemented with the protease inhibitors 10 μM *N-(trans*-epoxysuccinyl)-L-leucine 4-guanidinobutylamide, 10 μM pepstatin and 1 mM 4-(2-aminoethyl)benzenesulfonyl fluoride and immediately placed in a boiling water bath for three minutes. Samples were cooled, clarified by centrifugation and analyzed by immunoblotting. p120 and p68 signal intensities were quantitated using a Storm 840 imager and ImageQuant TL 7.0 software.

For analysis of membrane association, a saponin-treated trophozoite pellet was resuspended in PBS supplemented with 10 μM *N-(trans*-epoxysuccinyl)-L-leucine 4-guanidinobutylamide, 10 μM pepstatin and 1 mM 4-(2-aminoethyl)benzenesulfonyl fluoride and lysed by sonication. The lysate was split into two aliquots and centrifuged at 100,000 *x* g for 1 hour at 4 °C. The supernatant and pellet fractions of one aliquot were separated and set aside. The pellet of the second aliquot was resuspended in 0.1 M sodium carbonate pH 11 using a Dounce homogenizer and then centrifuged as above. Both sets of supernatant and pellet fractions

were prepared in SDS-containing buffer and analyzed by immunoblotting. Amounts of sample loaded were normalized to that of the crude trophozoite lysate.

Stability assays

Recombinant PfA-M1 (77 ng) was diluted from a stock solution into 100 mM buffer (Tris-HCl, pH 8.5 and 8.0, sodium HEPES pH 7.5, sodium MES pH 5.5, sodium acetate, pH 5.0) containing 100 mM NaCl and 0.1% Triton X-100 to a final volume of 200 μL and incubated at 37 °C. Immediately after addition of enzyme, and at ten minute intervals thereafter, 10 μL aliquots were transferred to 140 μL of ice-cold 100 mM HEPES pH 7.5 containing 100 mM NaCl and 0.1 % Triton X-100 and stored on ice. After all samples had been collected, they were warmed to 37 °C and mixed with 50 μL of 100 mM HEPES pH 7.5, 100 mM NaCl, 0.1 % Triton X-100 containing 300 mM arginyl-β-naphthylamide (Arg-bNA) and changes in fluorescence were monitored as described in "Enzyme assays and kinetic analyses".

Enzyme assays and kinetic analyses

To assess the effects of pH on steady state kinetic parameters, recombinant PfA-M1 (116 ng) was added to solutions of 100 mM buffer (sodium acetate pH 5.0; sodium MES pH 5.5, 6.0 or 6.5; sodium HEPES pH 7.0 or 7.5; Tris-HCl pH 8.0 or 8.5) containing 0.1% Triton X-100, 4% dimethyl sulfoxide, sufficient NaCl to bring the total ionic strength to 150 mM, and Arg-bNA concentrations between approximately $0.2K_M$ and $5K_M$. Assays were carried out in 200 μL final volumes at 37 °C. Changes in fluorescence were detected using a Victor^3 microplate fluorometer (PerkinElmer) with excitation and emission wavelengths of 340 and 410 nm, respectively. Kinetic parameters were determined by non-linear regression fit to the Michaelis-Menten equation $n = Vs/(K_m + s)$ using Kaleidagraph 4.1 (Synergy Software) where V is the limiting velocity and s is the substrate concentration. k_{cat} was calculated from the relationship $V = k_{cat}[E]$. In some cases, substrate inhibition was observed; therefore, initial rates were fit to the equation for uncompetitive substrate inhibition, where $n = Vs/(K_m + s + s^2/K_{si})$ and K_{si} is the inhibition constant. Inhibition of PfA-M1 by bestatin and bestatin methyl ester was assayed at pH 5.5 and pH 7.5 and inhibition constants were calculated using the Dixon method (45).

Mass spectrometry

Purified native PfA-M1 preparations enriched in p120 or p68/p35 were resolved on a denaturing, reducing 7.5% polyacrylamide gel. Gel slices containing individual PfA-M1 polypeptides (p120, p68 or p35) were treated with 10 ng/μl trypsin or endoproteinase Glu-C in 25 mM ammonium bicarbonate overnight at 37 ºC. The digests were analyzed on a 4800 MALDI TOF/TOF mass spectrometer (Applied Biosystems) with a matrix of 4 mg/ml α-cyano-4-hydroxy cinnamic acid in 50% (v/v) acetonitrile supplemented with 0.2% (v/v) trifluoroacetic acid and 20 mM ammonium citrate. A mass spectrum was obtained for each digest in reflector positive operating mode for the mass to charge range of 800 to 4000, averaging data from approximately 1000 individual laser shots. Tandem mass spectra were then obtained for significant peaks observed in the MS spectrum utilizing the MS/MS 1kV positive operating mode. Each tandem mass spectrum was typically the sum of approximately 1500 individual laser shots. A peak list for each digest was generated using 4000 Series Explorer software. Peak lists were submitted to a local Mascot Server v. 2.2 (Matrix Science Inc.) search engine using a database containing PfA-M1. The tandem mass spectra were also validated manually by ensuring that the spectra contained at least four consecutive -y or -b ions matching the predicted amino acid sequence.

RESULTS

Cellular distribution of PfA-M1

To assess the cellular distribution of endogenous, untagged PfA-M1 at high ultrastructural resolution, we localized the enzyme by cryo-immunoelectron microscopy using polyclonal affinity purified anti-PfA-M1 antibodies. Labeled parasite sections clearly reveal that PfA-M1 is present throughout the lumen of the food vacuole and in the nucleus (Fig. 3-1A and Supplemental Fig. 3-S2). The few gold particles observed outside of these two compartments might represent newly-synthesized PfA-M1 prior to delivery to the food vacuole or nucleus. A similar distribution of PfA-M1 was observed in immunofluorescence assays with parasites fixed with either paraformaldehyde/glutaraldehyde (Fig. 3-1B) or in 1:1 methanol/ethanol (Supplemental Fig. 3-S3). In contrast, fixation conditions that were close to those used previously to localize PfA-M1 (e.g., 25% methanol/75% acetone, -20 °C; (15,17)) yielded a diffuse distribution across the parasite (data not shown). This result suggests that the previously-

reported apparent cytosolic distribution (15,17) might stem from the use of fixation conditions that did not effectively preserve the relevant cellular compartments.

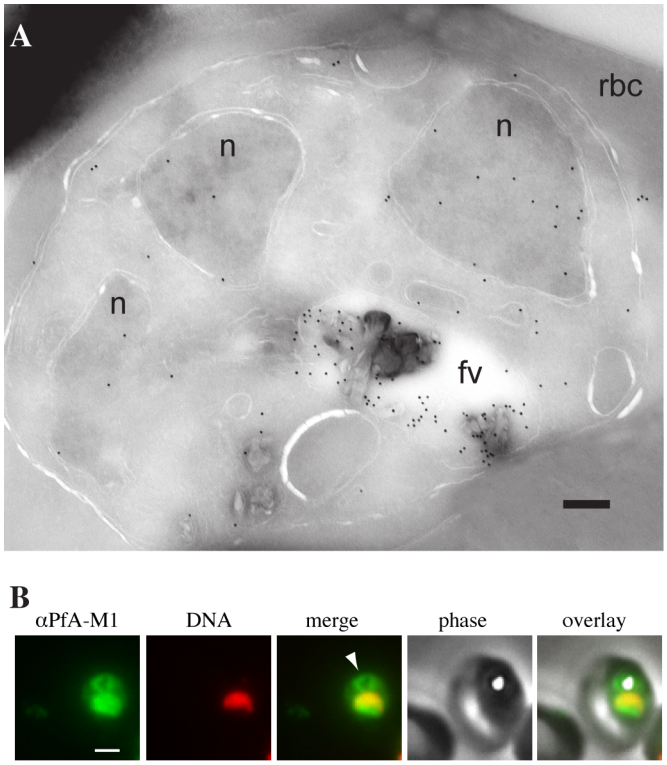

Figure 3-1: Localization of PfA-M1 in intraerythrocytic *P. falciparum*. (A) Detection of PfA-M1 in a parasite cryosection with affinity purified anti-PfA-M1 antibodies. fv, food vacuole; n, nucleus; rbc, red blood cell. Scale bar, 250 nm. (B) Localization of PfA-M1 in an aldehyde-fixed parasite by indirect immunofluorescence. Anti-PfA-M1 fluorescence is pseudocolored green and DAPI fluorescence (DNA) is pseudocolored red. Food vacuole fluorescence is identified by co-localization with the hemozoin crystal in the phase image (bright spot internal to the parasite) and is indicated with an arrowhead in the "merge" image. Scale bar, 1 mm.

PfA-M1 contains a unique, 194-amino acid N-terminal extension (NTE) that precedes the catalytic domains (Suppl. Fig. 3-S4). This sequence is present in PfA-M1 orthologs from other *Plasmodium* species but, unlike the catalytic domains, is not highly conserved (Suppl. Fig. 3-S4). One feature that is conserved is a hydrophobic stretch of amino acids near the N-terminus that could serve as a signal for translocation into the endoplasmic reticulum. One possible role for the NTE could be to mediate the dual targeting of PfA-M1 to the vacuole and the nucleus. To determine whether the PfA-M1 NTE contains targeting information, we fused this sequence to yellow fluorescent protein (YFP) and introduced the fusion into the parasite genome by Bxb mycobacteriophage integrase-mediated recombination ((42); Suppl. Fig. 3-S1A). Transgene

expression was driven by the PfA-M1 promoter from a single copy of the expression cassette. Confocal live-cell imaging revealed the presence of YFP in both the food vacuole and the cytosol (Fig. 3-2B). Thus, the PfA-M1 NTE appears to direct a dual distribution of the protein. The accumulation of the NTE-YFP fusion in the cytosol rather than the nucleus suggests that a nuclear localization signal resides outside of the NTE (i.e., in the four M1-family domains of PfA-M1). While the intensity of food vacuole fluorescence may appear to be low, the fluorescent form of YFP is in equilibrium with a protonated, non-fluorescent form with a pK_a of 5.7 (43). If the cytosol has a pH of 7.2 and the vacuole a pH of 5.2 (both values were previously reported using a pH-sensitive GFP variant (29)) then the difference in pH will diminish the vacuolar fluorescence intensity by about 3-fold.

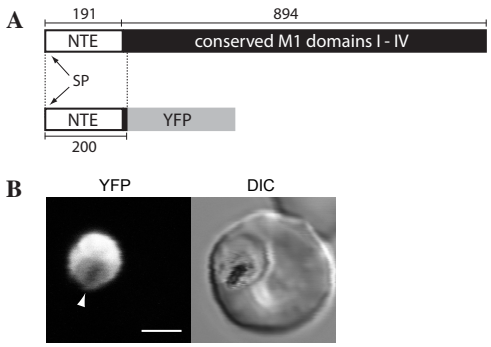

Figure 3-2: Localization of a PfA-M1 N-terminal extension (NTE)-YFP fusion. (A) Schematic diagram of full-length PfA-M1 (upper) and of the PfA-M1 NTE-YFP fusion (lower). The location of the signal peptide (SP) in the NTE is indicated. Lengths of protein segments are indicated as numbers of amino acids. (B) Confocal microscopic image of a live parasite expressing the NTE-YFP reporter. The position of the food vacuole is indicated with an arrowhead. The dark area in the center of the vacuole likely results from the exclusion of YFP by the hemozoin crystal. Note that YFP is substantially less fluorescent at the acidic pH of the vacuole (see text). DIC, differential interference contrast. Scale bar, 3 mm.

Characterization of endogenous PfA-M1 polypeptides

Polyclonal antibodies against recombinant PfA-M1 recognized three polypeptides in SDS protein extracts of whole trophozoites (Fig. 3-3A). Two of these, named p120 and p68, have been described previously (15). A third species, designated p35, was detected with our antibody. To gain insight into the nature of the p120, p68 and p35 species, they were purified from saponin-treated parasites, resolved on an SDS-polyacrylamide gel, digested with trypsin or endoproteinase Glu-C and subjected to tandem mass spectrometry. Results for all three species

are presented in Supplemental Fig. 3-S5 and Supplemental Table 3-S1. Peptides from p120 mapped to all four conserved domains of PfA-M1. Peptides obtained from p68 corresponded to sequences in domains I, II, III and the first 40 residues of domain IV but not to the C-terminal 290 amino acids of domain IV. Rather, all peptides originating from the p35 fragment were located in the C-terminal 290 residues of domain IV. These data suggest that the p68 and p35 polypeptides are N- and C-terminal fragments of PfA-M1, respectively. One peptide from the tryptic p35 digest appeared to derive from the amino terminus of the p35 fragment, as the first residue of this peptide (Leu796) followed an Asn residue rather than the Arg or Lys residue expected for trypsin cleavage (Supplemental Table 3-S1). In the crystal structure of recombinant PfA-M1, Leu796 lies in a loop between two domain IV a-helices (18) and appears to be accessible to proteolysis. Cleavage at Leu796 would produce a C-terminal polypeptide with a predicted mass of 34.2 kDa, which agrees well with the mobility of this fragment on denaturing, reducing polyacrylamide gels (Fig. 3-3A). We therefore propose that the p68 and p35 fragments are generated by proteolytic cleavage within the loop sequence containing Leu796. No peptides from the NTE were recovered in our study; however, anti-peptide antibodies that were raised against the NTE (residues 111-123) recognize p120 but not p68 (15). Thus, the p120 species appears to retain at least some of the PfA-M1 NTE (Fig. 3-3D; (15)).

We next investigated the distribution of the p120 and p68/p35 species in the nucleus and food vacuole. We have previously generated a parasite line in which the genomic copy of the PfA-M1 coding sequence was modified to encode a C-terminal hemagglutinin (HA) epitope tag (24). Immunofluorescence localization with anti-HA antibodies revealed the presence of PfA-M1-HA in the nucleus; however, the HA tag was not present in the food vacuole, presumably due to its cleavage and degradation by vacuolar proteases (24). To determine whether p120 and/or p35 retained the HA tag (p68, being an N-terminal fragment, would not possess the tag), SDS extracts of parasites expressing PfA-M1-HA were subjected to immunoblotting with anti-HA antibody. Only p120 possessed the HA tag (Fig. 3-3A), which suggests that this species is the nuclear form of PfA-M1. We then hypothesized that p68/p35 is the vacuolar form of PfA-M1, based on the proteolytic cleavage in the domain IV loop and the loss of the HA tag from p35 derived from PfA-M1-HA. If this is the case, p68/p35 should be enriched with respect to p120 in food vacuole preparations. The amounts of p120 and p68 were compared in saponin-treated trophozoites and in food vacuoles. The p68 species was enriched 5-fold over p120 in the food

vacuole preparations compared to whole trophozoites (Fig. 3-3B). The presence of residual p120 in the food vacuole preparations was likely due to incomplete elimination of intact trophozoites. Together, these results suggest that p120 and p68/p35 inhabit different subcellular compartments. We propose that p120 is the nuclear isoform of PfA-M1 and that p68/p35 is the vacuolar isoform.

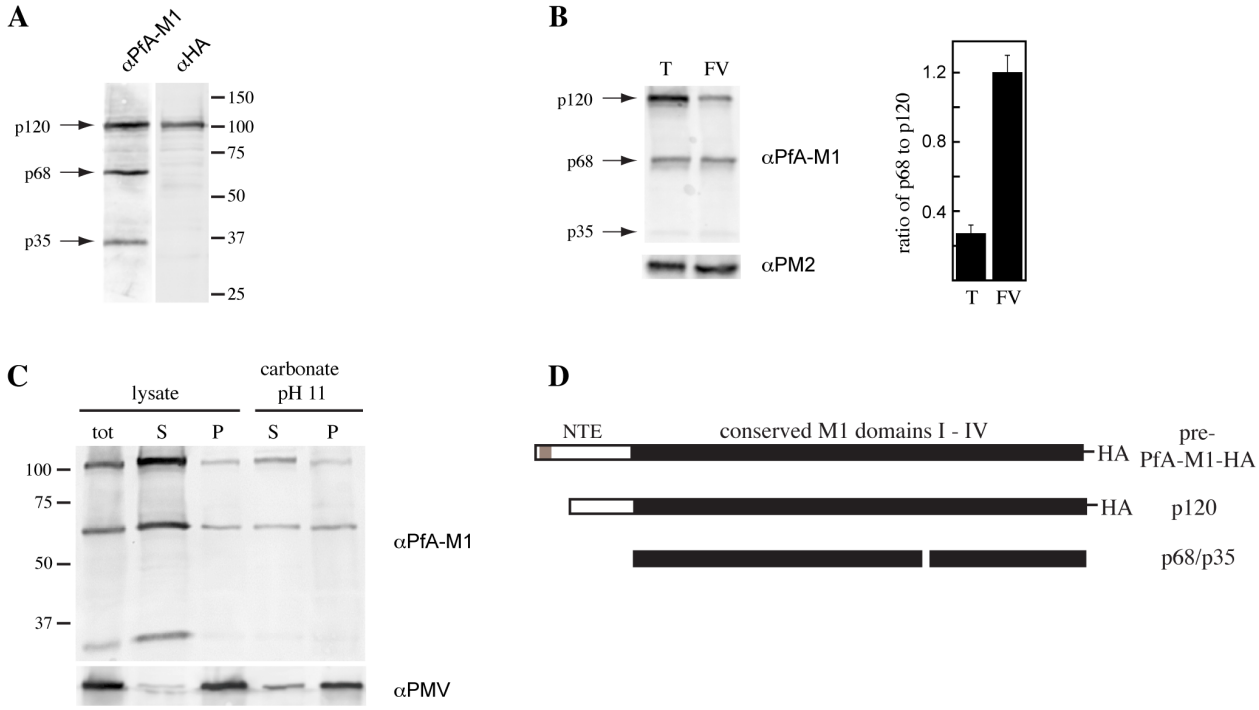

Figure 3-3: Characterization of PfA-M1 isoforms. (A) Immunoblots of an SDS extract of proteins from trophozoite-stage parasites expressing HA-tagged PfA-M1 (designated PfA-M1-HA). Left lane: anti-PfA-M1 blot showing the three major PfA-M1 polypeptides, p120, p68 and p35 (indicated with arrows at left). Right lane: the same extract probed with an anti-HA antibody. Sizes of markers are indicated at right. (B) Comparison of the relative abundance of p68 and p120 in trophozoites and enriched food vacuoles. *Left side:* Immunoblots of SDS extracts of proteins from saponin-treated trophozoites (T) and enriched food vacuoles (FV). The three PfA-M1 species (upper panel) are indicated with arrows at left. A control blot (lower panel) reveals similar levels of the food vacuole marker plasmepsin II (aPMII; lower panel) in both lanes. *Right side:* Signal intensities of p68 and p120 bands were determined from immunoblots and expressed as a p68:p120 ratio for comparison. Error bars are the standard deviation from three independent trophozoite/food vacuole preparations. (C) Fractionation of a crude lysate of saponin-treated trophozoites (lys) into soluble (S) and pellet (P) fractions. A membrane pellet was further fractionated into high pH-carbonate soluble and insoluble pellet fractions. The upper panel was developed with anti-PfA-M1 serum. The lower panel was probed with anti-plasmepsin V (aPMV) to demonstrate that an integral membrane protein associates with the pellet but not the soluble fractions. (D) Schematic models of full-length, HA-tagged PfA-M1 (pre-PfA-M1-HA) and the p120 and p68/p35 isoforms incorporating the data presented here and in Allary *et al* (15). N-terminal sequences of p120 and p68 have not been experimentally determined and are therefore estimates. The N-terminal residue of p35 is indicated with an arrow. The NTE is represented as an open box with the signal peptide indicated by the gray region.

Because pre-PfA-M1 has a putative signal anchor/transmembrane domain close to the amino terminus of the NTE (Suppl. Fig. 3-S4; (16)), we examined whether p120 or p68/p35 was associated with membranes. Immunoblot analysis of soluble and membrane fractions from a lysate of saponin-treated trophozoites revealed that most of the p120 and p68/35 resides in the soluble fraction (Fig. 3-3C). Much of that remaining in the membrane fraction was released by high pH carbonate treatment, which implies a peripheral interaction with membranes. As a control, the fractionation of plasmepsin V was analyzed and this single-transmembrane helix integral membrane protein (39) was found to reside mainly in the carbonate-insoluble membrane fraction (Fig. 3-3C).

Comparison of steady-state kinetic parameters of recombinant PfA-M1 and native PfA-M1 isoforms

Native PfA-M1 was obtained from saponin-treated trophozoites that express an HA-tagged form of the M17-family leucine aminopeptidase PfLAP (24). PfLAP and PfA-M1 both catalyze the hydrolysis of fluorogenic aminopeptidase substrates (46); thus, the presence of PfLAP could potentially confound a kinetic analysis of PfA-M1. Purification of PfA-M1 to near homogeneity was achieved by ion exchange and size exclusion chromatography (Suppl. Fig. 3-S6). PfLAP was separated from PfA-M1 on the first ion exchange column (Suppl. Fig. 3-S6). The p68 and p35 polypeptides co-eluted on the size exclusion column, which suggests that these two species form a stable complex. The p120 isoform of PfA-M1 was partially resolved from p68/p35, which enabled the isolation of fractions highly enriched in either p120 or p68/p35 (Suppl. Fig. 3-S6). To generate recombinant PfA-M1, residues 192 to 1085 were fused to an N-terminal hexahistidine tag followed by a tobacco etch virus (TEV) protease site and expressed in *E. coli*. The PfA-M1 N-terminal extension was omitted from the recombinant protein to best represent the p68/p35 vacuolar isoform, which has lost much of the NTE (15). After metal affinity chromatography, the hexahistidine tag was removed by TEV protease treatment and the cleaved protein was further purified (Suppl. Fig. 3-S6).

The steady-state parameters for hydrolysis of the amide bond in the fluorogenic substrate arginyl-b-naphthylamide (Arg-bNA) at pH 7.5 and 37 °C were determined for p68/p35, p120 and recombinant PfA-M1 (Table 3-1). The p68/p35 and p120 isoforms had very similar values of k_{cat}, K_m and k_{cat}/K_m, which indicates that neither the presence of an extended NTE in p120 nor the

cleavage that takes place to generate the p68 and p35 fragments has a dramatic effect on catalysis. The catalytic efficiency of recombinant PfA-M1 at pH 7.5 was identical within experimental error to that of p68/p35. Because the quantities of purified native enzyme were very limited, analysis of the effects of pH on PfA-M1 activity was conducted with the recombinant enzyme.

Table 3-1: Kinetic parameters for native and recombinant PfA-M1. The far right column is the ratio of kcat/Km at pH 7.5 to that at pH 5.5 for the indicated substrate. rPfA-M1, recombinant PfA-M1.

Enzyme	Substrate	pH	K_M (μM)	k_{cat} (s^{-1})	k_{cat} / K_M ($M^{-1} \bullet s^{-1}$)	k_{cat} / K_M 7.5: 5.5
p68/p35	Arg-βNA	7.5	86 ± 1	11 ± 1.1	(1.3 ± 0.1) x 10^5	
p120	Arg-βNA	7.5	110 ± 10	9.3 ± 1.0	(8.5 ± 1.1) x 10^4	
rPfa-M1	Arg-βNA	7.5	170 ± 10	21 ± 2	(1.2 ± 0.1) x 10^5	14 ± 1
		5.5	1100 ± 300	9.4 ± 0.8	(8.7 ± 2.4) x 10^3	
	Ala-βNA	7.5	210 ± 10	36 ± 2	(1.7 ± 0.1) x 10^5	46 ± 3
		5.5	4400 ± 400	16 ± 1	(3.7 ± 0.1) x 10^3	

Effects of pH on PfA-M1 stability, catalysis and inhibition

Most experimental determinations of food vacuole pH fall in the range 5.2 to 5.7 (26-29). To assess the feasibility of a catalytic role for PfA-M1 in the food vacuole, the stability of PfA-M1 activity at 37 °C over the pH range 5.0 to 8.5 was determined. PfA-M1 exhibited high stability within this range (Fig. 3-4A), with ≥ 90% of the starting activity remaining after one hour at all pH values tested.

Steady-state parameters for cleavage of Arg-bNA by PfA-M1 were determined over the pH range 5.5 to 8.5. The turnover number (k_{cat}) was not strongly affected by pH; this parameter was unchanged over the pH range 6.0 to 8.0, and dropped by a factor of two at pH 5.5 (Fig. 3-4B). In contrast, the Michaelis constant (K_m) increased below pH 6.5 and was 7-fold higher at pH 5.5 than at pH 7.5 (Fig. 3-4C, Table 3-1). The net effect of these changes on the catalytic efficiency (k_{cat}/K_m) was a ten-fold decrease at pH 5.5 *vs*. 7.5; however, the catalytic efficiency at pH 5.5 nevertheless remained high at ~10^4 $M^{-1}\bullet s^{-1}$. The catalytic efficiency at pH 5.0 (estimated by using a substrate concentration that is much lower than the K_m value) was over a magnitude lower than that at pH 5.5 but still greater than 10^2 $M^{-1}\bullet s^{-1}$ (Fig. 3-4D). These data suggest that the major effect of decreasing pH to 5.5 is on the interaction of substrate with enzyme. Because the substrate used in these analyses, Arg-bNA, has a positively-charged sidechain, it was possible

that the effect of pH on catalysis was due to enzyme-sidechain interactions. Thus, we examined the effect of pH on cleavage of alanyl-b-naphthylamide. The decrease in catalytic efficiency at pH 5.5 compared to 7.5 was a similar order of magnitude as that with arginyl-b-naphthylamide (Table 3-1), which indicates that ionizable groups other than that in the substrate sidechain are responsible for the observed pH effects.

To further probe the relationship between pH and substrate-enzyme interaction, we evaluated the effect of pH on inhibition of PfA-M1 by the substrate analogs bestatin and bestatin methyl ester. The inhibition constant (K_i) for bestatin increased 30-fold at pH 5.5 compared with pH 7.5 (Table 3-2). To determine whether the negative charge of the C-terminal carboxylate group of bestatin contributed to the pH effect, K_i values were determined for a variant of bestatin in which the carboxylate group was methylated and therefore uncharged. The potency of bestatin methyl ester was somewhat reduced relative to that of bestatin at both pH 5.5 and 7.5; however, the change in potency of bestatin methyl ester at pH 5.5 *vs*. 7.5 was about the same as that for bestatin (Table 3-2).

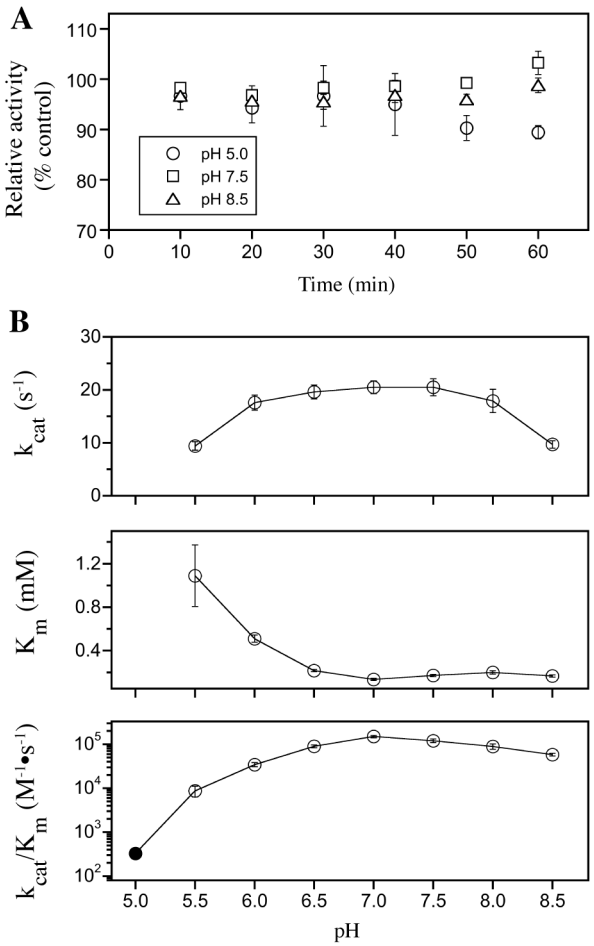

Figure 3-4: Effects of pH on PfA-M1 stability and steady state kinetic parameters. (A) Stability of PfA-M1 at pH 5.0 (circles), pH 7.5 (squares) and pH 8.5 (triangles) was assessed by incubating enzyme for the indicated times and pH values at 37 °C and measuring residual activity at pH 7.5. Error bars are standard deviations from triplicate experiments. (B) Effect of pH on steady-state parameters for the hydrolysis of Arg-b-NA at 37 °C and a constant ionic strength of 150 mM. Open circles: parameters were obtained by fitting rate data to the Michaelis-Menten equation or to an equation describing uncompetitive substrate inhibition (see Experimental Procedures). Filled circle: estimate of k_{cat}/K_m under conditions where the [S] >> K_m. Error bars are the standard deviation from triplicate experiments. Note that the ordinate has a linear scale in the k_{cat} and K_m plots and a logarithmic scale in the k_{cat}/K_m plot.

Table 3-2: Effect of pH on PfA-M1 inhibition.
The far right column is the ratio of the Ki at pH 5.5 to that at pH 7.5.

Inhibitor	pH	K_i (μM)	K_i 5.5 : 7.5
bestatin	7.5	0.12 ± 0.2	32 ± 7
	5.5	3.8 ± 0.5	
bestatin-OMe	7.5	0.48 ± 0.4	46 ± 7
	5.5	22 ± 3	

DISCUSSION

Aminopeptidases of the M1 family have evolved to fill a broad spectrum of biological roles in all three domains of life. In humans, M1 family members are key mediators of blood pressure regulation, neuropeptide levels and antigen processing, to name just a few examples (47). Our studies reveal that the sole M1-family aminopeptidase in *P. falciparum*, PfA-M1, has been recruited to fulfill specific roles in the physiology of the intraerythrocytic parasite. We propose that one of these roles is the generation of amino acids from globin peptides in the food vacuole lumen. The accumulation of PfA-M1 in the nucleus implies a second function, the details of which remain to be elucidated. These roles differ from what has been proposed previously for this protein. In this section, we interpret our results alongside those from prior studies.

Early immunofluorescence localization studies of PfA-M1 indicated a cytosolic distribution with possible accumulation around the food vacuole (15,17). In a previous study, we tagged endogenous PfA-M1 with YFP and localized the fusion in live parasites (24). The YFP tag was observed to concentrate in two subcellular structures, the food vacuole and the nucleus. To resolve the discrepancy between these and the earlier results, we undertook immunoelectron and immunofluorescence studies of native (untagged) PfA-M1 using affinity-purified polyclonal antibodies. These analyses support our earlier conclusion that PfA-M1 resides primarily in the food vacuole and the nucleus. Importantly, the immunoelectron microscopy and membrane fractionation studies revealed that PfA-M1 is a soluble enzyme distributed throughout the lumen of the food vacuole. It therefore seems unlikely that PfA-M1 is anchored into the food vacuole membrane with the catalytic domains outside the vacuole or in vacuole-associated vesicles, as has been previously proposed (16,25). By examining a range of fixation conditions for indirect immunofluorescence, we also observed vacuolar and nuclear concentrations of PfA-M1 with this technique. However, some fixation conditions appeared not to preserve the relevant subcellular structures, giving rise to a diffuse distribution of PfA-M1 that could be interpreted as cytosolic.

To determine whether the 194-residue PfA-M1 N-terminal extension contributed to dual vacuolar/nuclear targeting, we introduced an NTE-YFP fusion into parasites in monocopy with expression driven by the PfA-M1 5' untranslated region. YFP was present in the food vacuole of transfected parasites, which indicates that the NTE is sufficient for trafficking to this organelle. Interestingly, a fusion of the first 30 amino acids of the NTE (which contains a putative signal

anchor) to green fluorescent protein resulted in the expression of an integral membrane protein that is trapped in the endoplasmic reticulum (16). Thus, it appears that the signal anchor directs entry into the endoplasmic reticulum. Further transit to the food vacuole may require the presence of a longer NTE, which may be needed for cleavage of the signal anchor and may provide a vacuolar targeting signal. In our study, the NTE-YFP fusion did not concentrate in the nucleus; rather, the protein appeared to have a diffuse, cytosolic distribution in addition to the vacuolar pool. This result indicates that a subpopulation of the NTE-YFP fusion avoids translocation into the ER. Furthermore, it appears that the sequence that causes PfA-M1 to localize to the nucleus resides in the catalytic region of PfA-M1, which was not present in this fusion. It has been reported that the episomal expression of an N-terminally truncated form of PfA-M1 in *P. falciparum* generates a cytosolic distribution with no protein in the food vacuole (18). We suggest that the absence of important targeting information from this truncated form of PfA-M1 accounts for the lack of vacuolar protein.

Previously, three isoforms of PfA-M1 have been reported: p120, p96 and p68. We have identified a new species, p35, and demonstrate that p68 and p35 are N- and C-terminal fragments of PfA-M1, respectively. The p68 and p35 species, which are generated by proteolytic cleavage of a domain IV loop, remain associated during purification and exhibit catalytic activity that is very similar to that of the p120 species. A schematic diagram of p120 and p68/p35 isoforms that is consistent with existing data is shown in Fig. 3-3D. We propose that the p120 form resides in the nucleus and that the p68/p35 complex inhabits the food vacuole, based on the selective retention of a C-terminal HA tag in p120 and its depletion relative to p68 from enriched food vacuole preparations. The p96 isoform of PfA-M1 was initially thought to arise from artifactual proteolytic cleavage of p120 (15) but more recently it has been suggested that p96 is generated in the parasitophorous vacuole during trafficking to the food vacuole (16). We do not observe PfA-M1 in the parasitophorous vacuole in live cells expressing PfA-M1-YFP or in fixed parasites analyzed by immunofluorescence; however, it is possible that the sensitivity of these experiments is inadequate to detect low amounts of protein. We do sometimes observe the p96 species in immunoblots of parasite lysate and PfA-M1 purifications (Suppl. Fig. 3-S6A, B) but the amounts are minor in comparison to p120 and p68/p35.

It has been asserted that PfA-M1 does not have adequate activity at pH values below 6 to function as a catalytic aminopeptidase within the food vacuole (16,18,25). Reflecting this line of

thinking, the enzyme has been referred to as a "neutral" aminopeptidase (46). To assess the validity of this proposal, we undertook a detailed kinetic characterization of the catalytic properties of PfA-M1 over the pH range 5.0 to 8.5. Importantly, enzyme activity was highly stable at 37 °C throughout this pH range. The k_{cat} for PfA-M1-catalyzed hydrolysis of fluorogenic substrates is relatively insensitive to pH, whereas the K_m increases steeply as the pH drops below 6.5. At pH values below 5.5, the K_m was too high to permit individual measurement of k_{cat} and K_m; however, an estimate of k_{cat}/K_m at pH 5.0 indicates that this parameter continues to decline below pH 5.5. Importantly, however, the k_{cat}/K_m was greater than 10^2 $M^{-1} \bullet s^{-1}$ at pH 5.0 and around 10^4 $M^{-1} \bullet s^{-1}$ at pH 5.5. For comparison, the k_{cat}/K_m values for the hydrolysis of several peptide substrates by *P. falciparum* aminopeptidase P, an enzyme also located in the food vacuole, are around 10^4 $M^{-1} \bullet s^{-1}$ at pH 5.5 (13). Given that most experimental measurements of food vacuole pH fall into the range of 5.2 to 5.7 (26-29), it would appear that the catalytic efficiency of PfA-M1 is sufficient for a role in the production of amino acids from globin-derived peptides. The *in vivo* substrates of PfA-M1 are unknown but likely consist of a diverse pool of di- and oligopeptides generated by vacuolar enzymes including falcilysin, dipeptidyl aminopeptidase 1 and aminopeptidase P (10-13). The kinetic parameters for cleavage of physiological substrates could be even more favorable than those reported here for a non-natural, fluorogenic substrate. Our data support a model for hemoglobin catabolism in which amino acids are generated in the food vacuole lumen. We cannot exclude the possibility that some (di)peptides move from the vacuole lumen to the cytosol; however, it seems unlikely that peptide transport is an obligate step for amino acid production. Rather, our model leads to the prediction of one or more amino acid transporters in the food vacuole membrane.

So why has it been reported that PfA-M1 has negligible activity at pH values below 6 (18)? Prior analyses of the pH-activity relationship were conducted with a single concentration of a fluorogenic substrate and the results were reported as fractional activity (16,18). These types of studies do not yield the catalytic efficiency of the enzyme and may lead to unwarranted conclusions (48). Our data are consistent with the proposal that PfA-M1 does not operate at its pH optimum at the acidic pH of the food vacuole. The relevant question, however, is not whether activity is optimal but rather whether it is sufficient for the purpose at hand. In this regard, we believe that the observation that k_{cat} does not change dramatically down to pH 5.5 is a key insight, as the pH-dependent increase in K_m can be compensated for by high substrate

concentrations. Indeed, the concentration of the hemoglobin tetramer in the erythrocyte cytosol is 5 mM (49), which likely leads to high micromolar/low millimolar concentrations of peptides in the vacuole. It is plausible that this high concentration drives substrate binding to PfA-M1 and leads to the efficient generation of amino acid products. PfA-M1 is not the first M1-family aminopeptidase for which a role in an acidic environment is proposed; the mammalian enzyme aminopeptidase B processes neuropeptides in acidic secretory vesicles and retains substantial activity at pH 5 (50).

Why does the substrate K_m increase with pH? The pH dependence of inhibition by bestatin and bestatin methyl ester provides a clue. A co-crystal structure of PfA-M1 with bestatin reveals that the positively-charged amino terminus of the inhibitor interacts with a pair of glutamate sidechains in the active site (18). One explanation for the increase in inhibitor K_i and substrate K_m at acidic pH could be the protonation of one or both of these glutamates, which would likely destabilize the enzyme-substrate or enzyme-inhibitor complex. These results have important implications for inhibitor discovery against this enzyme. Efforts to identify new inhibitor chemotypes (for example, by high-throughput screening) should be carried out at pH ~5.5 to best represent the electrostatic environment of the active site as it occurs in the food vacuole.

A lingering question is the role of PfA-M1 in the nucleus. At present, it is not possible to propose a specific function; however, there are interesting precedents for participation of M1-family aminopeptidases in nuclear processes. Mammalian puromycin-sensitive aminopeptidase (PSA) has been localized to the nucleus and was found to associate with mitotic spindles (51). Interestingly, the PSA inhibitors puromycin and bestatin inhibited DNA synthesis and blocked the cell cycle in cultured COS cells. Homologs of PSA have also been implicated in homologous recombination during meiosis in plants (52) and in meiotic exit and anteroposterior axis formation in *Caenorhabditis elegans* (53). Investigation into the role of PfA-M1 in the *P. falciparum* nucleus is in progress.

ACKNOWLEDGEMENTS

We would like to thank K. DeCourcy for help with the confocal imaging, W. Beatty for carrying out the immunoelectron microscopy experiments, R. Helm for assistance with mass spectrometry, D. Fidock for the Bxb integrase plasmids and 3D7^{attB} parasite line, D. Goldberg for anti-PMII and anti-PMV antibodies, D. Jacobus for WR99210, M. Drew for critique of the manuscript and D. Waugh for the TEV protease expression vector. This work was supported by National Institutes of Health grant AI077638.

LIST OF ABBREVIATIONS

Ala-bNA, alanyl-b-naphthylamide; Arg-bNA, arginyl-b-naphthylamide; DAPI, 4',6-diamidino-2-phenylindole; HA, hemagglutinin; MS, mass spectrometry; NTE, N-terminal extension; PBS, phosphate-buffered saline; PSA, puromycin-sensitive aminopeptidase; TEV, tobacco etch virus; YFP, yellow fluorescent protein.

SUPPLEMENTARY INFORMATION

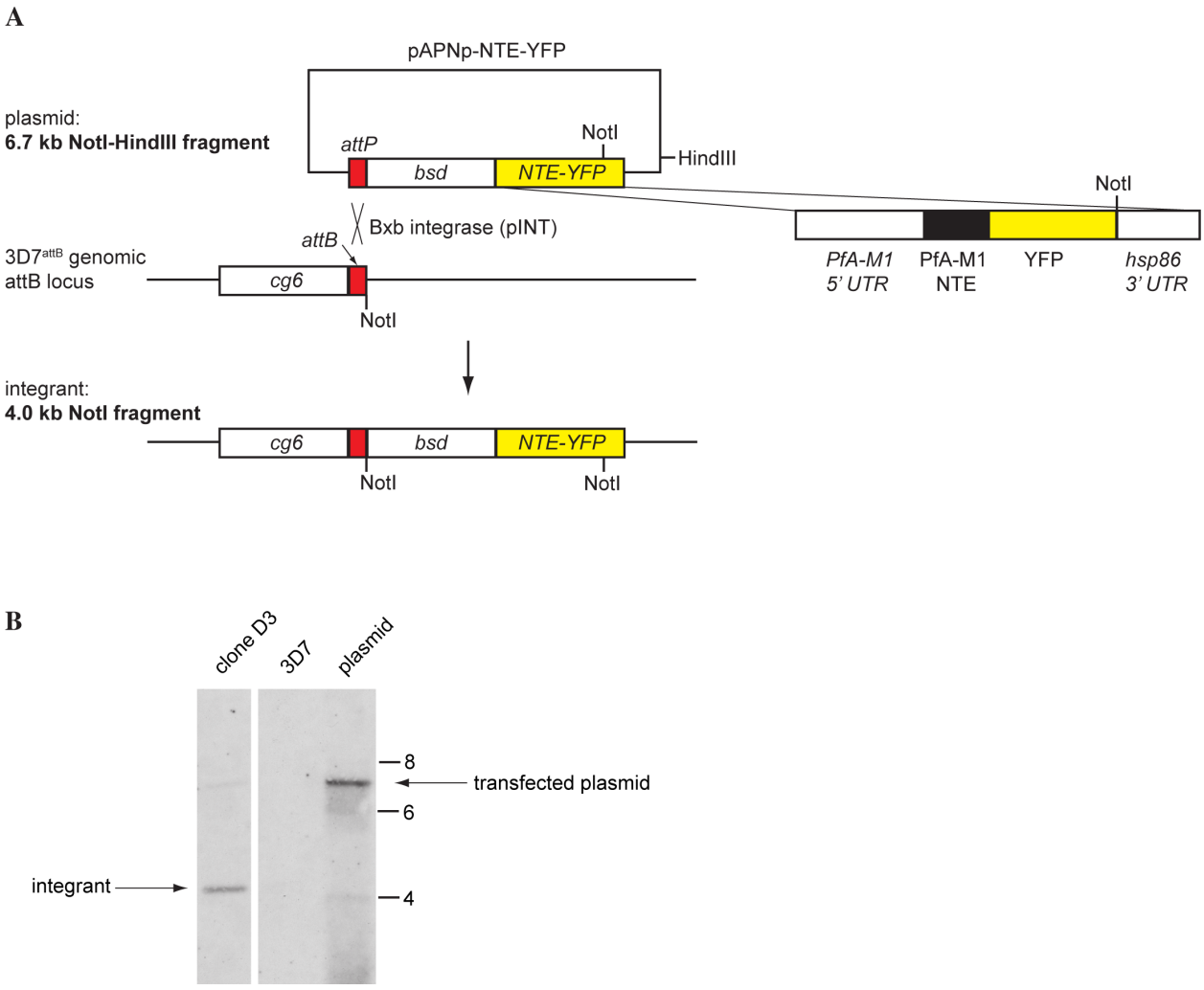

Supplemental Figure 3-S1: Creation of a parasite line (clone D3) expressing a fusion of the PfA-M1 N-terminal extension (NTE) with YFP. (A) Scheme for site-specific integration of plasmid pAPNp-NTE-YFP into the P. falciparum genome. The structure of the expression cassette is shown at the right of the plasmid. Bxb1 mycobacteriophage integrase-mediated recombination takes place between the attP element on the plasmid and the attB element that has been introduced into the cg6 locus in the parasite line 3D7attB (red boxes). Locations of HindIII and NotI sites are indicated. Expected sizes of bands after HindIII/NotI digestion are indicated at left. bsd, blasticidin resistance cassette; UTR, untranslated region. Sizes of boxes are not to scale. (B) Southern blot of total genomic DNA from parasite clone D3 and untransfected 3D7 parasites. The transfected plasmid pAPNp-NTE-YFP is in the right-most lane. The probe hybridized to the YFP coding sequence, which is absent from 3D7 parasites. Sizes of markers are indicated at right. Plasmid and integrant bands are indicated with arrows. All lanes are from the same blot and film exposure.

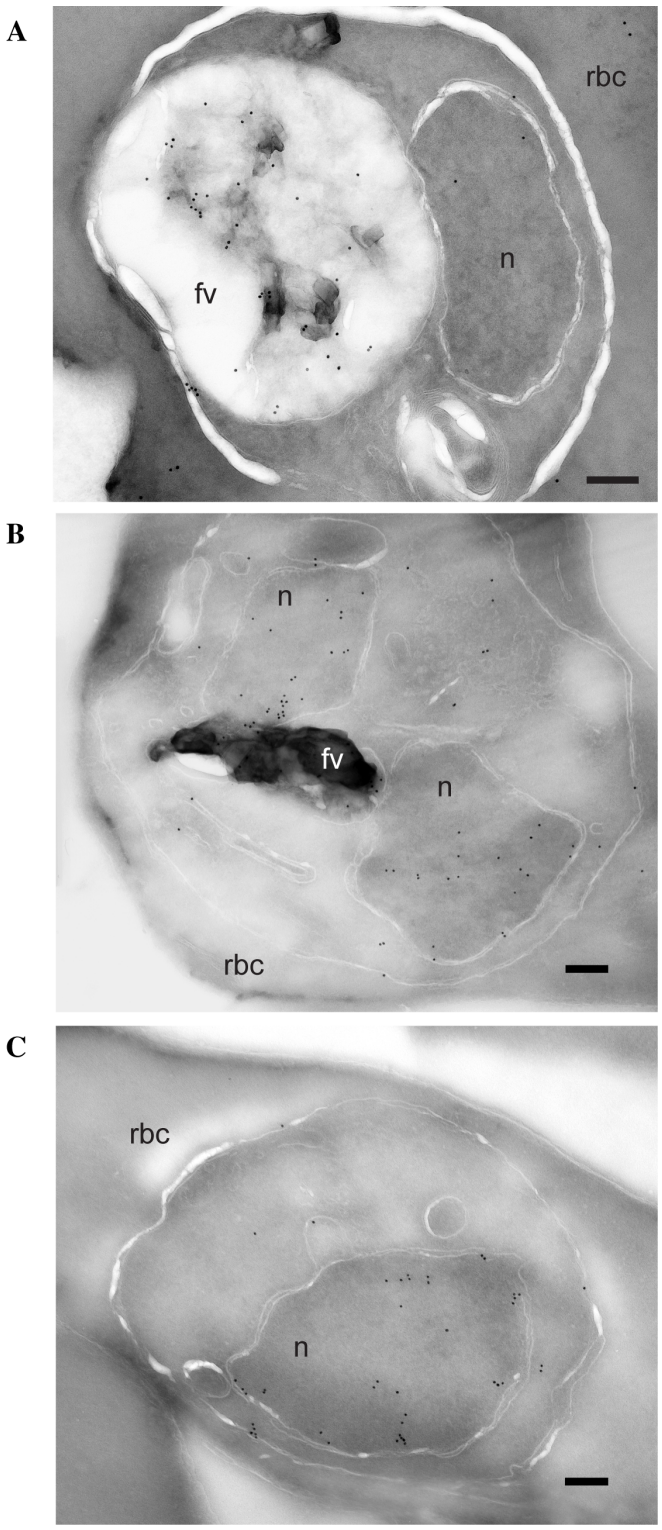

Supplemental Figure 3-S2: P. falciparum cryosections labeled with anti-PfA-M1. Note the distribution of label throughout the lumen of the food vacuole in A. B and C demonstrate labeling of the nucleus. The food vacuole does not appear in the section shown in C. fv, food vacuole; n, nucleus; rbc, red blood cell. Scale bar, 250 nm.

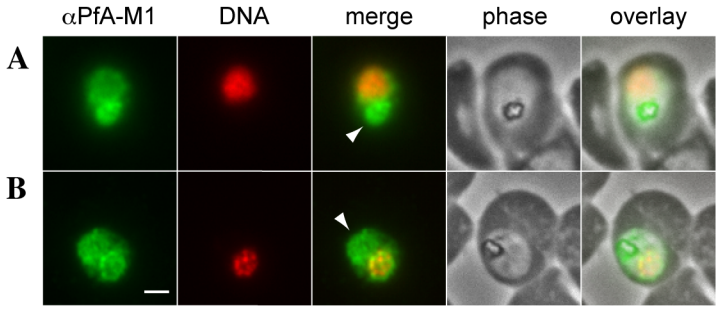

Supplemental Figure 3-S3: Immunofluorescence localization of PfA-M1 in parasites fixed with 50% methanol/50% ethanol at -20 °C. Anti-PfA-M1 fluorescence is pseudocolored green and DAPI fluorescence (DNA) is pseudocolored red. Food vacuole fluorescence is identified by co-localization with the hemozoin crystal and is indicated with an arrowhead in the "merge" image. Panel A clearly shows PfA-M1 label in the food vacuole, whereas a nuclear localization is more evident in panel B. Scale bar, 1 μm.

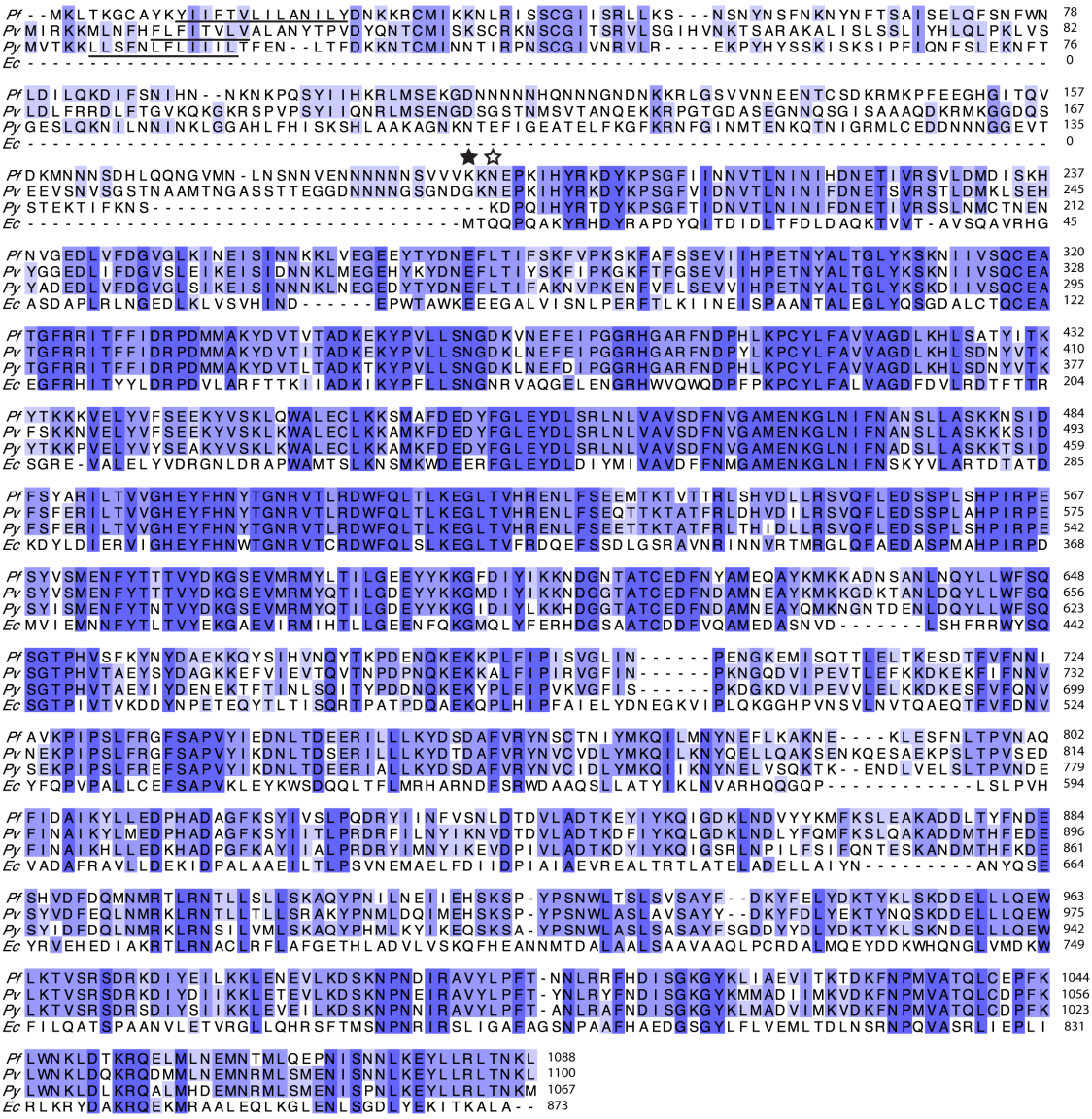

Supplemental Figure 3-S4: Alignment of PfA-M1 orthologs from P. falciparum (Pf), P. vivax (Pv) and P. yoelii (Py) with aminopeptidase N of E. coli (Ec). Conserved residues are shaded blue (darker shades indicate higher levels of conservation). The signal peptides in the Plasmodium sequences that are predicted with SignalP 3.0 are indicated with a black line. The first residue of recombinant PfA-M1 (K192) is indicated with a filled star. The last residue of the N-terminal extension (N194) is indicated with an open star. The alignment was generated with ClustalW and colored using Jalview 2.4 (AM Waterhouse et al (2009) Bioinformatics 25:1198-91).

A. p120

```
   1 MKLTKGCAYKYIIFTVLILANILYDNKKRCMIKKNLRISSCGIISRLLKSNSNYNSFNKN
  61 YNFTSAISELQFSNFWNLDILQKDIFSNIHNNKNKPQSYIIHKRLMSEKGDNNNNNHQNN
 121 NGNDNKKRLGSVVNNEENTCSDKRMKPFEEGHGITQVDKMNNNSDHLQQNGVMNLNSNNV
 181 ENNNNNNSVVVKKNEPKIHYRKDYKPSGFIINNVTLNININHDNETIVRSVLDMDISKHNV
 241 GEDLVFDGVGLKINEISINNKKLVEGEEYTYDNEFLTIFSKFVPKSKFAFSSEVIIHPET
 301 NYALTGLYKSKNIIVSQCEATGFRRITFFIDRPDMMAKYDVTVTADKEKYPVLLSNGDKV
 361 NEFEIPGGRHGARFNDPHLKPCYLFAVVAGDLKHLSATYITKYTKKKVELYVFSEEKYVS
 421 KLQWALECLKKSMAFDEDYFGLEYDLSRLNLVAVSDFNVGAMENKGLNIFNANSLLASKK
 481 NSIDFSYARILTVVGHEYFHNYTGNRVTLRDWFQLTLKEGLTVHRENLFSEEMTKTVTTR
 541 LSHVDLLRSVQFLEDSSPLSHPIRPESYVSMENFYTTTVYDKGSEVMRMYLTILGEEYYK
 601 KGFDIYIKKNDGNTATCEDFNYAMEQAYKMKKADNSANLNQYLLWFSQSGTPHVSFKYNY
 661 DAEKKQYSIHVNQYTKPDENQKEKKPLFIPISVGLINPENGKEMISQTTLELTKESDTFV
 721 FNNIAVKPIPSLFRGFSAPVYIEDNLTDEERILLLKYDSDAFVRYNSCTNIYMKQILMNY
 781 NEFLKAKNEKLESFNLTPVNAQFIDAIKYLLEDPHADAGFKSYIVSLPQDRYIINFVSNL
 841 DTDVLADTKEYIYKQIGDKLNDVYYKMFKSLEAKADDLTYFNDESHVDFDQMNMRTLRNT
 901 LLSLLSKAQYPNILNEIIEHSKSPYPSNWLTSLSVSAYFDKYFELYDKTYKLSKDDELLL
 961 QEWLKTVSRSDRKDIYEILKKLENEVLKDSKNPNDIRAVYLPFTNNLRRFHDISGKGYKL
1021 IAEVITKTDKFNPMVATQLCEPFKLWNKLDTKRQELMLNEMNTMLQEPNISNNLKEYLLR
1081 LTNKL
```

B. p68/p35

```
   1 MKLTKGCAYKYIIFTVLILANILYDNKKRCMIKKNLRISSCGIISRLLKSNSNYNSFNKN
  61 YNFTSAISELQFSNFWNLDILQKDIFSNIHNNKNKPQSYIIHKRLMSEKGDNNNNNHQNN
 121 NGNDNKKRLGSVVNNEENTCSDKRMKPFEEGHGITQVDKMNNNSDHLQQNGVMNLNSNNV
 181 ENNNNNNSVVVKKNEPKIHYRKDYKPSGFIINNVTLNININHDNETIVRSVLDMDISKHNV
 241 GEDLVFDGVGLKINEISINNKKLVEGEEYTYDNEFLTIFSKFVPKSKFAFSSEVIIHPET
 301 NYALTGLYKSKNIIVSQCEATGFRRITFFIDRPDMMAKYDVTVTADKEKYPVLLSNGDKV
 361 NEFEIPGGRHGARFNDPHLKPCYLFAVVAGDLKHLSATYITKYTKKKVELYVFSEEKYVS
 421 KLQWALECLKKSMAFDEDYFGLEYDLSRLNLVAVSDFNVGAMENKGLNIFNANSLLASKK
 481 NSIDFSYARILTVVGHEYFHNYTGNRVTLRDWFQLTLKEGLTVHRENLFSEEMTKTVTTR
 541 LSHVDLLRSVQFLEDSSPLSHPIRPESYVSMENFYTTTVYDKGSEVMRMYLTILGEEYYK
 601 KGFDIYIKKNDGNTATCEDFNYAMEQAYKMKKADNSANLNQYLLWFSQSGTPHVSFKYNY
 661 DAEKKQYSIHVNQYTKPDENQKEKKPLFIPISVGLINPENGKEMISQTTLELTKESDTFV
 721 FNNIAVKPIPSLFRGFSAPVYIEDNLTDEERILLLKYDSDAFVRYNSCTNIYMKQILMNY
 781 NEFLKAKNEKLESFNLTPVNAQFIDAIKYLLEDPHADAGFKSYIVSLPQDRYIINFVSNL
 841 DTDVLADTKEYIYKQIGDKLNDVYYKMFKSLEAKADDLTYFNDESHVDFDQMNMRTLRNT
 901 LLSLLSKAQYPNILNEIIEHSKSPYPSNWLTSLSVSAYFDKYFELYDKTYKLSKDDELLL
 961 QEWLKTVSRSDRKDIYEILKKLENEVLKDSKNPNDIRAVYLPFTNNLRRFHDISGKGYKL
1021 IAEVITKTDKFNPMVATQLCEPFKLWNKLDTKRQELMLNEMNTMLQEPNISNNLKEYLLR
1081 LTNKL
```

Supplemental Figure 3-S5: Locations in PfA-M1 of tryptic/Glu-C peptides obtained from p120, p68 and p35. (A) Sequences corresponding to peptides obtained from p120 are highlighted in blue. (B) Sequences corresponding to peptides obtained from p68 and p35 are highlighted in blue and red, respectively. Individual peptide sequences are provided in Supplemental Table 3-S1.

Supplemental Table 3-S1: Summary of tryptic/Glu-C PfA-M1 peptides identified by MS/MS.

*Pf*A-M1 isoform	*Pf*A-M1 residues	Peptide Sequence	Predicted mass (Da)	Observed mass (Da)
p120	350 - 369	KYPVLLSnGDKVNEFEIPGGR[2]	2205.1	2205.0
	360 - 369	KVNEFEIPGGR	1117.6	1117.5
	481 - 489	KNSIDFSYAR	1072.5	1072.5
	735 - 751	RGFSAPVYIEDNLTDEER	1954.9	1954.8
	757 - 764	KYDSDAFVR	972.4	972.4
	791 - 808	KLESFNLTPVNAQFIDAIK	2020.1	2020.0
	809 - 821	KYLLEDPHADAGFK	1475.7	1475.6
	822 - 831	KSYIVSLPQDR	1177.6	1177.6
	998 - 1008	RAVYLPFTNNLR	1307.7	1307.7
	1077 - 1085	EYLLRLTNKL	1133.7	1133.6
p68	238 - 252	KHNVGEDLVFDGVGLK	1598.8	1598.7
	312 - 324	KNIIVSQcEATGFR[3]	1494.7	1494.6
	350 - 369	KYPVLLSnGDKVNEFEIPGGR[2]	2205.1	2205.0
	360 - 369	KVNEFEIPGGR	1117.6	1117.5
	480 - 489	KKNSIDFSYAR	1200.6	1200.5
	481 - 489	KNSIDFSYAR	1072.5	1072.4
	541 – 548	RLSHVDLLR	952.6	952.5
	735 – 751	RGFSAPVYIEDNLTDEER	1954.9	1954.8
	757 – 764	KYDSDAFVR	972.4	972.4
	775 – 785	KQILmNYNEFLK[4]	1428.7	1428.6
p35	796 - 808	LTPVNAQFIDAIK[1]	1429.8	1429.7
	809 - 821	KYLLEDPHADAGFK	1475.7	1475.6
	822 - 831	KSYIVSLPQDR	1177.6	1177.6
	855 - 866	KqIGDKLNDVYYK[5]	1438.7	1438.6
	855 - 866	KQIGDKLNDVYYK	1455.7	1455.7
	908 - 922	KAQYPNILNEIIEHSK	1768.9	1768.8
	998 - 1008	RAVYLPFTNNLR	1307.7	1307.6
	1077 - 1085	EYLLRLTNKL	1133.7	1133.6

Cleavage occurs after underlined residue;
[1]Likely N-terminal peptide of p35 isoform: preceding residue is Asn which does not correspond to Trypsin or Glu-C specificity;
Modified residue indicated by lower case: [2]Deamidation, [3]Carbamidomethyl, [4]Oxidation, [5]N-terminal pyro-Glu.

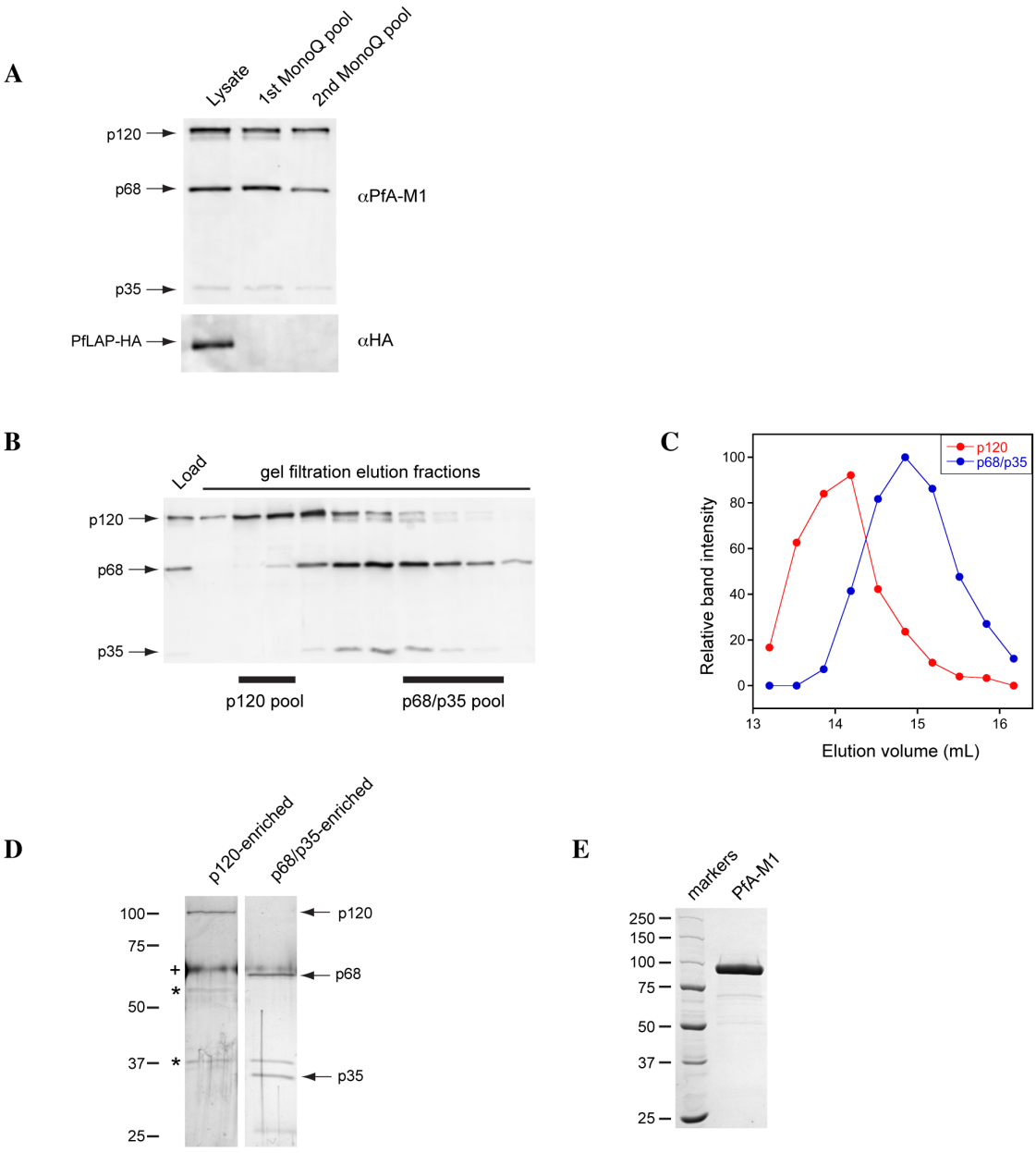

Supplemental Figure 3-S6: Purification of native and recombinant PfA-M1. (A) Separation of PfA-M1 from PfLAP-HA. Anti-PfA-M1 (upper panel) and anti-HA (lower panel) immunoblots of parasite lysate and the first two steps of the purification reveal that PfA-M1 is separated from PfLAP-HA on the first MonoQ column. Equal amounts of PfA-M1 activity were loaded in each lane. (B) Anti-PfA-M1 immunoblot of the material loaded onto a Superdex 200 size exclusion column (Load) and of eluted fractions that contained PfA-M1. Fractions that were combined into a p120-enriched pool or a p68/p35-enriched pool are indicated below the blot. (C) Quantitation of p120 and p68 band intensities from the immunoblot in (B) demonstrates partial resolution of these species. (D) Enriched p120 and p68/35 pools were resolved on a reducing SDS-polyacrylamide gel and silver stained. The positions of p120, p68 and p35 are indicated with arrows. Impurities are indicated with an asterisk. A contaminating protein that appears in the marker lane (not shown) and is probably keratin is indicated with a plus sign. Both lanes are from the same gel. (E) Purified recombinant PfA-M1 (2 µg) resolved on a reducing SDS-polyacrylamide gel and stained with Coomassie blue.

REFERENCES

1. Breman, J. G. (2001) *Am. J. Trop. Med. Hyg.* **64**, 1-11
2. Krugliak, M., Zhang, J., and Ginsburg, H. (2002) *Mol. Biochem. Parasitol.* **119**, 249-256
3. Loria, P., Miller, S., Foley, M., and Tilley, L. (1999) *Biochem. J.* **339**, 363-370
4. Liu, J., Istvan, E. S., Gluzman, I. Y., Gross, J., and Goldberg, D. E. (2006) *Proc. Natl. Acad. Sci. USA* **103**, 8840-8845
5. Martin, R. E., and Kirk, K. (2007) *Blood* **109**, 2217-2224
6. Lew, V. L., Tiffert, T., and Ginsburg, H. (2003) *Blood* **101**, 4189-4194
7. Rosenthal, P. J., Sijwali, P. S., Singh, A., and Shenai, B. R. (2002) *Curr. Pharm. Des.* **8**, 1659-1672
8. Goldberg, D. E. (2005) *Curr. Top. Microbiol. Immunol.* **295**, 275-291
9. Rosenthal, P. J. (2004) *Int. J. Parasitol.* **34**, 1489-1499
10. Eggleson, K. K., Duffin, K. L., and Goldberg, D. E. (1999) *J. Biol. Chem.* **274**, 32411-32417
11. Klemba, M., Gluzman, I., and Goldberg, D. E. (2004) *J. Biol. Chem.* **279**, 43000-43007
12. Wang, F., Krai, P., Deu, E., Bibb, B., Lauritzen, C., Pedersen, J., Bogyo, M., and Klemba, M. (2011) *Mol. Biochem. Parasitol.* **175**, 10-20
13. Ragheb, D., Bompiani, K., Dalal, S., and Klemba, M. (2009) *J. Biol. Chem.* **284**, 24806-24815
14. Kolakovich, K. A., Gluzman, I. Y., Duffin, K. L., and Goldberg, D. E. (1997) *Mol. Biochem. Parasitol.* **87**, 123-135
15. Allary, M., Schrevel, J., and Florent, I. (2002) *Parasitology* **125**, 1-10
16. Azimzadeh, O., Sow, C., Geze, M., Nyalwidhe, J., and Florent, I. (2010) *Malar. J.* **9**, 189
17. Florent, I., Derhy, Z., Allary, M., Monsigny, M., Mayer, R., and Schrevel, J. (1998) *Mol. Biochem. Parasitol.* **97**, 149-160
18. McGowan, S., Porter, C. J., Lowther, J., Stack, C. M., Golding, S. J., Skinner-Adams, T. S., Trenholme, K. R., Teuscher, F., Donnelly, S. M., Grembecka, J., Mucha, A., Kafarski, P., Degori, R., Buckle, A. M., Gardiner, D. L., Whisstock, J. C., and Dalton, J. P. (2009) *Proc. Natl. Acad. Sci. USA* **106**, 2537-2542
19. Cunningham, E., Drag, M., Kafarski, P., and Bell, A. (2008) *Antimicrob. Agents Chemother.* **52**, 3221-3228

20. Gardiner, D. L., Trenholme, K. R., Skinner-Adams, T. S., Stack, C. M., and Dalton, J. P. (2006) *J. Biol. Chem.* **281**, 1741-1745
21. Stack, C. M., Lowther, J., Cunningham, E., Donnelly, S., Gardiner, D. L., Trenholme, K. R., Skinner-Adams, T. S., Teuscher, F., Grembecka, J., Mucha, A., Kafarski, P., Lua, L., Bell, A., and Dalton, J. P. (2007) *J. Biol. Chem.* **282**, 2069-2080
22. Curley, G. P., O'Donovan, S. M., McNally, J., Mullally, M., O'Hara, H., Troy, A., O'Callaghan, S. A., and Dalton, J. P. (1994) *J. Eukaryot. Microbiol.* **41**, 119-123
23. Vander Jagt, D. L., Baack, B. R., and Hunsaker, L. A. (1984) *Mol. Biochem. Parasitol.* **10**, 45-54
24. Dalal, S., and Klemba, M. (2007) *J. Biol. Chem.* **282**, 35978-35987
25. Whisstock, J. C., McGowan, S., Trenholme, K. R., Gardiner, D. L., and Dalton, J. P. (2009) *Proc. Natl. Acad. Sci. USA* **106**, E56
26. Bennett, T. N., Kosar, A. D., Ursos, L. M., Dzekunov, S., Singh Sidhu, A. B., Fidock, D. A., and Roepe, P. D. (2004) *Mol. Biochem. Parasitol.* **133**, 99-114
27. Klonis, N., Tan, O., Jackson, K., Goldberg, D., Klemba, M., and Tilley, L. (2007) *Biochem. J.* **407**, 343-354
28. Krogstad, D. J., Schlesinger, P. H., and Gluzman, I. Y. (1985) *J. Cell Biol.* **101**, 2302-2309
29. Kuhn, Y., Rohrbach, P., and Lanzer, M. (2007) *Cell. Microbiol.* **9**, 1004-1013
30. Diaz-Perales, A., Quesada, V., Sanchez, L. M., Ugalde, A. P., Suarez, M. F., Fueyo, A., and Lopez-Otin, C. (2005) *J. Biol. Chem.* **280**, 14310-14317
31. Addlagatta, A., Gay, L., and Matthews, B. W. (2006) *Proc. Natl. Acad. Sci. USA* **103**, 13339-13344
32. Ito, K., Nakajima, Y., Onohara, Y., Takeo, M., Nakashima, K., Matsubara, F., Ito, T., and Yoshimoto, T. (2006) *J. Biol. Chem.* **281**, 33664-33676
33. Suda, H., Takita, T., Aoyagi, T., and Umezawa, H. (1976) *J. Antibiot.* **29**, 100-101
34. Lambros, C., and Vanderberg, J. P. (1979) *J. Parasitol.* **65**, 418-420
35. Kapust, R. B., Tozser, J., Copeland, T. D., and Waugh, D. S. (2002) *Biochem. Biophys. Res. Commun.* **294**, 949-955
36. Kapust, R. B., Tozser, J., Fox, J. D., Anderson, D. E., Cherry, S., Copeland, T. D., and Waugh, D. S. (2001) *Protein Eng.* **14**, 993-1000

37. Harlow, E., and Lane, D. (1999) *Using antibodies: a laboratory manual*, Cold Spring Harbor Laboratory Press, Cold Spring Harbor
38. Francis, S. E., Banerjee, R., and Goldberg, D. E. (1997) *J. Biol. Chem.* **272**, 14961-14968
39. Klemba, M., and Goldberg, D. E. (2005) *Mol. Biochem. Parasitol.* **143**, 183-191
40. Tonkin, C. J., van Dooren, G. G., Spurck, T. P., Struck, N. S., Good, R. T., Handman, E., Cowman, A. F., and McFadden, G. I. (2004) *Mol. Biochem. Parasitol.* **137**, 13-21
41. Trang, D. T., Huy, N. T., Kariu, T., Tajima, K., and Kamei, K. (2004) *Malar. J.* **3**, 7
42. Nkrumah, L. J., Muhle, R. A., Moura, P. A., Ghosh, P., Hatfull, G. F., Jacobs, W. R., Jr., and Fidock, D. A. (2006) *Nat. Methods* **3**, 615-621
43. Griesbeck, O., Baird, G. S., Campbell, R. E., Zacharias, D. A., and Tsien, R. Y. (2001) *J. Biol. Chem.* **276**, 29188-29194
44. Saliba, K. J., Folb, P. I., and Smith, P. J. (1998) *Biochem. Pharmacol.* **56**, 313-320
45. Dixon, M. (1953) *Biochem. J.* **55**, 170-171
46. Skinner-Adams, T. S., Stack, C. M., Trenholme, K. R., Brown, C. L., Grembecka, J., Lowther, J., Mucha, A., Drag, M., Kafarski, P., McGowan, S., Whisstock, J. C., Gardiner, D. L., and Dalton, J. P. (2010) *Trends Biochem. Sci.* **35**, 53-61
47. Albiston, A. L., Ye, S., and Chai, S. Y. (2004) *Protein Pept. Lett.* **11**, 491-500
48. Cornish-Bowden, A. (2004) *Fundamentals of enzyme kinetics*, Portland Press, London
49. Hellerstein, S., Spees, W., and Surapathana, L. O. (1970) *J. Lab. Clin. Med.* **76**, 10-24
50. Hwang, S. R., O'Neill, A., Bark, S., Foulon, T., and Hook, V. (2007) *J. Neurochem.* **100**, 1340-1350
51. Constam, D. B., Tobler, A. R., Rensing-Ehl, A., Kemler, I., Hersh, L. B., and Fontana, A. (1995) *J. Biol. Chem.* **270**, 26931-26939
52. Sanchez-Moran, E., Jones, G. H., Franklin, F. C., and Santos, J. L. (2004) *Plant Cell* **16**, 2895-2909
53. Lyczak, R., Zweier, L., Group, T., Murrow, M. A., Snyder, C., Kulovitz, L., Beatty, A., Smith, K., and Bowerman, B. (2006) *Development* **133**, 4281-4292

Chapter 4

Manipulating the substrate specificity of PfA-M1 by active site mutagenesis

Seema Dalal, Daniel Ragheb, and Michael Klemba

ABSTRACT

M1 aminopeptidases are involved in many cellular processes and display diverse preferences for N-terminal amino acids. Structural work on the *E. coli* M1 homolog has highlighted Met_{260} in its active site as a potential factor in the altered substrate specificities exhibited by these enzymes. Sequence analysis of other M1 family aminopeptidases has indicated the equivalent of the Met_{260} is a variable position among proteins with distinct functions. We have undertaken a kinetic analysis of this residue's role in substrate preference using the *P. falciparum* M1 homolog, PfA-M1, as a model enzyme. We have mutated the equivalent residue, Val_{459}, in recombinant PfA-M1 to eleven different amino acids that are represented in this position from sequences of other M1 aminopeptidases. Kinetic analysis of these PfA-M1 variants with dipeptide substrates has revealed unique trends in specificity associated with the properties of the mutated residue. In particular, enzymes with large, hydrophobic substitutions for Val_{459} were generally tighter binders of substrate and had lower turnover rates relative to the wild-type enzyme indicating a shift in catalytic efficiency. Replacement of Val_{459} with a proline has mimicked the narrow substrate specificity exhibited by the M1 homolog leukocyte-derived arginine aminopeptidase, which also has a proline in the corresponding position. These data are presented as preliminary results in an ongoing study on the unique role of this residue in the substrate specificity of M1 aminopeptidases.

INTRODUCTION

M1 family proteins are metalloproteases identified as members of a core of peptidases expressed by organisms in all kingdoms of life (1). They are defined by a canonical zinc-binding motif, consisting of two histidines and a glutamate (HEXXH), and an exopeptidase motif (GXMEN) (2). Within eukaryotes, the evolution and expansion of this family of proteases has implied an inherent, malleable quality that allows them to fulfill multiple physiological roles (1). These include general peptide catabolism, hormonal processing, antigen interactions, blood pressure regulation and cell cycle control in mammalian systems (3,4). In humans alone, there are twelve M1 aminopeptidase homologs that have been identified (6). Although structurally similar, these enzymes serve in specific capacities and are distinguished in nomenclature, such as aminopeptidases A, B, and N, leukocyte-derived arginine aminopeptidase, and puromycin-sensitive aminopeptidase (7). Most M1 aminopeptidases have the ability to hydrolyze many kinds of N-terminal amino acids in different preferential order, permitting residues such as Ala, Phe, Arg, and Lys in the P1 and P1' position of substrates (Schechter and Berger nomenclature) (5). Enzyme substrate specificity can also vary greatly; some homologs cleave various P1 residues similar to the *E. coli* homolog PepN (3). Others cleave a restricted set of N-terminal amino acids such as aminopeptidase B, which strictly hydrolyzes arginine and lysine in the P1 position (8). These altered specificities are the result of particular key active site components, apart from the identified catalytic residues, that allow M1 aminopeptidase specificity to be manipulated.

Crystallographic studies of the *E. coli* aminopeptidase N homolog PepN have highlighted the role of Met_{260}, the residue that immediately precedes the GAMEN motif in sequence, as playing a distinct role in specificity of the S1 pocket (9). In the absence of a large P1 residue, the PepN Met_{260} occupies the active site cavity, providing an N-terminal cushion for small amino acids. However, when the long side chain of a substrate, such as arginine, enters the pocket, Met_{260} undergoes a conformational change to allow the P1 amino acid to interact with other active site residues. A model of the Met_{260} rotation from their studies can be found in Supplemental Figure 4-S1. The observation that rotation of this methionine allows the enzyme to coordinate different sized residues raises the question as to how the other amino acids found in lieu of it would affect substrate binding. According to primary sequence alignment and crystal structure comparisons, the corresponding residue in the *P. falciparum* M1 aminopeptidase, PfA-

M1, is Val_{459}. (alignment not shown, (10)). Sequence alignments of other M1 aminopeptidases reveals that numerous other amino acids are found in this position. In this study we have attempted to determine if the identity of this residue is the main point of variability contributing to altered substrate specificity of this enzyme.

This chapter introduces the preliminary results of an ongoing study on the significance of the Val_{459} in the P. falciparum enzyme PfA-M1. In general, there is a partial bias for hydrophobic amino acids in the corresponding residue among M1 homologs. Previously characterized enzymes, such as PepN, aminopeptidase A, and the human leukocyte-specific arginyl aminopeptidase, have Met, Thr, and Pro residues in the equivalent position. Based on a comparison of primary sequences and survey of the literature, we decided to mutate the PfA-M1 Val_{459} residue to eleven different amino acids to best represent the variety of M1 aminopeptidases. The amino acids placed in lieu of Val_{459} in the active site were Gly, Ala, Ser, Thr, Leu, Ile, Met, Phe, Tyr, Trp and Pro. We used dipeptides with different N-terminal residues and a fixed P1' Ala to analyze the catalytic differences caused by changes in the S1 pocket. The future plans for this study of M1 family aminopeptidases are also discussed.

EXPERIMENTAL PROCEDURES

Cloning and mutagenesis

We have previously cloned the PfA-M1 gene from 3D7 parasites as described in Chapter 3 (see *Expression and purification of recombinant PfA-M1*). To perform mutagenesis on the Val_{459} residue, a section of the PfA-M1 gene was subcloned into the psp72 vector in between the restriction sites for BamH1 and NdeI. The point mutation was done using the Quickchange II XL site-directed mutagenesis kit (Stratagene) using degenerate primers, with the forward primer 5' AGTTGCTGTTTCTGACTTTAATNYKGGTGCTATGGAAAATAAAGG and reverse primer 5' CCTTTATTTTCCATAGCACCMRNATTAAAGTCAGAAACAGCAACT (with the mutation underlined). These primers produced point mutations for the Leu, Pro, Phe, Ser, and Thr substituted enzymes. For the other PfA-M1 variants we used the following combination of primers:

Met: forward, 5' AGTTGCTGTTTCTGACTTTAATATGGGTGCTATGGAAAATAAAGG, reverse 5' CCTTTATTTTCCATAGCACCCATATTAAAGTCAGAAACAGCAACT

Ala: forward, 5' AGTTGCTGTTTCTGACTTTAATGCTGGTGCTATGGAAAATAAAGG, reverse 5' CCTTTATTTTCCATAGCACCAGCATTAAAGTCAGAAACAGCAACT
Ile: forward, 5' AGTTGCTGTTTCTGACTTTAATATTGGTGCTATGGAAAATAAAGG, reverse 5' CCTTTATTTTCCATAGCACCAATATTAAAGTCAGAAACAGCAACT
Gly: forward, 5' AGTTGCTGTTTCTGACTTTAATGGAGGTGCTATGGAAAATAAAGG, reverse 5' CCTTTATTTTCCATAGCACCTCCATTAAAGTCAGAAACAGCAACT
Tyr: forward 5' AGTTGCTGTTTCTGACTTTAATTATGGTGCTATGGAAAATAAAGG, reverse 5' CCTTTATTTTCCATAGCACCATAATTAAAGTCAGAAACAGCAACT
Trp: forward 5' AGTTGCTGTTTCTGACTTTAATTGGGGTGCTATGGAAAATAAAGG, reverse 5' CCTTTATTTTCCATAGCACCCCAATTAAAGTCAGAAACAGCAACT.

Mutations in the psp72 vector were confirmed by DNA sequencing, and the entire PfA-M1 gene confirmed once segments were subcloned back into the pet45b expression plasmid.

Expression and purification

We have previously been able to over-express and purify a cleavable, N-terminal hexahistidine tagged form of the *P. falciparum* aminopeptidase PfA-M1 in *E. coli* as described in Chapter 3 *(*see *Expression and purification of recombinant PfA-M1)*. In order to control for extraneous metal contamination in the protein preparations (see *Metal content determination* below) we employed a Talon® His-tag Affinity column that uses cobalt ions to coordinate the N-terminal tag and is reported to resist metal leakage. We also incubated the proteins with the 100 μM metal chelator EDTA to scavenge extra metal in the solution, and then supplemented samples with the equivalent concentration of Zn^{2+} to attempt to fully occupy active sites with the metal while dialyzing against IMAC Buffer A overnight. Removal of the N-terminal histidine tag by cleavage with TEV protease and subtractive IMAC was done to prevent the affinity tag from affecting kinetic analysis. Gel filtration chromatography allowed us to both observe the oligomerization states for the variants of PfA-M1 as well as remove extra, unbound Zn^{2+}. Chromatograms of the absorbance spectra at 280 nm indicated that all the mutated forms of PfA-M1 migrated as expected monomers indicating substitution in the Val_{459} position did not cause misfolding or aggregation of the protein.

Metal content determination

The concentration of metal associated with PfA-M1 and mutated forms of the enzyme were determined by ion exchange chromatography and post-column chromogenic analysis. Metal ions were separated on an IonPac CS5A analytical column (250 *x* 4mM) preceded by a Ionpac CG5A guard column (50 *x* 4mM) by a Model AS50 Ion Chromatography System 3000 (Dionex, Sunnyvale, CA). Metal resolved on a column equilibrated in chelating elution buffer, consisting of 7 mM pyridine-2,6-dicarboxylic acid (PDCA), 66 mM KOH, 5.6 mM K_2SO_4, 74 mM HCOOH, was immediately mixed with 0.12 g/L of 4-(2-pyridylazo)resorcinol (PAR) delivered by a post-column pneumatic controller. Peaks corresponding to ions were detected at 530 nm and peak areas were integrated by Chromoleon software (Dionex). Protein samples were vortexed in a 1:1 ratio with 1 M nitric acid and centrifuged at 16,000 *x* g for 10 minutes to collect precipitate prior to injection. Metal concentrations were calculated using a standard curve of Nickel, Zinc, and Cobalt standards (Sigma-Aldrich) diluted in the same mixture of buffer and nitric acid.

Kinetic analysis with dipeptide substrates

Enzyme assays were conducted with dipeptide substrates (Sigma-Aldrich, Bachem) and analyzed by reverse phase ultra-performance liquid chromatography. Different amounts of protein ranging from 13 *ng* to 1.6 *ug* (depending on enzyme and substrate combination) were pre-incubated in 100 mM HEPES pH 7.5 and 110 mM NaCl for 10 minutes at 30 °C before addition of substrate concentrations between 0.2*x* and 10*x* the Michaelis constant (K_M). The 50 μL assay was allowed to progress for 15 minutes before reactions were effectively stopped by addition of 100 μL of 500 mM sodium borate pH 9.5. We confirmed that initial rates were linear for the duration of the reaction by a time-point assay. 15 μL aliquots of the diluted reactions were transferred to new wells where 5 μL of the primary amine derivatization reagent, AccQ Tag Ultra (6-aminoquinolyl-N-hydroxysuccinimidyl carbamate) was immediately added (Waters, Milford, MA). Derivatization reactions were allowed to continue until completion for 10 minutes at room temperature, and then diluted with 100 μL of 500 mM sodium borate pH 9.5 prior to injection. To ensure a molar excess of 3:1 of reagent to primary amine, dipeptide hydrolysis reactions were sometimes diluted to a final concentration of 0.75 mM prior to derivatization. Reactions were injected onto a reverse phase Acquity C18 column (2.1 *x* 100

mM, 1.7 μm) equilibrated with 5% AccQ Tag Ultra Eluent A solution (containing acetonitrile and formic acid) using an Acquity Ultra Performance Liquid Chromatography instrument. Peaks with absorbance at 216 nm corresponding to substrate and product were resolved using a gradient of increasing AccQ Tag Ultra Eluent B solution and integrated using Empower software (Waters, Milford, MA). Product concentrations were determined by fitting peak integration size to a standard curve of derivatized P1 or P1' residues, Gly or Ala respectively, in assay buffer. Rates were fit to the Michaelis-Menten equation

$$v = \frac{[E]_o[S]k_{cat}}{K_m + [S]}$$

(where v is the initial rate, $[E]_0$ the amount of enzyme, and [S] the substrate concentration) by non-linear regression in Kaleidagraph 4.1 (Synergy Software).

RESULTS

Metal content determination

In order to assess the effects of mutating the Val_{459} residue on zinc-binding in the active site, we identified and quantified the metal content for each form of PfA-M1. The rationale behind assessing the metal content was two-fold. First, it was important to ensure that the metal complexed with the enzymes was in fact Zn^{2+} as predicted by the conserved M1 metal binding motif and revealed by crystal structure (10). The presence of other metals in the active site, although perhaps structurally permissible, would likely be an artifact of the expression and purification process. Identifying the bound metal as Zn^{2+} allowed us to directly compare the kinetic parameters between the enzymes. In addition to identifying Zn^{2+} in the active site, we sought to determine the ratio of metal to enzyme. Substoichiometric levels of metal could be indicative of an altered active site structure that is detrimental to zinc-binding and consequently prevent accurate kinetic analysis. Metalloproteins are routinely assessed for transition metal binding using a bifunctional ion exchange column, such as the Dionex IonPac CS5A, in conjunction with the metal-complexing chromophore PAR. PAR has previously been used to quantitate Zn^{2+}, Co^{2+}, Ni^{2+}, Cu^{2+}, and Fe^{2+} at micromolar levels by chromatographic methods (11).

Protein sample mixed with nitric acid was injected and metal amounts determined using standards diluted in the same buffer. The results of these analyses are in Table 4-1 below. Only the metal Zn^{2+} was detected from the purified protein samples, which was not present in a detectable concentration in either the gel filtration buffer or nitric acid blanks. The ratios of metal to enzyme ranged from 1.1:1 to 1.5:1 indicating there was at least full occupancy of Zn^{2+} for each variant of PfA-M1. The presence of metal concentrations exceeding those of enzyme, although surprising, may be related to the limitation of determining protein concentration by absorbance at 280nm using an extinction coefficient calculated for denatured peptide sequences. A ratio exceeding 1:1 for the wild-type enzyme indicated these results were not a consequence of the amino acid substitution in the active site. Using this analysis, we determined that the mutations did not lead to severe perturbation of metal-binding.

Table 4-1: Determination of Zn^{2+} content in PfA-M1 variants. Concentrations of zinc from the PfA-M1 protein samples were assessed in triplicate by ion exchange chromatography and compared to protein concentrations calculated by absorbance at 280 and the PfA-M1 extinction coefficient.

PfA-M1 variant	Ratio Zn: Protein
Val (Wild-type)	1.2 ± 0.1
Gly	1.5 ± 0.1
Ala	1.3 ± 0.1
Ser	1.4 ± 0.1
Thr	1.2 ± 0.1
Leu	1.1 ± 0.1
Ile	1.4 ± 0.1
Met	1.3 ± 0.1
Phe	1.3 ± 0.1
Tyr	1.5 ± 0.1
Trp	1.5 ± 0.1
Pro	1.5 ± 0.1

Kinetic analysis of PfA-M1 variants with dipeptide substrates

Our kinetic analysis was carried out with X-Ala dipeptides, where the P1 residues were chosen to reflect different side chain properties with small, large, bulky, non-polar, polar, and charged groups. The use of fixed P1' Ala substrates enabled us to assess changes in S1 specificity and minimize contacts with the S2 subsite. Individual amino acids can be resolved on a reverse phase column by ultra-performance liquid chromatography and derivatized amino termini followed by absorbance at 216 nm. We first analyzed the wild-type PfA-M1 and full set of enzymes against four substrates: Ala-Ala, Leu-Ala, Phe-Ala, and Arg-Ala. Common trends among the variants with similar residue replacements, as discussed below, prompted us to select a subset of enzymes to analyze with more substrates. For the sake of clarity in considering the data, K_M, k_{cat}, and catalytic efficiency parameters are displayed individually and as normalized to the wild-type enzyme.

PfA-M1 variants display altered substrate specificities

The individual kinetic parameters for the twelve forms of PfA-M1 with substrates Ala-Ala, Leu-Ala, Phe-Ala, and Arg-Ala are represented graphically in Figure 4-1. The data indicated that changing the identity of the single residue in the PfA-M1 active site changed both the K_M and k_{cat} values among enzymes. In spite of the complexity of the results, there were certain trends in catalysis among the different substrates. Enzymes where larger, hydrophobic residues replaced Val_{459} generally had reduced K_M values among the substrates (Figure 4-1A). This was not true for all combinations of these PfA-M1 variants and substrates (such as Ile_{459}) but was nevertheless a discernable pattern. The Pro_{459} variant had entirely different results from the other enzyme forms, revealing restricted substrate specificity, as discussed further below. The aromatic substitutions were consistently tighter binders of substrate than the wild-type enzyme and their smaller counterparts (such as Ala_{459} and Thr_{459}). In some instances, such as the Leu_{459} and Met_{459} enzymes, hydrophobic substitutions did not bind an individual substrate well, as was the case with Arg-Ala.

Changes in the K_M for some PfA-M1 variants were correlated by shifts in relative turnover rates as shown in Figure 4-1B. Within the same clusters of enzymes that exhibited lower K_M values, particularly those with aromatic substitutions for Val_{459}, there was a trade-off where the k_{cat} was also decreased relative to the other variants. This inverse correlation between K_M and product turnover was true for three of the four substrates analyzed with the full set of proteins, the exception being Arg-Ala. With the case of this P1 amino acid, in spite of low Michaelis constants, the k_{cat} values were not reduced relative to the wild-type protein but rather remained robust. The length of the arginine side-chain likely allows it to hydrogen bond with residues at the top of the S1 subsite perhaps contributing to preference for it among most of the enzymes. Interestingly the low K_M subset of proteins still had reduced turnover rates relative to the enzymes with smaller residue substitutions, indicating it may not be an entire departure from the trend but rather a dampened effect due to the substrate.

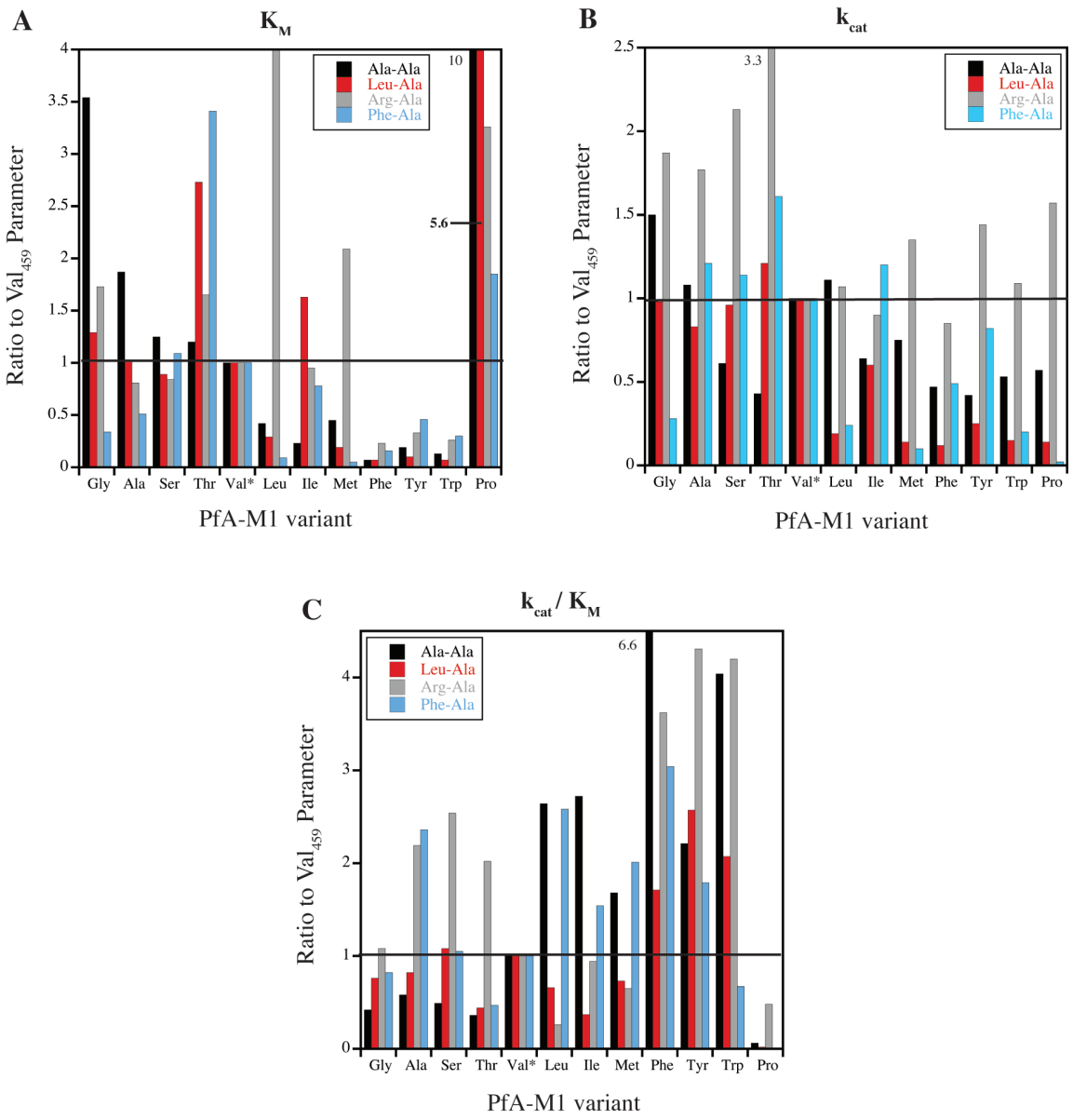

Figure 4-1: Relative K_M, k_{cat}, and k_{cat} / K_M values for PfA-M1 Val_{459} variants with Ala-Ala, Leu-Ala, Phe-Ala, and Arg-Ala. Michaelis-Menten parameters derived from substrate saturation curves are displayed graphically for the four substrates with all eleven PfA-M1 residue 459 variants and the wild-type enzyme, listed in order of relative side-chain size of the substituted amino acid (except for Pro because of its distinct structure). Values are normalized to the wild-type PfA-M1 (Val_{459}), which is indicated with an *. To facilitate comparison of parameters in the plot, a bar is set at a ratio of 1.

The catalytic efficiency of an enzyme is expressed as the ratio of k_{cat} over K_M, quantifying an enzyme's ability to both bind substrate and catalyze the reaction towards product. As one might expect, sharp changes in either parameter will dramatically affect the catalytic efficiency of an enzyme as displayed in Figure 4-1C. The PfA-M1 variants that displayed lower K_M values,

in spite of their reduced turnover rates, were the most efficient enzymes. This was a direct consequence of their increased ability to bind substrates.

The major exception to the trends observed by changing the Val_{459} position was its replacement with proline. The Pro_{459} enzyme was a generally poor enzyme with Ala-Ala, Leu-Ala, and Phe-Ala as expressed in millimolar Michaelis values and very low k_{cat} constants (or in the case of Ala-Ala, a K_M close to 100 mM with a high k_{cat}). However, with Arg-Ala as a substrate, the Pro_{459} enzyme was able to turnover the substrate much better than any other P1-Ala combination and even better than certain other enzymes. In this instance, it is of use to consider the actual kinetic parameters for the Pro_{459} enzyme as presented in Supplemental Figure 4-S2. While relative to wild-type PfA-M1 the K_M for Arg-Ala is still increased, it is only 1.1 mM, which in concert with a k_{cat} of 17.4 s^{-1} yields a catalytic efficiency of 1.6×10^4 M^{-1} s^{-1}. This indicates that the PfA-M1 Pro_{459} variant was primarily selective for a P1 Arg residue, a drastic shift in specificity for an M1 aminopeptidase.

In light of the patterns we observed from these results, we decided to expand our studies with fewer enzymes and a larger set of substrates. We omitted enzymes from our further work that had generally similar parameters among the different substrates, such as glycine and serine (comparable to alanine), isoleucine (comparable to leucine), and tyrosine and tryptophan (comparable to phenylalanine). The results from these analyses are displayed in Figure 4-2.

Exploring kinetic trends among a subset of PfA-M1 variants with more substrates

Given the differences in specificity among individual enzymes, we decided to analyze some of the PfA-M1 forms with P1 Gly, Val, Met, Tyr, and His containing substrates. This increased list of substrates would allow us to examine if the previously observed trends continued, or if there were further changes in specificity. As a note, we used Gly-Leu instead of Gly-Ala in our analysis because we were unable to determine kinetic parameters with the latter due to an extremely high K_M (which was subsequently reduced with a P1' Leu residue).

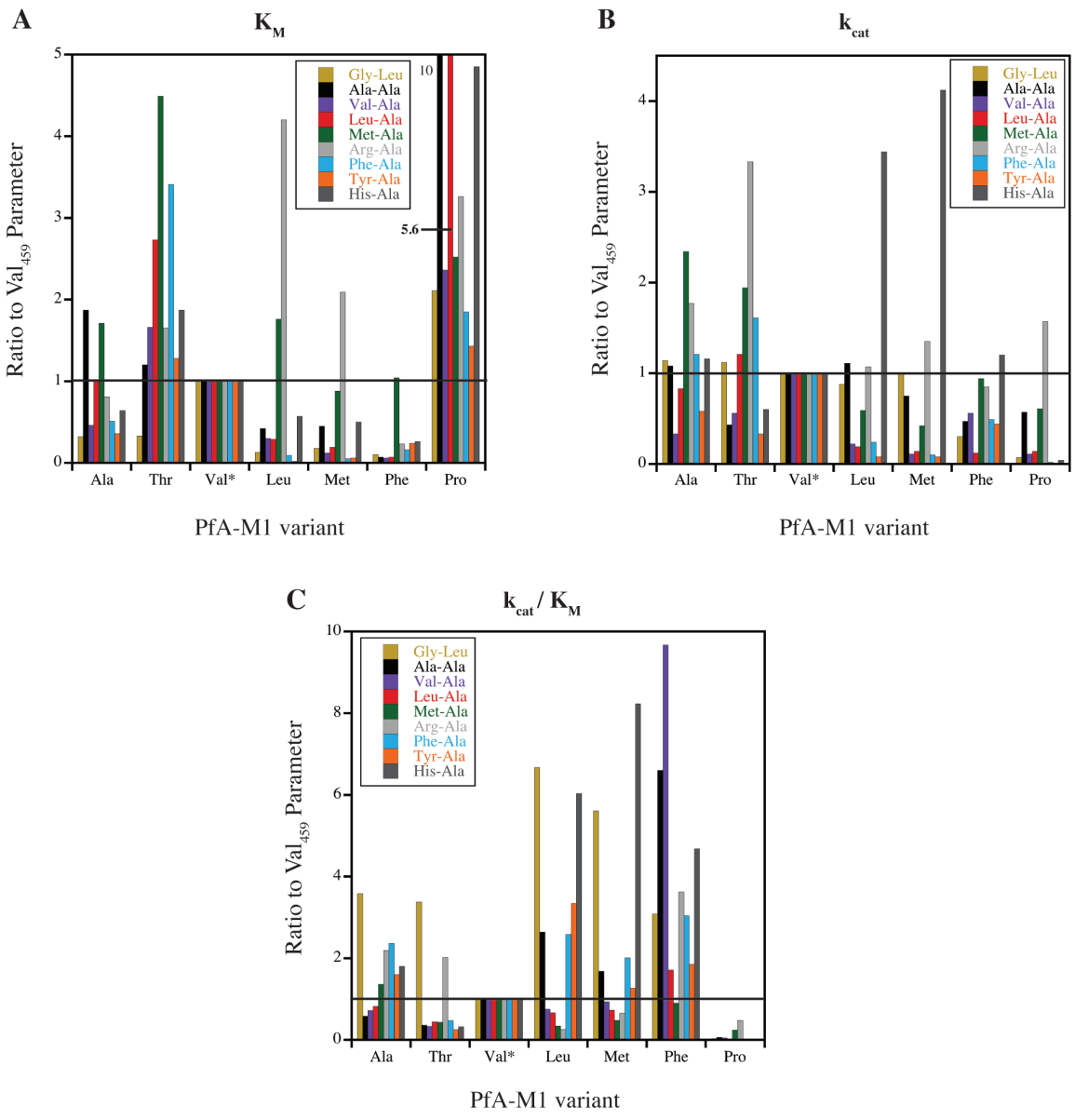

Figure 4-2: Analysis of subset of PfA-M1 Val_{459} variants with expanded list of P1 residues. Kinetic parameters for six PfA-M1 residue 459 variants and the wild-type enzyme are displayed with nine substrates of different size and side-chain properties. PfA-M1 variants are arranged according to substituted residue size (except for proline) and values are normalized to the wild-type enzyme (Val_{459}), which is indicated with an *. To facilitate comparison of parameters in the plot, a bar is set at a ratio of 1.

As with the previous results, the data pointed to a complexity of interactions in the active site of the PfA-M1 variants that resulted in altered K_M and k_{cat} parameters. For the most part, the large, hydrophobic substituted residues still exhibited lower Michaelis and turnover constants, although there were individual disparities (such as the Phe_{459} variant with Met-Ala). The Thr_{459} enzyme, on the other hand, had a combination of large K_M values relative to wild-type (and other

variants) but also varied in terms of its turnover rates, indicating its own individual preference for substrates.

One specific result of interest was the difference in kinetic parameters for the PfA-M1 enzymes with Gly-Leu. Glycine lacks a side-chain group that would interact with the Val_{459} position. As a result, changes in parameters with this substrate could be indicative of structural modifications in the active site beyond the mutated residue. As displayed in K_M, k_{cat}, and catalytic efficiencies, enzymes varied among one another and from the wild-type enzyme with preference for Gly-Leu. These changes indicated that varying the Val_{459} position not only affected the interactions between the single residue and the N-termini of substrates, but also to some degree altered the active-site pocket.

Our analysis also revealed that in addition to Arg-Ala, the Pro_{459} form of PfA-M1 also displayed preference for a P1 Met residue. The side chain of methionine, although slightly shorter than arginine and lacking the charged guanidinium group, is also long enough to extend into the S1 pocket. Despite a K_M that is two-fold greater than that of Val_{459}, increased turnover rates with methionine indicated the Pro_{459} variant was efficient in hydrolyzing this residue (see Supplemental Figure 4-S2). These data for the Pro_{459} enzyme are the most directly relatable to physiological observations. The human leukocyte-derived arginine aminopeptidase (L-RAP) has been shown to have peculiar specificity for an M1 aminopeptidase enzyme in its preference mainly for Lys and Arg P1 residues (12). The equivalent Val_{459} residue in L-RAP is also a proline in the human enzyme. It is plausible, considering our results, that preference for arginine is a consequence of precluding other substrates in the active site as a form of negative selection for particular P1 groups.

DISCUSSION

We have determined from our analysis of mutated forms of PfA-M1 that changing the identity of the Val_{459} position in the active site is an important factor in the substrate specificities of the enzyme displayed in altered kinetic parameters. Among the different PfA-M1 forms, a subset with large, hydrophobic residues in lieu of Val_{459} displayed relatively low K_M values and correspondingly low k_{cat} constants. In these cases, it appears as though the enhanced ability to bind substrates comes with a trade-off in increased activation energies, allowing the substrate but not transition state to be more readily stabilized. Further, our analysis revealed that in the case of

the Pro_{459} form, the substrate specificity of the enzyme could be dramatically narrowed for two substrates, Arg- and Met-Ala. While one cannot rule out specificity changes made by compensatory mutations in active sites among homologs, it is clear that this residue plays a significant role in of itself.

Even though it is difficult to directly connect the identity of this residue with physiological necessity, certain hypotheses can be drawn about structure-function relationships. As an example, the differences between the wild-type PfA-M1 enzyme and the Phe_{459} variant kinetic parameters are curious in light of the enzyme's role in hemoglobin catabolism in the food vacuole of *P. falciparum*. The temptation in analyzing kinetic data is to consider catalytic efficiency alone as the benchmark for substrate specificity of an enzyme. While this remains true in terms of overall preference for a substrate in one environment, given the context of the PfA-M1 vacuolar role the disparity between the K_M and k_{cat} parameters may give better insight into the need for the Val_{459} residue. In Chapter 3 we proposed that a crucial aspect of the malaria enzyme's ability to function is its resistance to changes in k_{cat} even as the K_M values increased with dropping pH levels. In the presence of high concentrations of hemoglobin peptides, the saturating environment makes k_{cat} the key parameter for efficient turnover of substrate. We have determined in this study that at pH 7.5 the increased catalytic efficiency of the Phe_{459} form is a consequence of its low K_M and in spite of a relatively low k_{cat}. Inferring from our observations in Chapter 3, one could thus propose that in the food vacuole of the parasite where the Phe_{459} variant's K_M values would be greater, its ability to efficiently cleave amino acids would compromised given its low turnover rates. This would likely hold true for all the low K_M enzymes from this study where k_{cat} values seemed to correspondingly drop. It is of note that compared to all the other forms, the wild-type enzyme retains the highest average k_{cat} among the different substrates.

It is feasible that selective pressure for the Val_{459} in PfA-M1 was driven by a need for robust turnover rates at an acidic pH. This does not take into consideration the still undiscovered role of the enzyme in the nucleus, which would also affect the selection process. Notwithstanding, the next step in understanding the malaria enzyme's vacuolar recruitment and catabolic function is to attempt to replace the endogenous form of PfA-M1 in the parasite with Val_{459} variants that exhibited altered substrate specificity (such as Phe and Pro) and assess the phenotypes. One might expect that the specificity switches would have deleterious effects on the

endpoint of hemoglobin catabolism, but it is difficult to predict how that would subsequently affect the parasite. If mutations are accepted (such that the parasite can still survive with altered PfA-M1 activity), the effects can be monitored by changes in parasite growth rates, morphology, and amino acid production (as profiled by those secreted into the medium). This *in vivo* extension of our study will lay important groundwork for understanding the specific need for PfA-M1 in the parasite.

To further strengthen the conclusions drawn from our *in vitro* experiments, we are pursuing a similar study of the bacterial enzyme PepN's Met_{260} residue, by mutating it to valine (to mimic the *P. falciparum* protein), phenylalanine and proline. The ability to shift specificity in PePN will highlight the significance of the residue outside of the context of a single enzyme. Preliminary results from the *E. coli* study indicate that we can reproduce the results and tune the specificity of this protein in a similar fashion to PfA-M1 (data not shown).

Finally, we have yet to determine the significance of the Pro_{459} enzyme's altered specificity. Arginine and methionine P1 substrates were hydrolyzed efficiently by the Pro_{459} form and conversely not well tolerated by Leu_{459} and Met_{459} variants indicating an ability of the protein to turn off preference for certain substrates. The human leukocyte-derived arginine aminopeptidase (L-RAP) also has a proline in the corresponding residue of Val_{459} and prefers arginine and lysine in the P1 position (12). The ability of these M1 homologs to limit substrate specificity is presumably a consequence of this proline. To further explore this, we will use X-ray crystallography to give structural insight into how this proline causes such a dramatic change in specificity. We have begun attempts to solve the structure of the Pro_{459} PfA-M1 form and are currently optimizing crystal growth conditions. In addition we will also attempt to crystallize the Phe_{459} variant to understand any active site modifications induced by the presence of this aromatic residue.

As a way to analyze the effects on specificity caused by varying this position in non-mutagenic context, we will examine the three M1 aminopeptidase homologs expressed by the protozoan parasite, *Toxoplasma gondii*. These enzymes, which have a high degree of similarity with one another and the *P. falciparum* protein, possess an alanine, methionine, and proline in the corresponding Val_{459} position. Characterizing these enzymes will be a useful counterpart to our PfA-M1 studies, serving to confirm our results and help further understand the significance of this residue. Although beyond the scope of this study, eventually connecting the enzymes

with their *in vivo* locations and function would open the door to comprehending the role of this active site position in the complex nature of M1 aminopeptidases.

ACKNOWLEDGEMENTS

We would like to thank Dr. M. Hernick for the use of the Dionex ICS-3000 system for metal analysis.

LIST OF ABBREVIATIONS

EDTA, Ethylenediaminetetraacetic acid; IMAC, immobilized metal affinity chromatography; PAR, 4-(2-pyridylazo) resorcinol; PDCA, pyridine-2,6-dicarboxylic acid; PepN, *E. coli* M1 aminopeptidase homolog; TEV, tobacco etch virus.

SUPPLEMENTARY INFORMATION

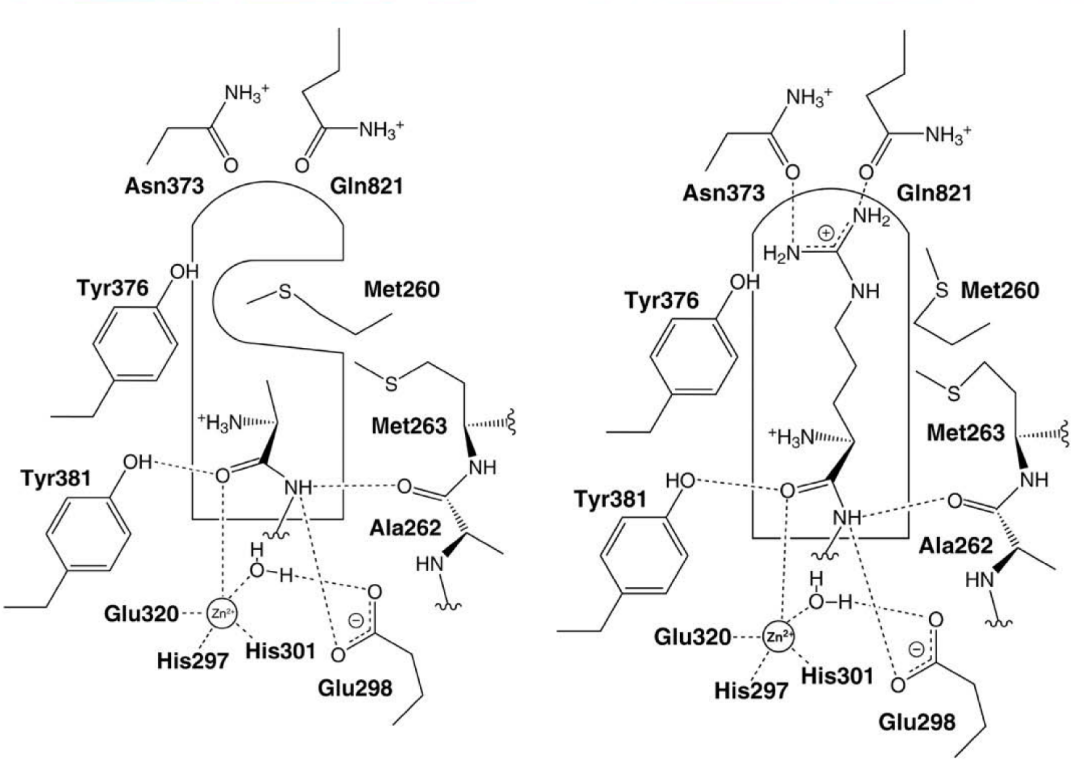

Supplemental Figure 4-S1: "Expected substrate-binding models of aminopeptidase N." Model of predicted interactions in the S1 pocket site of the bacterial M1 aminopeptidase PepN, with P1 residue Ala (left) and Arg (right). This is Figure 7 from Ito, K., et al. (2006) *J. Biol. Chem.* **281**, 33664 – 33676.

Substrate	K_m (mM)	k_{cat} (s^{-1})	k_{cat}/K_m (M^{-1} s^{-1})
Gly-Leu	15.5	1.0	6.5 X 10^1
Ala-Ala	~99	~25	~2.5 X 10^2
Val-Ala	12.9	0.1	7.9
Leu-Ala	2.9	1.4	4.8 X 10^2
Met-Ala	0.6	6.9	1.1 X 10^4
Arg-Ala	1.1	17.4	1.6 X 10^4
Phe-Ala	9.4	0.5	5.3 X 10^1
Tyr-Ala	6.2	0.1	1.6 X 10^1
His-Ala	22.9	0.1	4.4

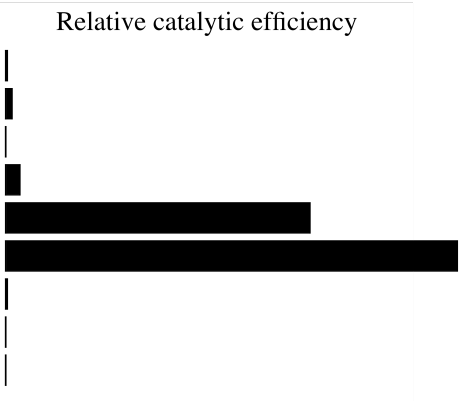

Supplemental Figure 4-S2: Individual kinetic parameters for the PfA-M1 Pro_{459} variant. Relative k_{cat} / K_M values are displayed graphically for each substrate.

REFERENCES

1. Page, M. J., and Di Cera, E. (2008) *J Biol Chem* **283**, 30010-30014
2. Hooper, N. M. (1994) *FEBS Letters* **354**, 1-6
3. Chandu, D., and Nandi, D. (2003) *Microbiology* **149**, 3437-3447
4. Peer, W. A. (2011) *Ann Bot* [Epub ahead of print]
5. Schechter, I., and Berger, A. (1967) *Biochem Biophys Res Commun* **27**, 157-162
6. Diaz-Perales, A., Quesada, V., Sanchez, L. M., Ugalde, A. P., Suarez, M. F., Fueyo, A., and Lopez-Otin, C. (2005) *J Biol Chem* **280**, 14310-14317
7. Albiston, A. L., Ye, S., and Chai, S. Y. (2004) *Protein Pept Lett* **11**, 491-500
8. Cadel, S., Pierotti, A. R., Foulon, T., Creminon, C., Barre, N., Segretain, D., and Cohen, P. (1995) *Mol Cell Endocrinol* **110**, 149-160
9. Ito, K., Nakajima, Y., Onohara, Y., Takeo, M., Nakashima, K., Matsubara, F., Ito, T., and Yoshimoto, T. (2006) *J. Biol. Chem.* **281**, 33664-33676
10. McGowan, S., Porter, C. J., Lowther, J., Stack, C. M., Golding, S. J., Skinner-Adams, T. S., Trenholme, K. R., Teuscher, F., Donnelly, S. M., Grembecka, J., Mucha, A., Kafarski, P., DeGori, R., Buckle, A. M., Gardiner, D. L., Whisstock, J. C., and Dalton, J. P. (2009) *Proceedings of the National Academy of Sciences* **106**, 2537-2542
11. Atanassova, A., Lam, R., and Zamble, D. B. (2004) *Anal Biochem* **335**, 103-111
12. Tanioka, T., Hattori, A., Masuda, S., Nomura, Y., Nakayama, H., Mizutani, S., and Tsujimoto, M. (2003) *J Biol Chem* **278**, 32275-32283
13. Addlagatta, A., Gay, L., and Matthews, B. W. (2006) *Proceedings of the National Academy of Sciences* **103**, 13339-13344

Chapter 5

Summary and conclusions

The evolution of *P. falciparum* has involved its ability to invade human red blood cells and efficiently proteolyze host hemoglobin in an acidic organelle known as the food vacuole. Hemoglobin catabolism is required for parasite survival, and essential enzymes involved in this pathway are potential drug targets. The work presented in this dissertation provides the biochemical basis for the catalytic roles of two *P. falciparum* aminopeptidases that have been recruited to the food vacuole to participate in hemoglobin degradation.

The presence of PfAPP in the food vacuole is the first known case in which an aminopeptidase P homolog has been found in an acidic environment. The enzyme is unique in its ability to hydrolyze amino acids from the N-terminus of peptides that contain a proline in the second position. Similar to previous studies done on PfAPP, we confirmed the dual distribution of the enzyme to the food vacuole and cytosol by immunolocalization. Our kinetic analyses revealed that the enzyme is maximally active with Mn^{2+} as well as structurally stable and catalytically efficient in an acidic environment. These results set it apart from the human homolog, indicating a specialization of function for the parasite enzyme. They further substantiated PfAPP participation in hemoglobin catabolism.

The aminopeptidase PfA-M1, which has a broader substrate specificity range, was also localized to the food vacuole of the parasite in addition to its nucleus. The presence of this enzyme in an acidic environment is very irregular for members of the M1 family of proteases. Our immunolocalization studies with wild-type parasite lines have corroborated the location of protein in the nucleus and food vacuole. The *P. falciparum* specific N-terminal extension in sequence was shown by fluorescent reporter protein to contribute to the vacuolar targeting of PfA-M1. Our study also determined that the vacuolar form of PfA-M1 is soluble and an efficient catalyst in acidic conditions, meaning the enzyme likely carries the burden of amino acid production in the vacuole.

The recruitment of these two enzymes to the food vacuole enables the parasite to efficiently degrade hemoglobin. Given their respective substrate specificities, they likely work in concert to generate free amino acids. PfA-M1 is able to cleave dipeptides and hydrolyze the N-termini of small polypeptides generated by other vacuolar proteases, and PfAPP is able to hydrolyze those peptides containing prolines. Although an acidic pH is not the ideal environment for these enzymes (peak activity ranges from pH 7-7.5), their kinetic constants indicate that high substrate concentrations allow them both to function efficiently in the acidic

vacuole. These results underscore the tentative relationship between pH optima and physiological roles, in which the former can be misleading when understanding the actual cellular function of an enzyme.

Evolutionary adaptation to the food vacuole required the structural stabilization of the aminopeptidase P homolog in an acidic environment. While it is still unclear whether the pH-resilient stability and turnover rates are intrinsic qualities of the M1 family of aminopeptidases, PfA-M1 is also well equipped to function in the food vacuole. In designing strong inhibitors against these aminopeptidases, screening and assays should be performed at a biologically relevant pH values close to 5.5. Competitive inhibitors screened at neutral pH will likely not have the same potency *in vivo* given the changes in protonation states within enzyme active sites and the high concentrations of substrate available in the vacuole. Molecules with extremely low inhibition constants at an acidic pH could be more effective in disrupting PfAPP and PfA-M1 vacuolar function.

Alternatively, the presence of PfAPP and PfA-M1 in distinct secondary locations indicates that they are involved in processes other than hemoglobin catabolism. PfAPP likely acts in a housekeeping capacity in the cytosol by processing peptides generated by the proteasome. There is potential that the role of PfA-M1 in the nucleus may be more unique. Exploration of this function could present an alternative opportunity for inhibitor design leading to potent anti-malarial drug development.

In another final study presented here, the preliminary results from mutagenesis of the PfA-M1 active site have revealed a significant residue in the S1 pocket contributing to the substrate specificity of the M1 aminopeptidase homolog. Changing the identity of Val_{459} can dramatically alter the kinetic parameters of the enzyme as demonstrated with various different dipeptides. Continuing work on this residue will give insight into its importance among M1 aminopeptidases in general as well as help further elaborate on the roles of PfA-M1 in the parasite.